

PRESTRESSED CONCRETE RAILWAY CROSSTIE SUPPORT VARIABILITY AND
ITS EFFECT ON FLEXURAL DEMAND

BY

RICARDO JOSÉ QUIRÓS OROZCO

THESIS

Submitted in partial fulfillment of the requirements
for the degree of Master of Science in Civil Engineering
in the Graduate College of the
University of Illinois at Urbana-Champaign, 2018

Urbana, Illinois

Advisers:

Professor Christopher P.L. Barkan
Mr. J. Riley Edwards

ABSTRACT

The increased presence of instrumentation on railroad track components in revenue service operation has provided vast amounts of data with the potential for improving the current modeling of track systems. The continuous improvement of components and track design depends on fine-scale optimization of models, prevailing assumptions, and gaining additional understanding into the underlying mechanical processes that the track system undergoes during loading as trains pass over. For example, the current structural models used for concrete crosstie flexural analysis and design assume that the ballast bearing support is static and consistently located in a specific region under the crosstie. This assumption implies a linear behavior of the wheel-load bending moment relationship. However, field and laboratory data show that this relationship is actually non-linear and the difference between measured behavior and prevailing assumptions is significant. Previous work has shown that the interaction of the crosstie's deflected shape with the supporting ballast layer has the potential to modify the support distribution of the crosstie as load increases. To better understand the observed phenomenon and its implications, a generalized structural analysis model was developed along with an analytical model with the objective of explaining support redistribution under loading based on mechanics principles. The results show that the proposed algorithm explain the observed field data well and establishes a foundation for further analysis of this previously unquantified effect. The model I developed can serve as an initial structural analysis tool for the development of a mechanistic-empirical prestressed concrete crosstie design procedure.

ACKNOWLEDGMENTS

Over my academic and professional life, multiple people have provided invaluable aid, guidance, support, and mentorship. Without them, I would not be in the position to develop the present work, nor be the person I am today. I would like to express my sincere gratitude to every single one of them.

This work is first and foremost dedicated to my family. I am thankful to live in an era where technology can make me feel like home when needed. Even with thousands of kilometers between us, I always feel their continuous support. Thanks for my parents for always pushing me to pursue my ambitions, teaching me what's important in life, and providing both the education and environment necessary to thrive and fulfill my potential. Thanks to my brother for being the rock I can rely on in every subject and being my accomplice for the past two years.

My eternal gratitude to the RailTEC Infrastructure research management team. For their guidance and mentorship on the past two years, for pushing us out of our comfort zone and most importantly, for trusting and valuing our opinions. In many areas, I am a different person compared to the student who started this program, and they have played a key role in that. Thanks to Riley Edwards, Marcus Dersch, and Arthur Lima for their continuous support and trust in the help I could provide in different areas and projects. To Prof. Barkan for leading such a brilliant team in RailTEC and for his genuine interest in the personal well-being and growth of its members. To the RailTEC program coordination team for their help and assistance when needed. To the National University Rail Center for the amazing support in the development and growth of railroad education in the United States. Special thanks to Amtrak, for providing the funding necessary for the completion of my degree and especially to Steven Melniczuk for coordinating and guiding the project.

To my day-to-day family here at Illinois, fellow B118 students, where we shared not only a sometimes-messy workspace but also great memories that will always live with me. It was comforting and convenient to have people so close to throw ideas into the air, learn about different cultures, or planning a trip for brunch or dinner. I would like to single out specific members of the team such as Josue Cesar Bastos, Nao Nishio, Jake Branson, Tom Roadcap, Álvaro Canga, and Yubing Liang with whom I shared most of my time here and made every day a wonderful experience.

*Quiero vivir la vida aventurera
de los errantes pájaros marinos;
no tener, para ir a otra ribera,
la prosaica visión de los caminos.*

*Poder volar cuando la tarde muera
entre fugaces lampos ambarinos
y oponer a los raudos torbellinos
el ala fuerte y la mirada fiera.*

*Huir de todo lo que sea humano;
embriagarme de azul... Ser soberano
de dos inmensidades: mar y cielo,
y cuando sienta el corazón cansado
morir sobre un peñón abandonado
con las alas abiertas para el vuelo.*

“Vuelo Supremo” Julián Marchena Valle-Riestra

TABLE OF CONTENTS

| | |
|--|-----|
| CHAPTER 1: INTRODUCTION..... | 1 |
| CHAPTER 2: FIELD INSTRUMENTATION OF PRESTRESSED CONCRETE CROSSTIES FOR LOADING ENVIRONMENT QUANTIFICATION | 9 |
| CHAPTER 3: ANALYTICAL MODELING OF CROSSTIE BALLAST SUPPORT..... | 35 |
| CHAPTER 4: EFFECT OF WHEEL LOAD ON SUPPORT CONDITION DEFINITION | 57 |
| CHAPTER 5: SENSITIVITY OF REDISTRIBUTION MODEL AND EFFECTS OF TEMPERATURE ON SUPPORT CONDITION DEFINITION | 73 |
| CHAPTER 6: RECOMMENDATIONS AND FUTURE WORK..... | 90 |
| REFERENCES | 102 |

CHAPTER 1: INTRODUCTION

1.1 Introduction

The railway track structure is a system of components (Figure 1.1) expected to function together as a single unit. A primary function of the track structure is to support and distribute wheel loads from the rail vehicles to the subgrade (Hay, 1982; Kerr, 2003). The increase in bearing area in each of the track-system interfaces reduces the high pressures at the wheel-rail interface to levels that the subgrade can support. In the case of ballasted track, the interfaces of this system include:

- Wheel-Rail interface
- Rail-Crosstie interface
- Crosstie-Ballast interface
- Ballast-Subgrade interface

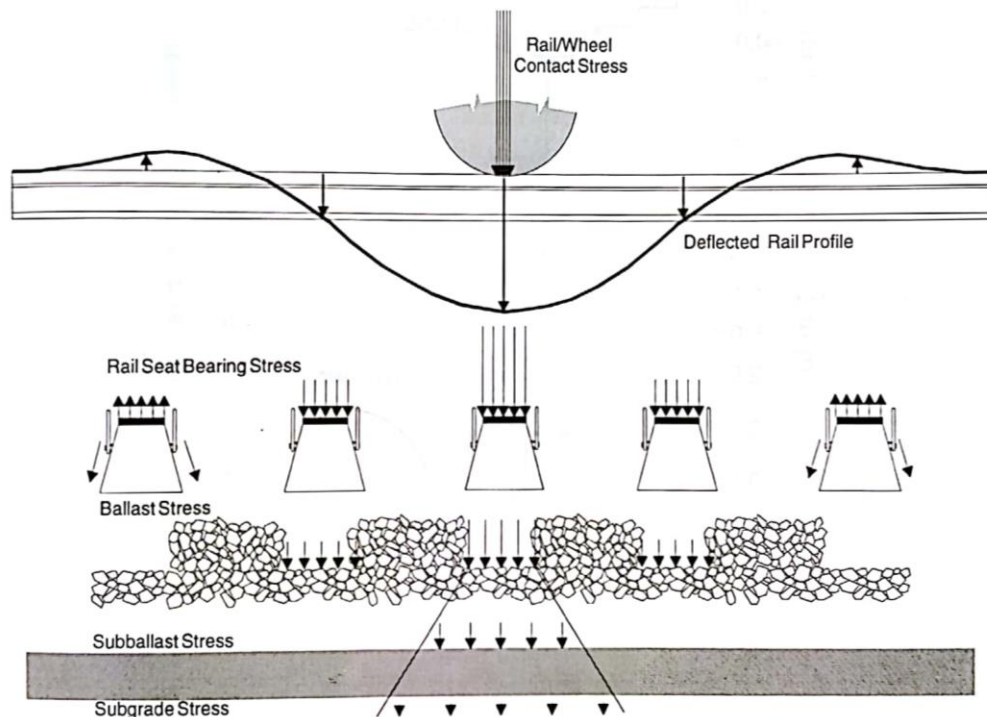


Figure 1.1: Typical wheel load distribution on track structure (Selig and Waters, 1994)

The wheel-rail interface is a sophisticated and well-researched area that gained greater attention with the study of elastic (or Hertzian) contact (Hertz, 1881) and continued with the mathematical developments of axle hunting behavior by Klingel (1883), Boedecker (1887), and Carter (1916) in the late 19th and early 20th centuries. Since then, problems of fatigue, wear, noise, vibration, adhesion, impact loads, and stability have been studied with increasing levels of sophistication through the use of computational analysis. This research and depth of understanding has led to the development of improved materials and manufacturing techniques that have had a significant impact on the life cycles of the wheel and rail (Knothe, 2008; Lewis and Olofsson, 2009).

Today, the rail-crosstie interface includes the load transfer between rail to the crosstie via a tie plate or rail pad. The loading environment of this interface has been analyzed using the theory of a continuously supported beam, an analytical method initially proposed by Winkler (1867), solved by Zimmerman (1941), and more recently documented by Kerr (2003). Experimentation at this interface was conducted by Talbot (1918), who measured pressures at the bottom of the rail as a part of a broader experimental program. More recent research has focused on the measurement of pressures with matrix-based tactile surface sensors (MBTSS) for both timber (Rose and Stith, 2004) and concrete (Rapp et al., 2012; Greve, 2015) crossties.

Difficulties in executing successful experimental research at the crosstie-ballast interface has limited the amount of research focused on this area of the track structure. The first North American efforts to quantify the characteristics of the interface were performed by Talbot (1919) who identified two problems: 1) the unloaded crosstie may not touch the ballast at all points and 2) the ballast may have different compaction levels along the length of the crosstie. These uncertainties increased the variability of measurements to a point where Talbot developed a

series of hypothetical support distributions (Figure 1.2). Based on this work, several authors introduced different models focused on either analysis (Clarke, 1957; Schramm, 1961; Cope, 1993) or design (Council of Standards Australia, 2003; UIC, 2004; AREMA, 2017a). Experimentation with load cells facilitated quantification of the pressures at the crosstie-to-ballast interface (Prause et al., 1977), with a known limitation that the instrumentation itself could potentially alter the results due to the installation process (i.e., the observer effect). Recent experimentation involves the use of less intrusive methods for pressure instrumentation (Sadeghi, 2008; McHenry et al., 2015; Gao et al., 2017a; Song et al., 2017). Current research efforts on the interface are oriented towards the development of under tie pads (UTP). However, this line of research is focused on aspects other than the flexural response of crossties, primarily focusing on topics related to the material characterization, train-track interaction (Johansson et al., 2008), track geometry (Schneider et al., 2011), reduction of vibrations and noise (Thompson, 2008), and the effects of pressure on the ballast particles (Gräbe et al., 2016).

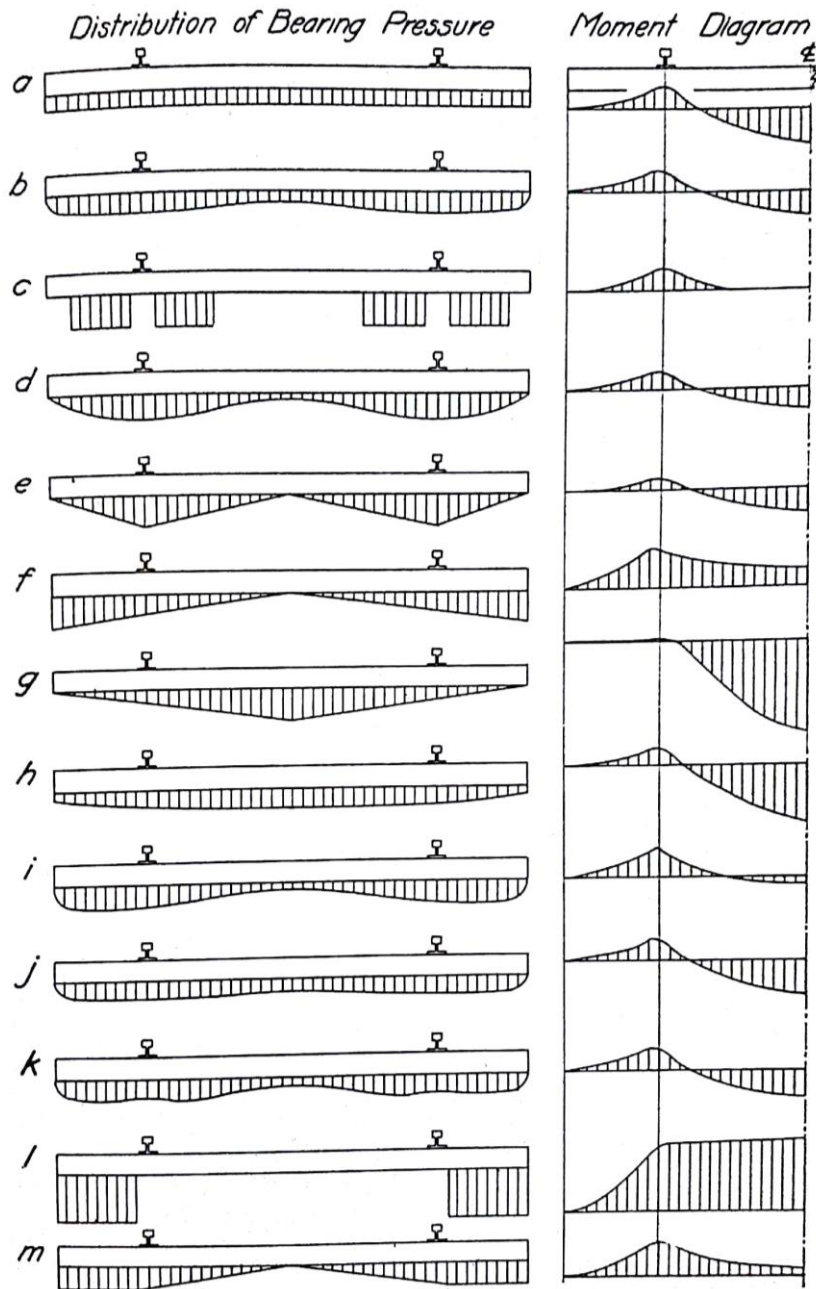


Figure 1.2: Hypothetical cross-tie support conditions (Talbot, 1919)

Finally, the ballast-subgrade interface has been subject to extensive research from a geotechnical engineering standpoint. The primary objective of this interface is to reduce the vertical pressures applied to the subgrade to a level that is below what the existing soil can withstand without excessive deformation and failure. General-purpose geotechnical models can

be used for modeling the load distribution through the ballast and subballast layers, including Boussinesq's (1885). Talbot's (1919) equation became the standard method for determining ballast pressure levels and minimum required ballast depths. Over the years, researchers and design standards have proposed alternative equations for this purpose, either based on experimental or analytical work (Clarke, 1957; Heath et al., 1972; Raymond, 1978; Li and Selig, 1998). Recently, numerical modeling based on the Discrete Element Modeling (DEM) technique has proven to be a viable way to characterize the pressure and distribution of loads in this particular interface (Tutumluer et al., 2007, 2009, 2011; Hou et al., 2018). Currently, research efforts focused on this interface also include the use of under ballast mats as a way to minimize vibrations, increase resiliency on transition zones, and reduce pressure to the subgrade (Hanson and Singleton, 2006; Lima, 2017).

1.2 Crosstie-ballast interaction importance

Talbot (1919) observed that “a light change in the distribution of the intensity of bearing pressure along the tie makes a relatively large change in the amount and distribution of the bending moments.” This interaction is particularly crucial for the case of concrete crossties, where the high stiffness and low resiliency of the material can generate cracking. In North America, the problem of crosstie cracking has been recognized as one of the most critical issues for the use of concrete crossties (Zeman, 2010; Van Dyk, 2015). At the same time, multiple authors have demonstrated the importance of maintaining adequate support conditions for concrete crossties, either by theoretical, experimental, or computational methods (Giannakos, 2010; Yu et al., 2017; Bastos et al., 2017).

Adequate characterization of this interface has the potential of yielding two valuable outcomes for the rail industry: 1) analytical models that correctly quantify and predict the flexural demand over the life-cycle of the component, 2) innovative designs or novel materials that could reduce the flexural demand on optimized components. In this work I aim to provide data that will be useful for the development of both objectives. The quantification of field-measured support conditions and analysis of potential factors contributing to the variability of the measurements could provide the necessary information for the development of more refined and complex analysis models. At the same time, this work offers arguments that could lead to a deeper understanding of the factors involved in the support condition estimation problem, and therefore may serve as valuable background for the development of new crosstie designs.

1.3 Objectives

The primary objectives of this research are to:

- Quantify the ballast support distribution of prestressed concrete crossties based on existing strain data gathered in the field under revenue service train operation.
- Develop a parametric analytical model that can evaluate potential sources of variability for concrete crosstie ballast support.
- Investigate the observed effects of wheel load and temperature differentials in the variability of concrete crosstie support conditions.
- Assess the potential implications of the variability of concrete crosstie support for future crosstie designs and the development of design standards.

1.4 Thesis Outline

This thesis is divided into six chapters including this introduction. The following paragraphs provide a brief description of the overall scope of each chapter.

In Chapter 2 I provide the results and analysis of the field instrumentation deployed on a shared heavy axle load (HAL) and higher-speed passenger rail corridor in the United States. The results presented include the distribution of wheel loads, flexural bending moments and the estimated support conditions of the field site. The chapter also provides a discussion on the potential variability of the measured bending moments due to possible changes in the support condition on sections of non-instrumented track.

In Chapter 3 I provide historical background on the problem of characterizing the crosstie support distribution. The different analysis models included in North American and international design standards that represent the state of the practice are presented in this chapter. Finally, the chapter includes the development of a parametric structural analysis model that can be used for the evaluation of the flexural response of crossties due to a wide range of potential support conditions.

In Chapter 4 I explain the limitations of the existing crosstie support condition analysis models when compared to field data. The chapter describes the observed non-linearity of the wheel load-bending moment relationship seen in field data. I present an innovative hypothetical ballast-crosstie interaction model that describes the aforementioned behavior. Using an adapted numerical back-calculator, I demonstrate that the support condition of the crosstie is dependent on the deflection of the component.

In Chapter 5 I present findings regarding the effect of temperature on the variability of support redistribution. The use of the numerical back-calculator and a filtered dataset facilitates

quantification of changes in the support condition of the component due to the thermal curling of the crosstie. This provides an explanation for the previously-observed effect of temperature gradients on the flexural response of crossties.

In Chapter 6 I summarize the findings presented in my thesis, provide recommendations stemming from the results, and offer ideas for future research.

CHAPTER 2: FIELD INSTRUMENTATION OF PRESTRESSED CONCRETE CROSSTIES FOR LOADING ENVIRONMENT QUANTIFICATION¹

2.1 Introduction and background

Field flexural bending moment demand data in concrete crossties provided the starting dataset used for the identification of sources of variability and relationships between loading characteristics and crosstie response. The overall objective of the field experimentation was to quantify the loading demands placed on individual crossties under a variety of operational conditions. Using analytical tools, the flexural demand could be used to back-calculate support characteristics and identify trends not readily apparent in the directly captured data.

Revenue service field experimentation was performed as part of a project funded by the National Railroad Passenger Corporation (Amtrak) aimed at the improvement of both the design of their concrete crosstie and the overall track structure (e.g. ballast depth). Wheel load and flexural field data representative of the operating conditions found on Amtrak's Northeast Corridor (NEC) were gathered, processed, and analyzed to establish a baseline for how the existing concrete crosstie design performs in the field. Information obtained from the analysis of these data provided answers to critical questions about the design and performance of both the track substructure and the concrete crossties.

Prior to this study, the University of Illinois at Urbana-Champaign (UIUC) gathered field data to better understand the loading environment and improve design methodologies on heavy axle load (HAL) freight, intercity passenger, and rail transit systems (Van Dyk et al., 2013; Edwards et al., 2017a). These efforts were accomplished, in part, through the analysis of data

¹ Much of Chapter 2 was submitted and published in the 2018 Transportation Research Record (TRR): Journal of the Transportation Research Board (TRB) (Quirós-Orozco et al., 2018)

from wayside inspection systems used for monitoring the performance of rolling stock such as the Wheel Impact Load Detector (WILD). On a component level, surface strain gauge instrumentation has been used to quantify flexural demands on concrete crossties (Van Dyk, 2015; Edwards et al., 2017b). In the case of the NEC, field instrumentation dates back to 1983 where one of the first WILD sites was deployed to investigate the causes of transverse rail seat cracks in concrete crossties (Harrison and Tuten, 1984). The use of both WILD sites and instrumented crossties facilitates comprehensive characterization of the demand to which the track and its components are subjected. These data, when evaluated in conjunction with supporting experimental laboratory data, facilitate the evaluation of the efficiency of a particular design with respect to the actual field loading demands.

2.2 Field site location

Amtrak's NEC is the most densely traveled rail corridor in the United States, with almost 11.7 million annual passengers traveling on Amtrak trains and another 250 million annual commuter rail passengers distributed among eight operators (Amtrak, 2012). Additionally, the corridor is also traversed by approximately 50 freight trains per day operated by two Class 1 freight railroads (Amtrak, 2012). As such, the corridor's infrastructure experiences a variety of loading conditions ranging from HAL freight operations to high-speed passenger train services. Historically, the track structure and components such as crossties have been designed through a process based mostly on practical experience (Van Dyk, 2015) or assumed simplistic static loading cases. Optimization of track components for highly variable loads and speed requires an in-depth understanding of the effect of each service.

2.3 Overview of field instrumentation

Field experimental data are divided into two categories, based on their type and source; 1) WILD sites and 2) UIUC's instrumented crossties. The former corresponds to data provided by Amtrak for three different sites along the NEC. These data are processed and tabulated by the WILD system manufacturer and include information related to vehicle speed, peak loads, number of axles per train, and railcar identity. The second source of data is a field site deployed by UIUC in Edgewood, MD with concrete surface strain gauges. This site provides information related to the flexural bending moment of the concrete crossties and offers secondary data regarding the field site's crosstie support conditions.

2.3.1 *Wheel Impact Load Detector*

A WILD is an electronic data collection device designed to measure and isolate vertical and lateral wheel forces using either rail mounted strain gauges or accelerometers (Barke and Chiu, 2005; LB Foster Salient Systems, 2015). While its primary objective is to evaluate the performance of the rolling stock and measure the impact forces caused by out-of-round or otherwise damaged wheels (Harrison et al., 2006; Barke and Chiu, 2005), WILD systems have also proven to be a practical mechanism for producing static wheel load approximations that can serve rail infrastructure researchers and practitioners (Van Dyk et al., 2014; Van Dyk, 2015; Edwards et al., 2018a). Specifically, static wheel load values are a critical input into the determination of impact factors. To obtain an estimate of static wheel load from the dynamic revenue service operating environment, WILD sites use an algorithm to back-calculate static load based on values of dynamic load from multiple instrumented cribs and knowledge of the railcar's speed. WILD-estimated static loads tend to be higher than the "true"

static load for a given vehicle. These differences can be attributed to 1) the inherent variability in measuring dynamic wheel loads in the field environment and 2) inaccuracies in the algorithm that back-calculates static loading.

A common strain-gauge-based WILD site is 15 meters (50 feet) in length, with a series of strain gauges micro-welded to the neutral axis of the rail web. They quantify the wheel load by either a direct mathematical or a calibrated relationship between strain and force (Barke and Chiu, 2005). Instrumentation is divided into several ballast cribs at various intervals to capture a single wheel's rotation up to five times, recording peak impact and average forces at a data collection rate of up to 30 kHz (Harrison and Tuten, 1984; Canadian National, 2011). Electronic signal processors housed in a wayside enclosure analyze the data using an algorithm that isolates wheel tread irregularities and computes both static and peak load values (Stratman et al., 2007). Rail infrastructure owners commonly define loading thresholds according to their operational procedures that facilitate the delivery of alerts when limits are exceeded (LB Foster Salient Systems, 2015).

Amtrak provided access to WILD data for three different locations on the NEC: Edgewood, Maryland, Marcus Hook, Pennsylvania, and Mansfield, Massachusetts (Figure 2.1). Amtrak operates intercity trains at all locations using Viewliner, Amfleet, and ACELA rolling stock. Each of the sites has different commuter rail and HAL freight operators (Table 2.1).



Figure 2.1: Location of WILD sites used for analysis

Table 2.1: Commuter and HAL operators on each WILD site location

| Site | Commuter Operator | HAL Operator |
|------------------------|---|------------------------------|
| Edgewood, MD | Maryland Area Regional Commuter (MARC) | Norfolk Southern Corporation |
| Marcus Hook, PA | Southeastern Pennsylvania Transportation Authority (SEPTA) | Norfolk Southern Corporation |
| Mansfield, MA | Massachusetts Bay Transportation Authority (MBTA) | CSX Transportation |

2.3.2 Concrete cross-tie surface strain gauges

Researchers in the Rail Transportation and Engineering Center (RailTEC) at UIUC have previously used surface mounted strain gauges to measure bending moments experienced by

concrete crossties under revenue service HAL freight trains (Wolf, 2015) and in rail transit applications (Edwards et al., 2018b). In the case of Amtrak's NEC, temporary instrumentation of concrete crossties was performed in 1983 to identify causes of premature cracks (Harrison and Tuten, 1984) and again in 2014 to investigate a later generation of crosstie design and performance questions (Mayville et al., 2014).

The field site comprised seven instrumented crossties and related electronic equipment (Figure 2.2). The crossties were located on Track 2, which primarily handles northbound traffic. Four crossties were instrumented with three strain gauges: two at the rail seats and one in the center of the crosstie. A fifth crosstie was instrumented with two additional strain gauges located halfway between each rail seat and center. Finally, two adjacent crossties were instrumented with a single strain gauge at the center to record additional bending data given the critical nature of this design region. Independent of strain gauge instrumentation, three thermocouples were deployed to capture ambient temperature, and the temperature at the top, and bottom of the crosstie. The strain gauges enabled quantification of bending strains at discrete locations along the length of the crosstie due to train loading and were oriented longitudinally along the chamfer near the top surface of the crosstie. Collection of data using the aforementioned instrumentation is automatically initiated through the use of a laser trigger oriented transversally to the track direction that continuously monitored the presence of trains over the site.

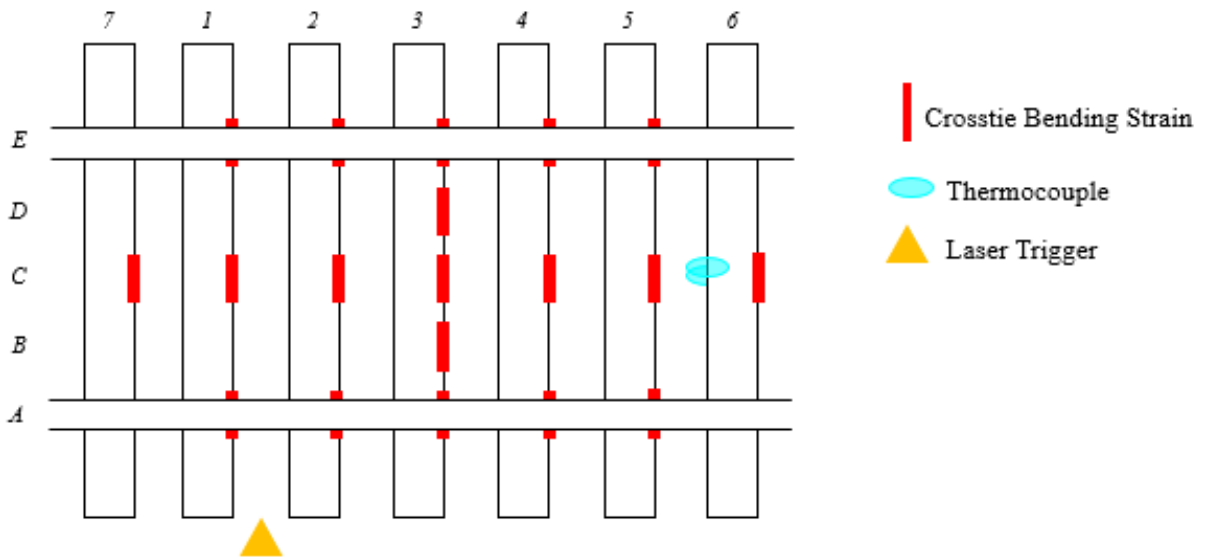


Figure 2.2: Plan view of instrumented crosstie section on Amtrak's NEC in Edgewood, MD

Concrete crosstie calibration factors determined in the laboratory were used to relate the measured strains to a known bending moment, using a process described by Edwards et al. (2017b). In summary, these parameters were found by instrumenting several crossties of the same design and vintage as those installed in track using the same strain gauge layout as in the field. A calibrated load was applied to each crosstie at their rail seats in a configuration adapted from the design validation tests presented in Chapter 30, Section 4.9 of the American Railway Engineering and Maintenance-of-way Association (AREMA) Manual for Railway Engineering (MRE) (AREMA, 2017a).

2.4 Data Analysis

2.4.1 Traffic Breakdown

For the six months of data collection, a total of 54,156 trains were analyzed, which represents 2,210,687 axles and 36.6 million gross tons (MGT) of traffic. While the Marcus

Hook, PA site had the highest amount of traffic in terms of absolute train count, the Edgewood, MD site had a higher number of axles and tonnage due to the larger volume of freight traffic (Figure 2.3). Both the Marcus Hook, PA and Mansfield, MA sites had a larger percentage of commuter trains and limited HAL freight operations (Figure 2.4).

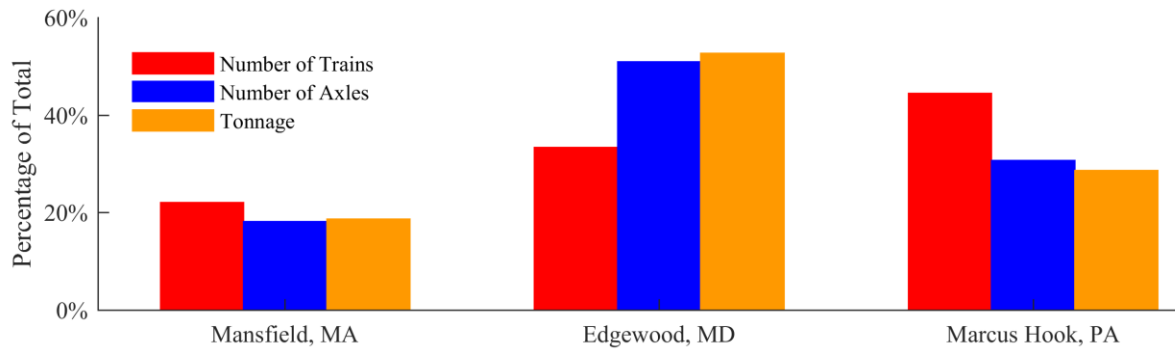


Figure 2.3: Distribution of traffic metrics by instrumentation site

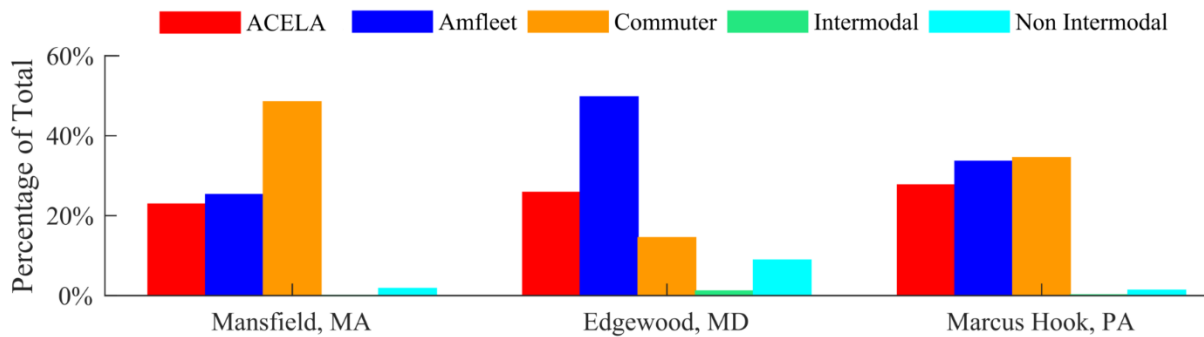


Figure 2.4: Distribution of services by instrumented site

The effect of freight railroad operations on the NEC is evident given that only 6% of total freight train movements accounted for 30% of the total tonnage (Figure 2.5). This value is similar to the total tonnage of the Amtrak operations. The “Other” category includes information obtained from trains with malfunctioning equipment identification (AEI) tags.

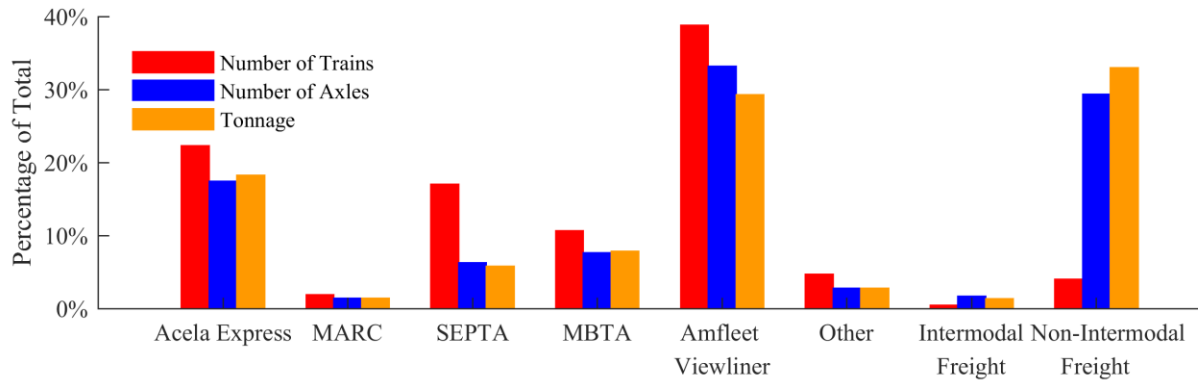


Figure 2.5: Distribution of traffic metrics by operator and service type

2.5 Static and Dynamic loads analysis

Data provided by the WILD sites include detailed static and peak vertical loads for each axle. In the case of static loads (Figure 2.6), the substantial difference between loaded and probably empty freight cars is evident in the data, especially for non-intermodal traffic.

Intermodal traffic, due to the varying nature of their payloads and differing car configurations, shows a more gradual change. For passenger trains, the differences between passenger cars and power units are evident. Most passenger coaches have similar weight, but there are substantial differences in the weights of their power units, with MBTA having the heaviest locomotives, followed by MARC, and finally Amtrak. SEPTA data show a different behavior as they operate electric multiple unit cars with more or less uniform weight on their axles. The highest recorded wheel load in the aforementioned time period was 51.2 kips from a non-intermodal freight car.

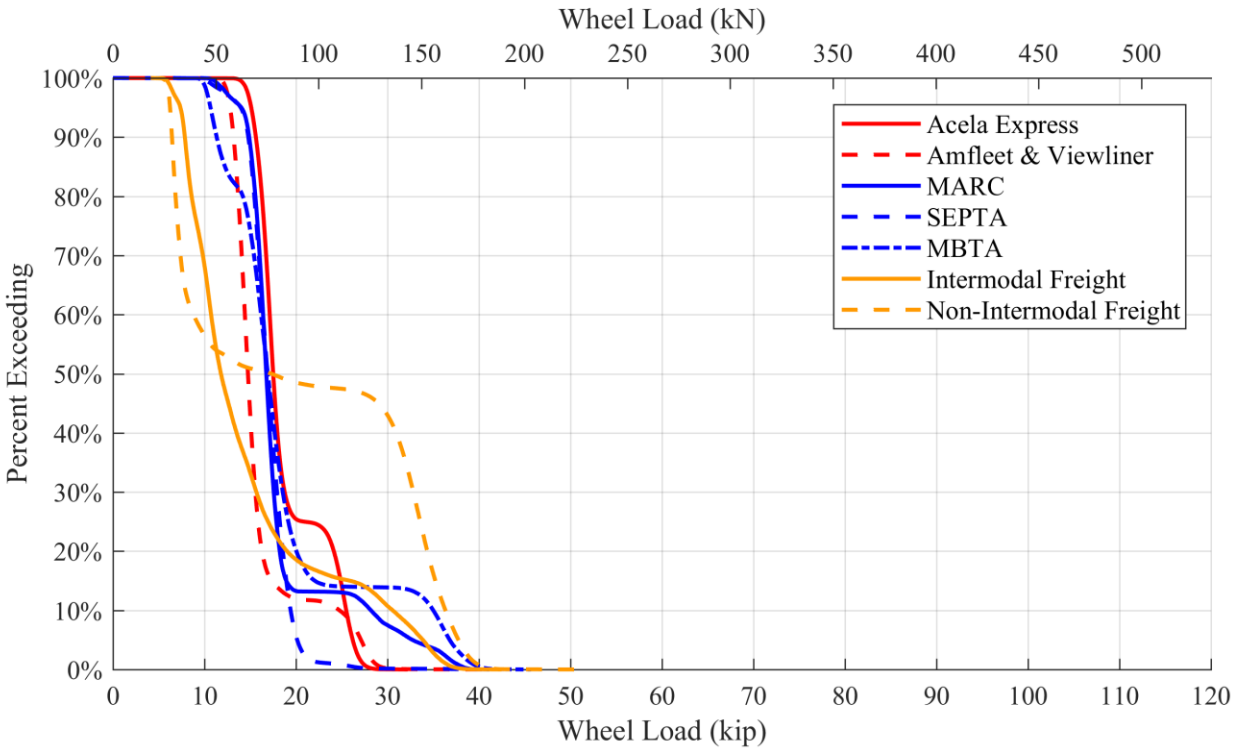


Figure 2.6: Static wheel load distribution by operator and vehicle type

Dynamic and impact effects increase the aforementioned static values. These peak loads (Figure 2.7) displayed greater variability, especially for the top 10% of the wheel load levels. Maximum wheel load peak values ranged as high as 122 kips for a non-intermodal vehicle. The differences between unloaded and loaded cars in freight operation were visible but less noticeable. This indicates that unloaded cars had a higher probability of generating larger impact factors than loaded cars, which was also noted by Van Dyk et al. (2017). Passenger cars that shared similar static load distributions displayed higher variability, indicating a substantial difference in the magnitude of impact factors for different operators. MBTA passenger cars had, on average, higher impact factors. The magnitude of these values put MBTA rolling stock at approximately the same magnitude of peak loads as those of non-intermodal freight trains.

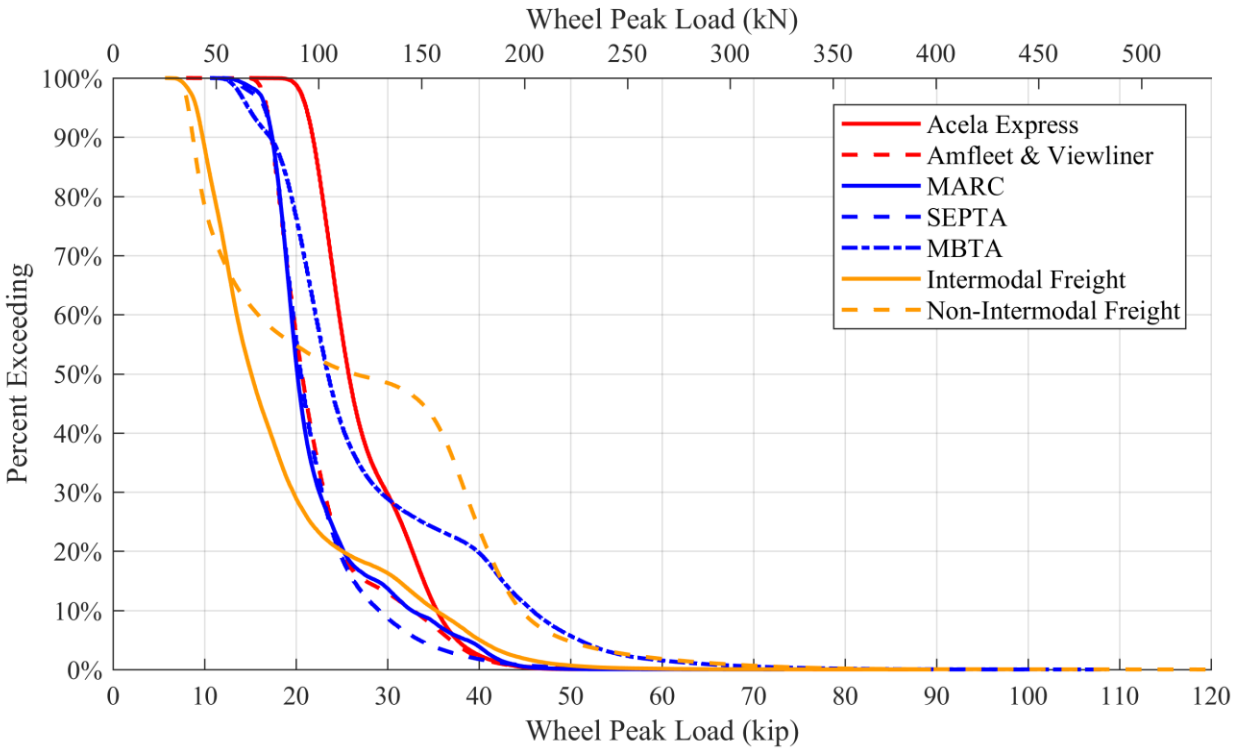


Figure 2.7: Peak load distribution by operator and vehicle type

2.6 Impact factor analysis

The aforementioned increase in peak loads compared to the static values is quantified as the impact factor, or ratio between peak and static loads. The current AREMA current recommended design procedure for concrete cross-ties defines the impact factor as the additional load over static values and proposes a value of 200% (AREMA, 2017a). In terms of the ratio between peak and static values, this translates to an impact factor of three. The relationship between peak and static loads for all train and operator categories was plotted (Figure 2.8). Each data point represents an individual wheel for each of the train and operator categories shown. Lines represent the different impact factor thresholds, all points under each line fall below the respective threshold. Also indicated is the percentage of wheels falling below each of the impact factor thresholds. Specific types of rolling stock can be identified by the corresponding different

color and concentration of data points. Differences between locomotives and passenger cars are evident for the passenger trains. Non-intermodal freight shows a substantial change in behavior between empty and loaded cars, with the former presenting substantially higher impact factors than the latter. Since empty or lightly loaded freight cars have a low static load, they caused relatively low dynamic loads compared to loaded cars even when their impact factors exceeded the recommended values.

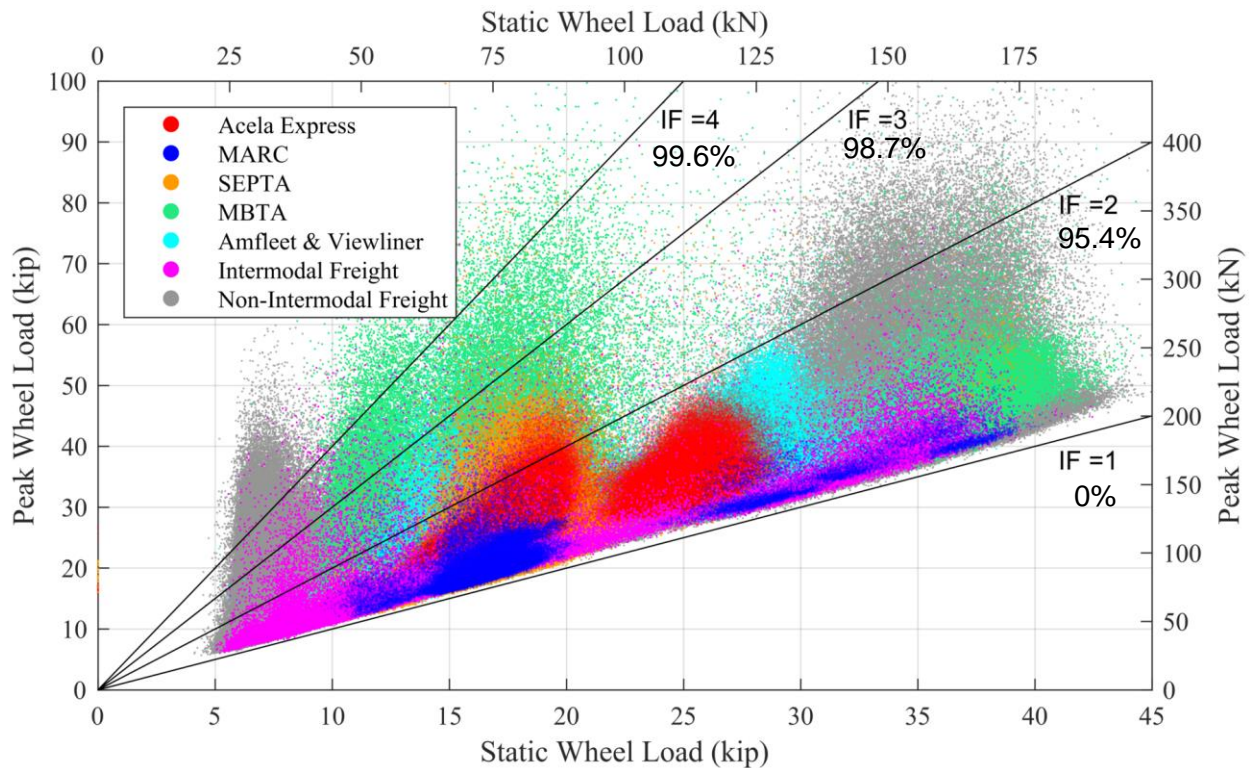


Figure 2.8: Relationship between static and peak wheel loads by vehicle classification

98.7% of all the wheels captured were below the impact load factor = 3. The majority of events above this line were probably due to empty freight cars with low static loads and therefore, low-magnitude impact forces. These can be identified when isolating wheels with an impact factor > 3 (Table 2.2). Average peak loads in these cases (non-intermodal freight vehicles) were relatively low compared to other vehicle types, indicating that most of these

exceptions were probably empty freight cars. For passenger trains the average peak wheel loads with an impact factor of three are similar, with the exception of Acela trainsets. More stringent wheelset maintenance requirements of these higher-speed trainsets can explain the low peak values.

Table 2.2: Distribution of exceptional Impact Factors (IF) by operator and rolling stock type

| Vehicle | Wheels with IF>3 (%) | Average peak load with IF>3 (kips) | Maximum peak load with IF>3 (kips) |
|--------------------------|--------------------------------|--|--|
| Acela | 0.0059 | 30.6 | 88.8 |
| MARC | 0.059 | 48.6 | 60.9 |
| SEPTA | 0.18 | 55.0 | 99.6 |
| MBTA | 4.1 | 52.1 | 108.5 |
| Amfleet-Viewliner | 0.031 | 50.9 | 90.1 |
| Intermodal | 0.95 | 36.4 | 89.4 |
| Non-Intermodal | 3.1 | 27.7 | 122.0 |

The proportion and distribution of wheels exceeding impact factor = 3 varied by operator (Figure 2.9). Amtrak, MARC, and SEPTA passenger trains generally had a low occurrence of wheels exceeding the aforementioned threshold while MBTA had the highest number of wheels that exceed the threshold. The difference between MBTA and other passenger operators was approximately two orders of magnitude, even surpassing those of non-intermodal freight trains. For passenger trains, the data also enable identification of locomotives, powered rail cars, and passenger cars. In all cases, the higher estimated static wheel loads correspond to locomotives (or power cars in the case of ACELA rolling stock.) The method of determining estimating static wheel loads and differences between estimated static wheel loads and known static loads is discussed in Section 2.3.1.

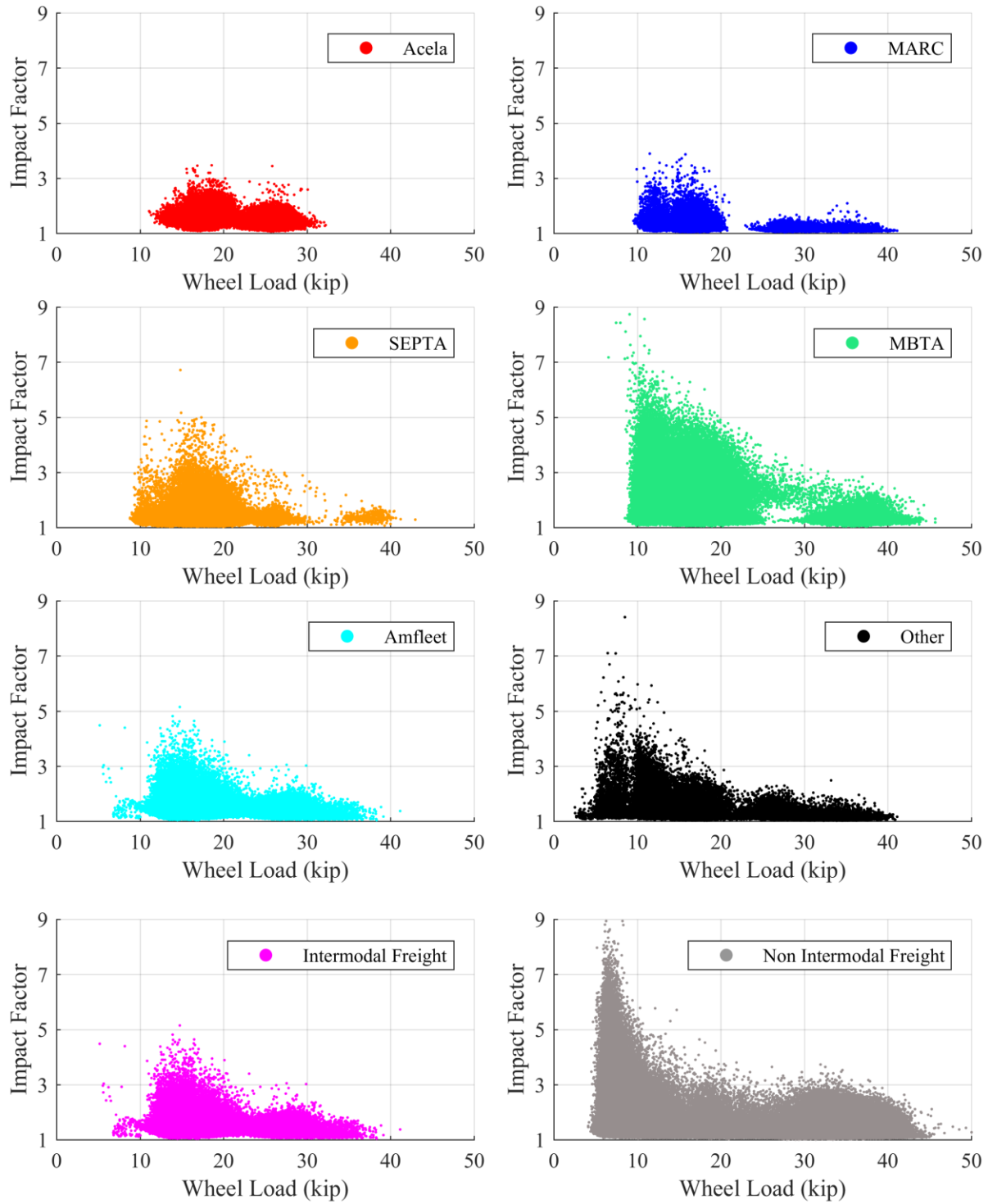


Figure 2.9: Distribution of wheel impact factors by train, operator type, and static² load

² See explanation in text of how static load is recorded by WILDs

2.7 Flexural bending moments on concrete crossties

2.7.1 Flexural bending moment results

The UIUC field site on Amtrak’s NEC in Edgewood, MD was operational for four distinct periods from 14 December 2016 until 10 May 2017 (Table 2.3). Each train recorded passing over the site was related to the respective WILD database entry in order to relate vehicle classification and wheel loads to their respective bending moments. This mapping also allowed me to validate the data collected for any potential failures of instrumentation. The recorded bending moments represent 4.5 out of the 7.6 MGT total traffic on the line during the aforementioned time period.

Table 2.3: Data collection periods for instrumented crossties

| Operation Period | Days | Trains Recorded |
|--------------------------------|-------------|------------------------|
| 14 Dec 2016-26 Jan 2017 | 44 | 1,769 |
| 22 Feb -26 Feb 2017 | 4 | 229 |
| 13 Mar-6 Apr 2017 | 25 | 1,081 |
| 7 Apr-10 May 2017 | 34 | 1,727 |
| Total | 107 | 4,806 |

Data filtering and processing techniques were used to identify peak data. The most common noise encountered when using strain gauges is related to typical alternate current (AC) interference at a frequency of 60 Hz (National Instruments, 2012). However, due to the presence of the electrified catenary of Amtrak’s NEC operating at 12 kV 25 Hz (Fisher, 1990), interference in the strain gauge signal was identified at 25 Hz through visual analysis of the frequency spectrum. Filtering techniques based on the Chebyshev Type II band stop filter were used to remove the interference at the 25 Hz frequency and its harmonics.

Each dataset was compared to its respective WILD site data to obtain a classification of the rolling stock, quantify the number of axles and speed, and refine the processing algorithms. Percent exceeding graphs were prepared for the distribution of center bending moments (Figure 2.10). The maximum recorded center negative bending moment is 150 kip-in. This bending moment was induced by a non-intermodal freight train axle, and it was also found to map to a high impact load. Other than this maximum observation, the data show little variability among different types of rolling stock. This indicates low sensitivity of bending moments to load increases, a condition commonly associated with crossties that have adequate support under the rail seats (Gao et al., 2017a).

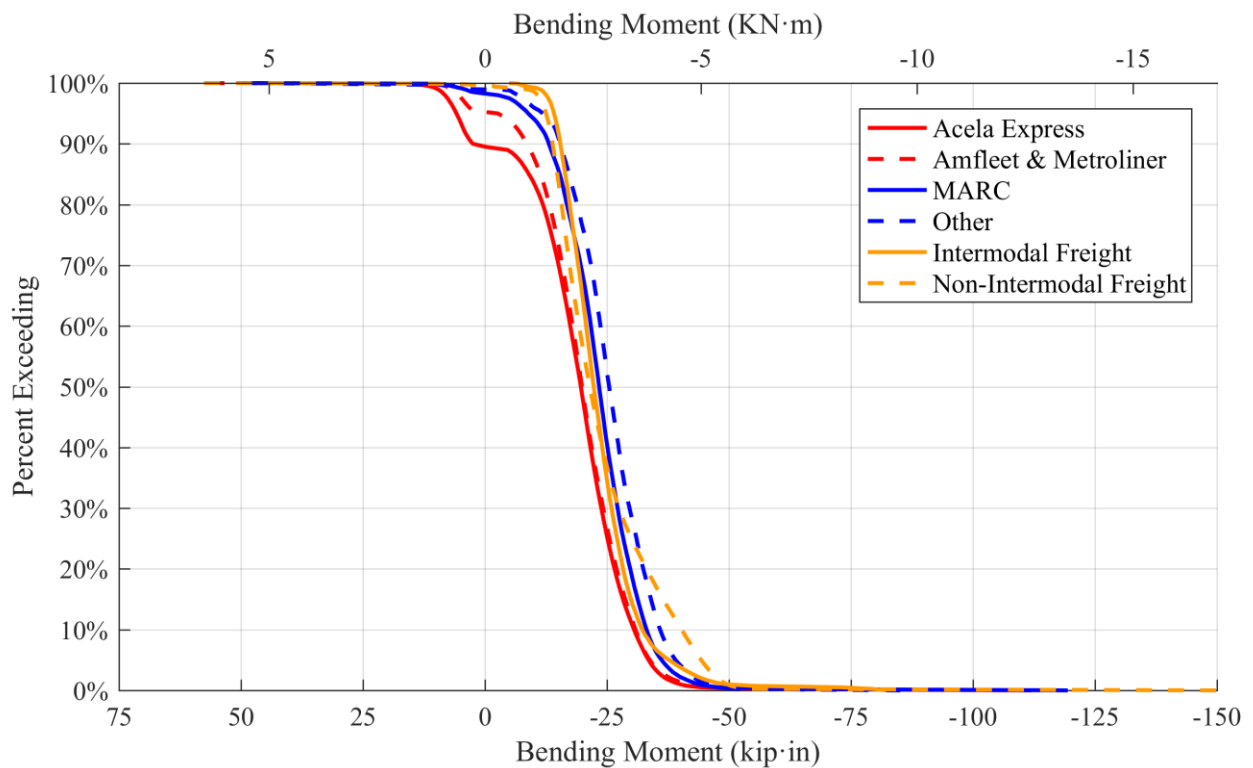


Figure 2.10: Flexural bending moments on the center crosstie region by train type

These values did not reach the specified flexural capacity of the crossties which was defined as 208 kip-in for the center region in negative bending (Amtrak, 2003). Center positive

bending moments were likely related to temperature curling effects and associated changes in support condition as well as relatively low magnitude vertical loads (Wolf et al., 2016).

Percent exceeding curves were prepared for the rail seat section of the crosstie by train type (Figure 2.11). The maximum recorded center negative bending moment was 275 kip-in. The data show increased variability between different types of rolling stock when compared with the center of the crosstie. The distribution of bending moments resembles the distribution of peak loads (Figure 2.7), which implies that the rail seat is more sensitive to wheel load increases. This behavior also aligned with the expected results for a crosstie with adequate support under the rail seat (Gao et al., 2017a). These values did not reach the specified flexural capacity of the crossties which were defined as 306 kip-in for the rail seat region in positive bending (Amtrak, 2003).

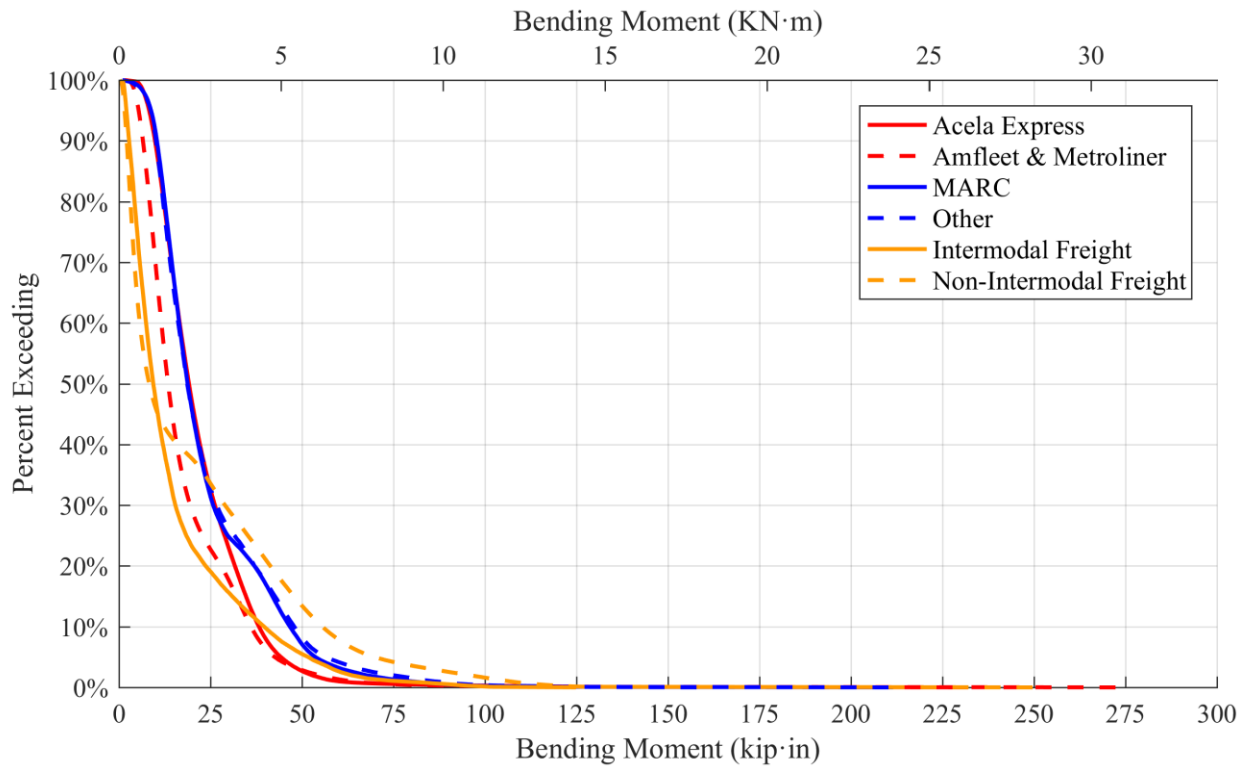


Figure 2.11: Flexural bending moments of prestressed concrete ties on rail seat region by train type

Detailed analysis of the top ten percent of bending moments (Table 2.4) provided the most likely range of design values that could be used for future track components. There was a substantial increase in the values from both center and rail seat bending from the 99.5% to 100% (maximum) percentiles. These loads and moments represent extreme scenarios that might define limit state cases for the design of crossties.

Table 2.4: Top ten percentile of peak wheel load and bending moment data by car classification for the Edgewood, MD field site

| Classification | Measured Data | 90% | 95% | 98% | 99% | 99.5% | 100% |
|-------------------------------|----------------------|------------|------------|------------|------------|--------------|-------------|
| Acela | Wheel Load (kips) | 33.9 | 35.2 | 36.2 | 37.5 | 38.6 | 50.5 |
| | C- Moments (kip-in) | -31 | -34 | -36 | -40 | -44 | -111 |
| | RS+ Moments (kip-in) | 38 | 44 | 51 | 60 | 80 | 232 |
| MARC | Wheel Load (kips) | 31.9 | 38.5 | 41.1 | 43.3 | 44.9 | 57.4 |
| | C- Moments (kip-in) | -33 | -36 | -39 | -44 | -48 | -119 |
| | RS+ Moments (kip-in) | 47 | 54 | 64 | 80 | 90 | 211 |
| Amfleet and Viewliner | Wheel Load (kips) | 35.4 | 39.2 | 41.3 | 43.4 | 45.2 | 68.8 |
| | C- Moments (kip-in) | -31 | -34 | -37 | -42 | -50 | -112 |
| | RS+ Moments (kip-in) | 36 | 43 | 52 | 64 | 75 | 276 |
| Other | Wheel Load (kips) | 32.5 | 37.2 | 40.3 | 43.8 | 46.8 | 65.3 |
| | C- Moments (kip-in) | -36 | -39 | -42 | -46 | -48 | -85 |
| | RS+ Moments (kip-in) | 48 | 56 | 70 | 86 | 95 | 160 |
| Intermodal Freight | Wheel Load (kips) | 31.8 | 40.9 | 44.2 | 47.9 | 50.5 | 73.2 |
| | C- Moments (kip-in) | -32 | -38 | -43 | -50 | -73 | -82 |
| | RS+ Moments (kip-in) | 40 | 52 | 61 | 77 | 90 | 125 |
| Non-Intermodal Freight | Wheel Load (kips) | 43.1 | 47.2 | 52.7 | 62.6 | 69.2 | 119.5 |
| | C- Moments (kip-in) | -40 | -44 | -47 | -50 | -52 | -150 |
| | RS+ Moments (kip-in) | 56 | 70 | 91 | 107 | 115 | 252 |

2.8 Crosstie support condition evaluation

Evaluation of ballast support conditions was performed using a numerical back-calculator. The algorithm takes input bending moment data from the aforementioned instrumented concrete crossties and approximated rail seat loads recorded at the WILD sites

(Gao et al., 2017a, 2017b). Understanding the expected support condition parameters is a fundamental element in the design process of prestressed concrete crossties as the bending moments are highly sensitive to variations of the support condition (Bastos, 2016). The computational algorithm divides the crosstie into six bins and optimizes the percentage of total ballast reaction in each bin that is required to recreate the bending moment collected using surface strain gauges in the field.

A subset of the aforementioned bending moment dataset was used in the back-calculator. Particular emphasis was placed on selecting train passes of similar load levels and negative temperature differentials in order to capture worst-case conditions for center negative bending moments. Upward curl in concrete crossties has the potential of inducing high ballast reaction in the center of the element and therefore maximizing the effect of load on the center negative bending moment (Wolf et al., 2016). Previous research on this topic has shown that negative temperature differentials are strongly related to high center negative bending moments (Wolf, 2015). For the purposes of my research, I needed to minimize the variance due to these factors. Therefore, the analysis was limited to a selected subset of non-intermodal freight locomotives on the night of 23 April 2017. Negative temperature differential recorded on site ranged from -4.4 to -5.4 degrees Fahrenheit (-2.5 to -3 Celsius). Locomotive wheels showed both the highest loads and least variation and therefore represented a uniform condition on which to perform the analysis. Figure 2.12 presents the results of the ballast pressure distribution of six locomotives passing the Edgewood, MD field site. Each line represents the average of the conditions calculated for each of the six axles of the individual locomotives. Even with the effect of upward temperature curling, there is a high concentration of support under the rail seats. It is possible to conclude that the dominant support condition at the site is one of a recently

tamped track, with adequate support at the rail seats. This aligns with related results presented in previous sections.

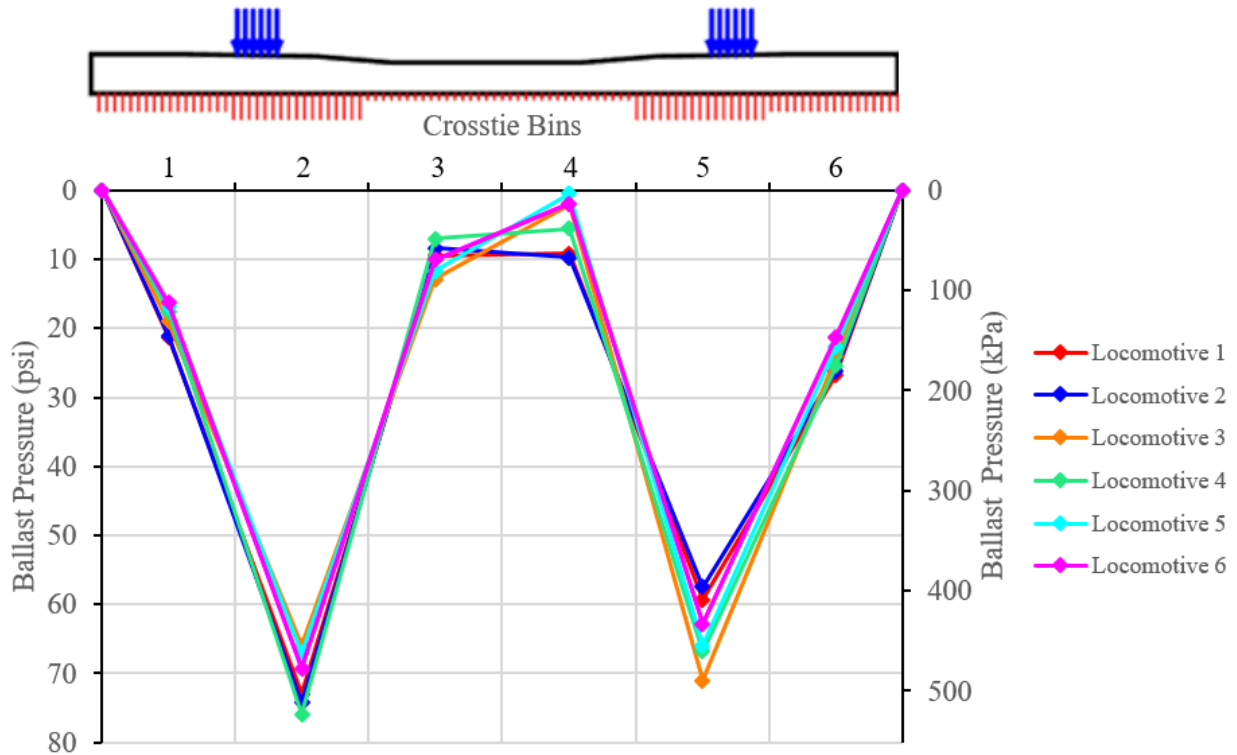


Figure 2.12: Average ballast pressure distributions for six freight locomotives on 23 April 2017

2.9 Variability of support condition

As discussed in Section 2.8, concrete crosstie flexural behavior is highly sensitive to changes in support conditions. While instrumentation is a valuable tool that aids in the characterization of the loading environment on the NEC, it only provides measurement at a single location that is unlikely to be representative of the broader conditions found on the entire NEC. It should also be noted that the Edgewood, MD site is located in tangent track that is well maintained based on visual observation and a review of track health data, generating a near-optimum condition for the long-term performance of track components. Other sections of the NEC, in which particular circumstances may make it difficult to maintain track, or segments with

high impact loads generated due to changes in the track stiffness (e.g., structure approaches), might experience a different flexural behavior. This change in support conditions would likely imply higher bending moments than those recorded in Edgewood, MD.

The aforementioned back-calculator algorithm can be used as a structural analysis model with different fixed hypothetical support conditions as inputs to generate bending moments as outputs. This is reverse of the process that is typically undertaken with the algorithm. Inputs also include all vertical peak loads obtained from the adjacent WILD site. A complete simulation of all the traffic going through the site can be modeled to create synthetic percent-exceeding curves. Five different support conditions were evaluated (Figure 2.13) and are related to the conditions validated by Bastos (2016) in a laboratory experimental setup. His observations were based on a crosstie divided into nine bins. His support values were then adapted for use in the back-calculator algorithm, which uses a six-bin support condition definition. For this, each bin was assigned to support a percentage of the total load applied to the crosstie.

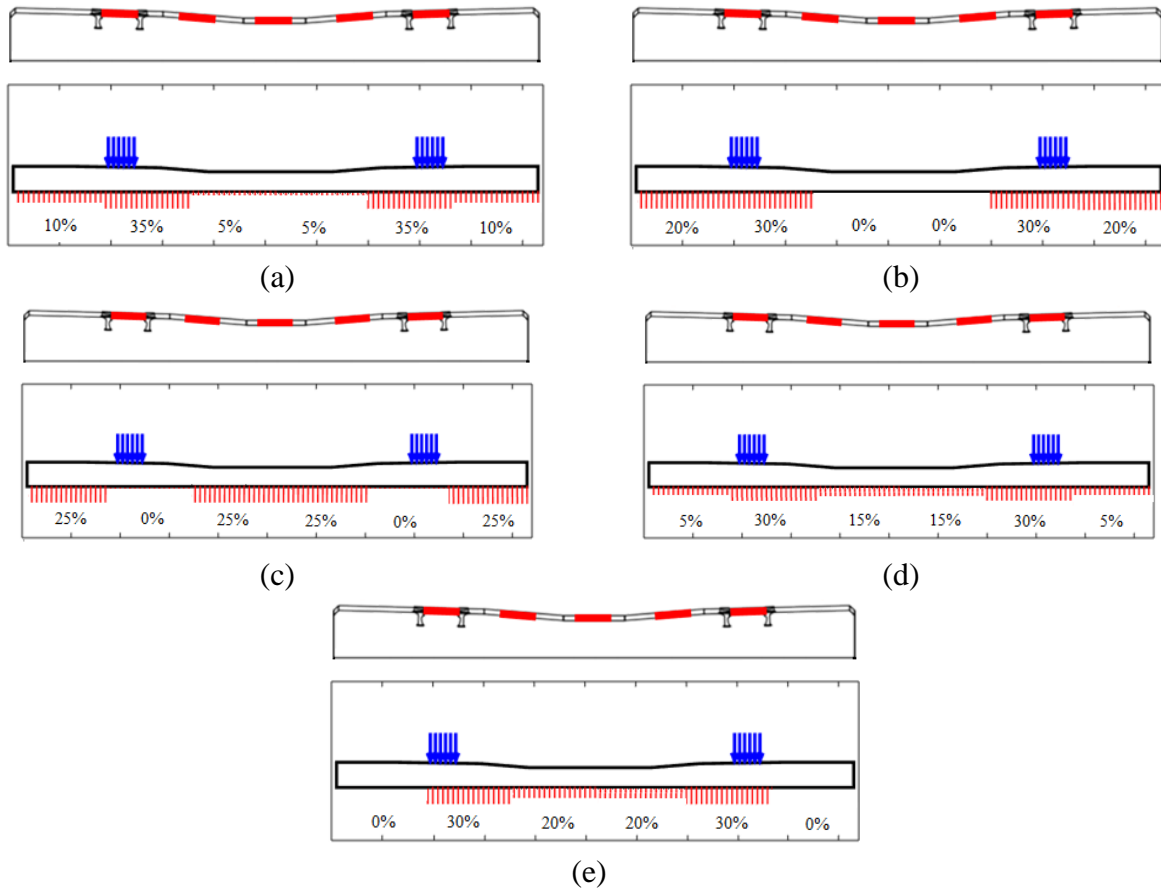


Figure 2.13: Potential support conditions analyzed for flexural demand variability analysis. (a) back-calculated support, (b) lack of center support, (c) lack of rail seat support, (d) light center binding, (e) moderate center binding

Results of this analysis are presented as percent-exceeding graphs for the crosstie-center region (Figure 2.14). A sharp increase in the top 10% of the data is expected due to the values of high impact loads measured along the NEC. Also shown in Figure 2.14 are the specification and laboratory results of the current crosstie design, calculated according to the standard testing protocols included in the AREMA MRE Chapter 30, Part 4 (2017a). Depending on the support case, simulated values can exceed current design first crack and even ultimate capacity, especially when subjected to high center binding. The effects of potential dynamic changes in the support condition due to the interaction between the crosstie's deformed shape and ballast,

which is explored in further chapters, is not yet considered. However, the data provide an upper bound of the bending moments that are feasible based on the current NEC wheel loading environment. If the track is maintained to the level observed at the Edgewood, MD field site, bending moments are not expected to exceed current specification values. This lack of exceedance of flexural values is a reliable indicator of good, long-term concrete crosstie performance.

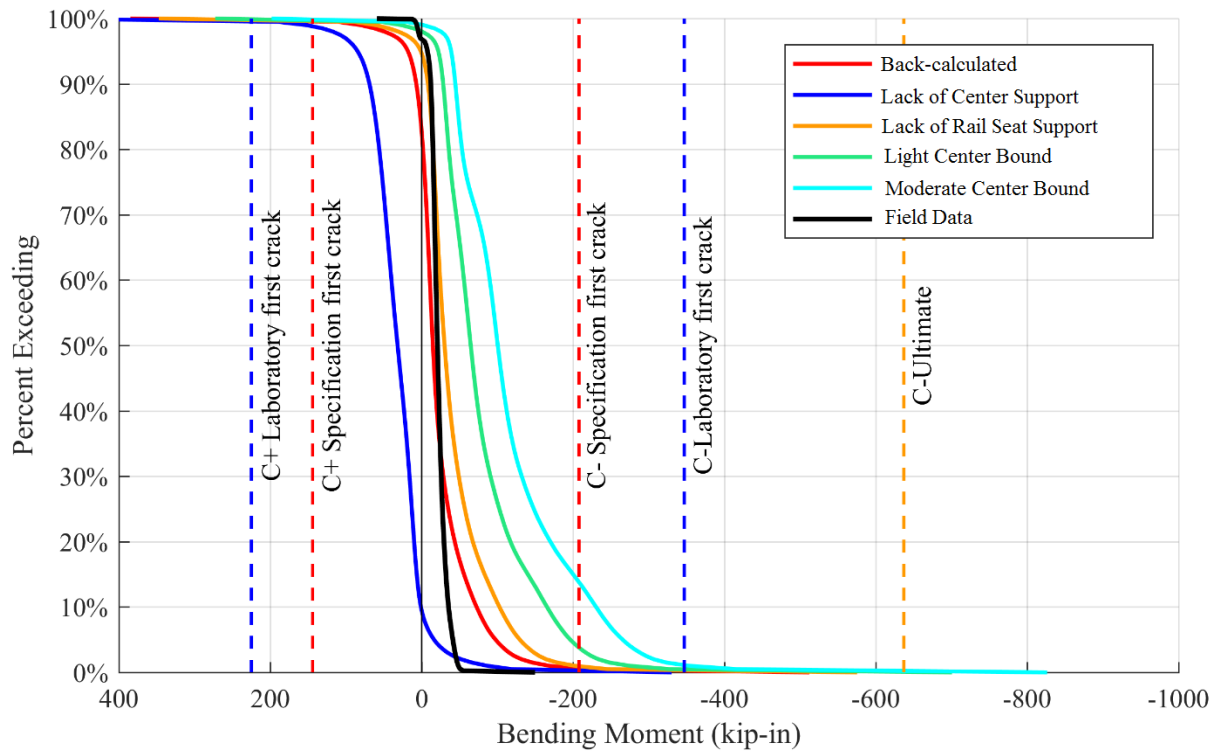


Figure 2.14: Extrapolated flexural bending moments of prestressed concrete crossties at the center region due to different support conditions based on field loading data

Rail seat flexural results show a significant reduction in the variability of the bending moments due to changes in the support condition (Figure 2.15). For the rail seat region, having adequate support immediately under the point of load application generates the highest bending moment. Therefore, the current characteristics of the Edgewood, MD field site induce the

highest possible rail seat demand that would be expected. In other words, it is unlikely that changes in the support condition will ever generate higher flexural values at the rail seat. Considering that the current specification value of 306 kip-in is surpassed neither by field measured data nor by analytical scenarios, it can be concluded that the current design provides a strong rail seat section that can be further optimized by potentially reducing the specification value.

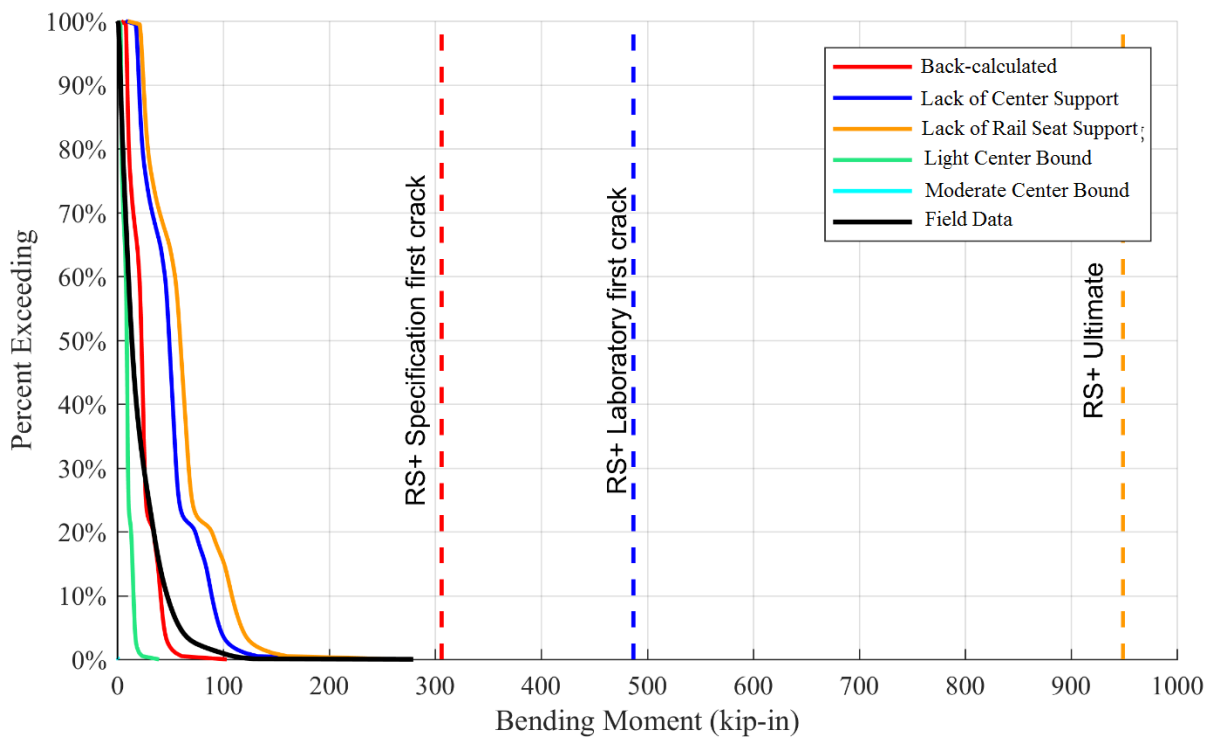


Figure 2.15: Extrapolated flexural bending moments of prestressed concrete cross-ties at the rail seat region due to different support conditions based on field loading data

2.10 Conclusions

Optimization of the track structure and its components requires comprehensive understanding of the effect and variability of loads. Field instrumentation such as WILD sites and instrumented cross-ties proved to be a valuable resource for addressing these questions

through loading and bending moment quantification. From field experimentation conducted on Amtrak's NEC at Edgewood, MD, and supporting laboratory experimentation at UIUC, several conclusions can be drawn:

- The NEC loading environment shows high variability of load levels between equipment types and operators.
- Crosstie center bending moments are less sensitive to load increases than rail seat bending moments, implying adequate support conditions under the rail seats at this field location.
- Considering measured field values, neither specification nor laboratory flexural capacities of the current crossties are exceeded by current train operation and track conditions.
- Back-calculation of existing support conditions at the Edgewood, MD site confirmed the previous observations and indicated sufficient support under the rail seats even when the crosstie is subjected to negative temperature differentials (upward curl).
- There is potential for high flexural demands in the center region of the crosstie that exceed current specification values and actual measured capacity in localized parts of the NEC (e.g. track transitions or other areas with poor support).
- Infrastructure owner experience with the performance of the current design on those more demanding sections of the NEC should guide any necessary increase in the center negative specification value to align with potential (extrapolated) flexural demands.
- For the rail seat region of the crosstie, there is no expected scenario in which Amtrak's flexural specification value can be surpassed and also indicates room for potential crosstie flexural design optimization.

- Maintaining track condition to the level quantified in the field will ensure bending moments not in exceedance of current specification values, which will likely be a reliable indicator of good long-term field performance.

Use of these data regarding the track structure and its performance could influence future designs that are better suited to the operational characteristics of Amtrak's NEC. Additionally, they provide a basis for the future implementation of a reliability-based design approach, in alignment with the broader vision for the mechanistic design of track systems.

CHAPTER 3: ANALYTICAL MODELING OF CROSSTIE BALLAST SUPPORT

3.1 Introduction

The ballast support distribution under crossties is a crucial element in the computation of the flexural bending moments (Sadeghi and Youldashkhan, 2005). Even small changes in the support condition of a crosstie can have a substantial effect on the magnitude of flexural demand (Wolf, 2015; Bastos, 2016). While the support under the crosstie was theorized to be uniform under the complete footprint of the crosstie (Hay, 1982), early research showed that in fact, support is highly variable (Talbot, 1919). Due to the rigidity and irregular shape of ballast particles, the crosstie may be supported by only 100-200 points of contact (Shenton, 1978), making it difficult to experimentally quantify interface pressures. Talbot (1919) cited significant variability in support conditions, even among adjacent crossties, and the effects of these different support conditions on the development of flexural bending moments. As an initial step to furthering this area of study, Talbot (1919) defined hypothetical, idealized distributions for the ballast pressure and the related flexural moment distribution of the crosstie (Figure 1.1). Recently, Wolf et al. (2015) performed a sensitivity analysis of the effects of support variability on the development of flexural bending moments in concrete crossties. Bastos (2016), performed a laboratory comparison of simulated support conditions and the effects on the measured bending moments. A review of these studies illuminates the importance of changes in support conditions on the magnitude of flexural demand placed on a crosstie.

3.2 Analytical ballast support models

It is necessary to quantify the contact pressure distribution of the ballast-crosstie interface before the crosstie can be analyzed in terms of its structural capacity (Doyle, 1980). This

distribution is dependent on the development of voids under the crosstie caused by repeated loading and unloading. In general terms, freshly tamped track is expected to exhibit ballast support concentrated within the zone below each rail seat. Under revenue service conditions the support tends to extend toward the crosstie center and simulates a uniform support scenario (Sadeghi and Barati, 2010). Lack of appropriate maintenance allows degradation of support in the area below the rails leading to center binding (i.e., the concentration of support under the center of the crosstie). This implies that the pressure distribution of the interface may be time-dependent (Doyle, 1980). This has led to the need to perform structural analysis on crossties and multiple crosstie ballast support definition models. One approximated in-field crosstie ballast support profile is presented by Prause (1974) (Figure 3.1). The effective bearing length (L) is considered to represent an equivalent distributed load with the average ballast pressure immediately under the crosstie.

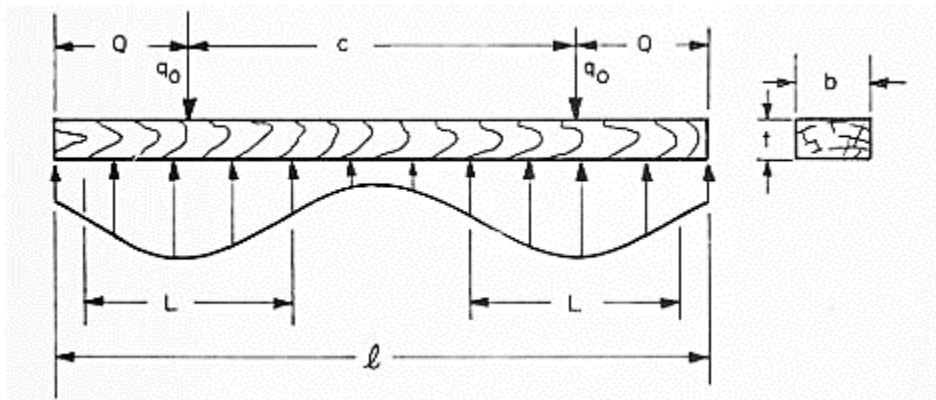


Figure 3.1: Pressure distribution along tie length (Prause et al., 1974)

In terms of effective bearing length for timber crossties, the American Railroad Engineering Association (AREA) defined this as the distance from the end of the sleeper to the “point inside of the edge of the rail base over which tamping operations extend” (Doyle, 1980). These distances were assumed by Magee to be dependent on crosstie length (Table 3.1).

Table 3.1: Effective bearing lengths proposed by Magee for timber crossties (Doyle, 1980)

| Crosstie length (in) | Effective bearing length (in) |
|----------------------|-------------------------------|
| 96 | 33 |
| 102 | 39 |
| 108 | 45 |

Clarke (1957) defined the effective length as a function of the crosstie length (l), gauge distance (g), and thickness (t) (Equation 3-1) (all units in millimeters). This can be simplified in the case of standard gauge track (1435 mm) (Equation 3-2).

$$L = (l - g) \left[1 - \frac{(l - g)}{125 t^{0.75}} \right] \quad 3-1$$

$$L = \frac{l}{3} \quad 3-2$$

Scharamm (1961) defines the area as a function of the crosstie length and gauge (Equation 3-3).

$$L = (l - g) \quad 3-3$$

In the models presented above, ballast support is concentrated under each rail seat, and the center of the crosstie is free from any ballast pressure. This is the objective of maintenance practices that aim to create a “non-pressure bearing center section of the crosstie” as it has been recognized that limiting the amount of bearing support under the center of the crosstie is key to minimizing the development of center negative bending moments (Cope, 1993). Early recommendations by the International Union of Railways (UIC) Office of Research and Experiments (ORE) set the length of this non-bearing area to 500 mm (19.7 in) (Doyle, 1980). Cope (1993) proposed a theoretical distance of 750 mm (30 in.); however, he recognized that

design practices have only partially succeeded in achieving this non-bearing zone and proposed introducing a reduced bearing force in this area (Figure 3.2).

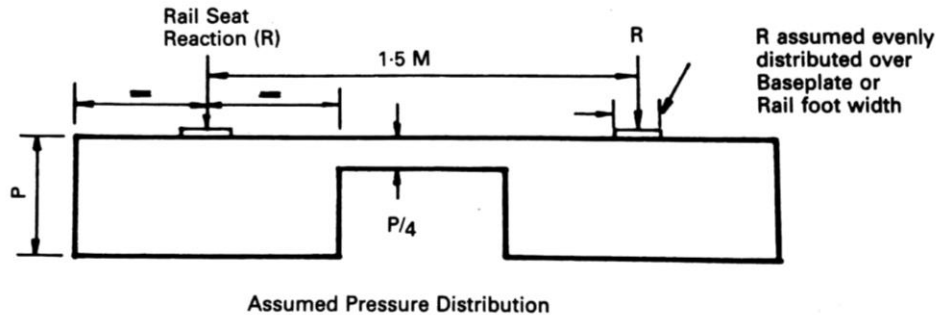


Figure 3.2: Assumed pressure distribution under crosstie (Cope, 1993)

Profillidis (2014), presented a model developed from field measurements performed by ORE that incorporates a trapezoidal support definition and a reduced center bearing area (Figure 3.3).

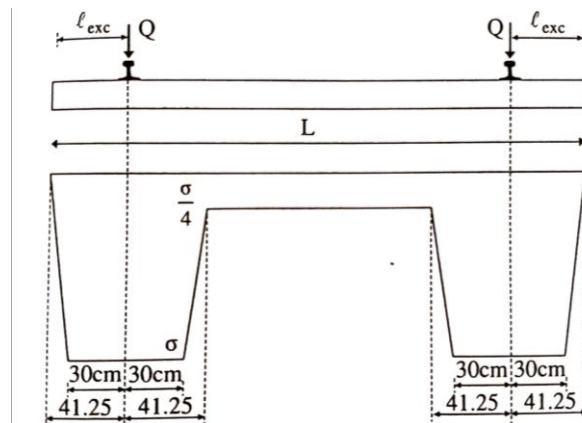
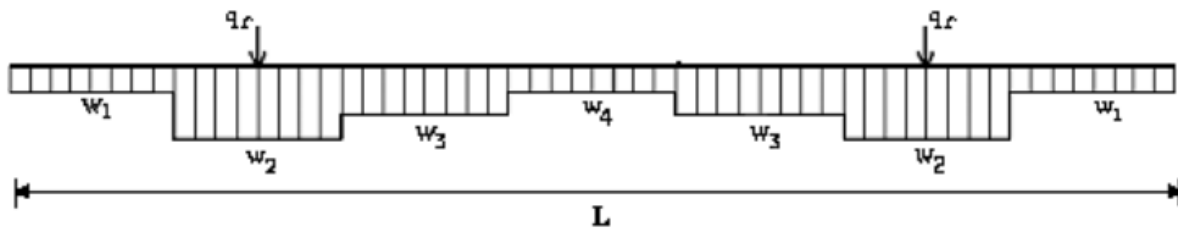


Figure 3.3: Stress distribution under the crosstie according to Profillidis (2014)

A different approach was taken by Sadeghi (2008) with a model based on experimental data gathered with load cell instrumented crossties. This model attempts to recreate the actual parabolic support distribution measured by the author. This parabolic distribution is simplified by dividing the crosstie into seven bins where each region has a load bearing ratio based on the

total length of the crosstie and the rail seat load. The model proposed contact alongside the complete length of the crosstie, with higher bearing ratios on the bins directly under the rail seat (Figure 3.4). The model also proposes two different sets of coefficients for two unique support conditions: 1) right after tamping, with higher support under the rail seats and 2) after cumulative loadings with a more distributed loading pattern.



After accumulative loadings

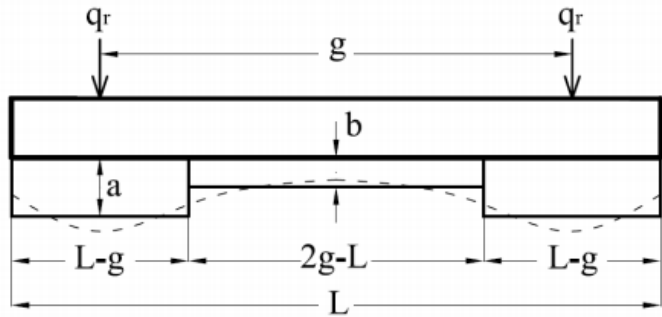
$$w_1 = 1.596q_r/L, w_2 = 2.436q_r/L, w_3 = 1.974q_r/L, w_4 = 1.687q_r/L$$

After tamping

$$w_1 = 1.267q_r/L, w_2 = 2.954q_r/L, w_3 = 1.967q_r/L, w_4 = 1.447q_r/L$$

Figure 3.4: Proposed model for crosstie pressure distribution (Sadeghi, 2008)

This model was later simplified for design purposes (Sadeghi and Barati, 2012) using an approach similar to what was proposed by Cope (1993), with a uniform high bearing area under each rail seat and a reduced bearing section at the center of the crosstie (Figure 3.5). The model also presents different coefficients tailored to the observed response of prestressed concrete, timber, and steel crossties.










| Sleeper Type | Parameter | |
|-----------------------|----------------|----------------|
| | a | b |
| Timber | $0.753q_r / L$ | $0.494q_r / L$ |
| Steel | $0.719q_r / L$ | $0.561q_r / L$ |
| Pre-stressed concrete | $0.709q_r / L$ | $0.581q_r / L$ |

Figure 3.5: Load distribution pattern under different cross-ties (Sadeghi and Barati, 2012)

Based on visual observation, Table 3.2 shows the variety in ballast configurations based on the previously described analytical models.

Table 3.2: Comparison of different analytical models of crosstie-ballast contact pressure distributions

| Name | Model | Notes |
|-------------|---|---|
| Uniform |  | $L_{eff}=51''$ (Half standard crosstie length) |
| Scharamm |  | $L_{eff}=42''$ $L_{eff} = (l - g)$ |
| Magee |  | $L_{eff}=39''$ (Based on experimental methods) |
| Clarke |  | $L_{eff}=34''$ $L_{eff} = (l/3)$ |
| Cope |  | Rail seat support length=42'' Center Bearing pressure is 25% of rail seat area |
| Profillidis |  | Rail seat support length≈23.6'' Center bearing pressure is 25% of rail seat area, trapezoid distribution under rail seat |
| Sadeghi |  | Rail seat support length=42'' Center bearing pressure is ≈82% of rail seat area |

3.3 Crosstie analytical models in design standards

Analysis models intended for design purposes are included within many international design standards such as AREMA (2017a), UIC 713 (2004), and the Australian Council of Standards AS 1085.14 (2003). The aforementioned design standards aim to balance realistic analytical models with reasonable “worst-case” scenarios capable of recreating the expected flexural demand in revenue service.

3.3.1 American Railway Engineering and Maintenance-of-Way Association (AREMA) Manual for Railway Engineering (MRE)

Currently, AREMA provides two recommendations for quantifying the effective bearing length, AREMA MRE Chapter 16, Part 10, Article 10.11.1 defines this length as two-thirds of the crosstie length (AREMA, 2017b) in alignment with Clarke (1957), an assumption that is more closely related to the calculation of average ballast contact pressures. At the same time, AREMA MRE Chapter 30 (Ties), Part 4, Article 4.4.1.2 proposes a different analysis model for crosstie design. The model (Figure 3.6), is comprised of a two-zone bearing area, similar to the model developed by Scharamm (1961). It incorporates a reduced distributed load on the desired non-bearing area, in alignment with Cope's (1993) recommendations. The center reaction factor (α) is related to the crosstie length (L) (Table 3.3).

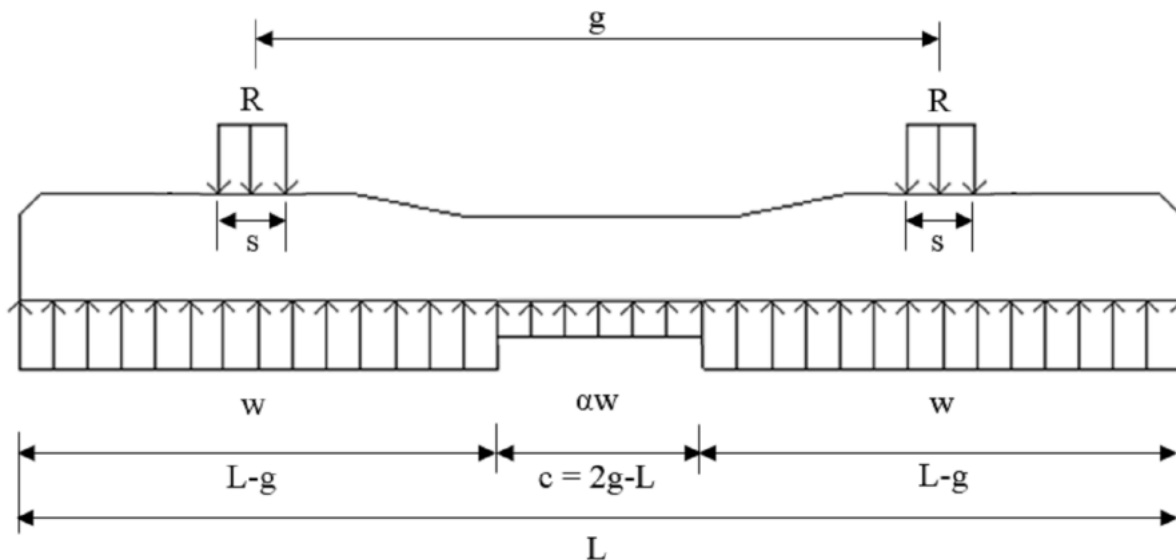


Figure 3.6: Analytical crosstie model proposed by AREMA (2017a)

Table 3.3: Center reaction factors proposed for AREMA crosstie analytical model (2017a)

| Crosstie Length | Center Reaction Factor (α) |
|-----------------|-------------------------------------|
| 7'-9" (2.360 m) | 0.66 |
| 8'-0" (2.440 m) | 0.68 |
| 8'-3" (2.520 m) | 0.74 |
| 8'-6" (2.590 m) | 0.84 |

Based on this support model and the notation described in Figure 3.6, the calculation of the design bending moments follows Equation 3-4 for the rail-seat-positive bending moment and Equation 3-5 for the center-negative bending moment.

$$RS_+ = \frac{1}{8} \left[\left(\frac{2R}{2(L-g) + \alpha(2g-L)} \right) (L-g)^2 - Rs \right] \quad 3-4$$

$$C_- = -\frac{1}{2} R \left[\frac{-L^2 - (1-\alpha)(2g-L)^2}{2(L - (1-\alpha)(2g-L))} - g \right] \quad 3-5$$

3.3.2 International Union of Railways (UIC) leaflet UIC 713. Design of monoblock concrete sleepers

UIC recommends three different analytical models for the computation of flexural bending moments. Model A (Figure 3.7a) is used for the calculation of rail seat positive bending moments and represents a freshly tamped track condition. The effective bearing area extends symmetrically from the center of the rail seat to the end of the crosstie and therefore, is the most demanding condition for the rail seat in terms of induced bending moments. This model is the same as the one proposed by Schramm (1961) and the one proposed in Japanese design standards (Indraratna et al., 2011). The second model (Figure 3.7b), incorporates a reduced bearing area under the center of the element, similar to some of the approaches described in the previous

section. The magnitude of the ballast pressure is reduced by 50% on the center of the crosstie and represents a partially consolidated track condition. As this model incorporates support under the center of the crosstie, it can generate center negative bending moments and therefore is used for the calculation of that specific flexural demand. This model is similar to the model proposed by AREMA, although the magnitude of the center reaction factor is higher in the AREMA version. The third model (Figure 3.7c) represents a fully consolidated track condition with uniform support. This model is recommended for the analysis of waisted crossties and increases the magnitude of center negative bending moments.

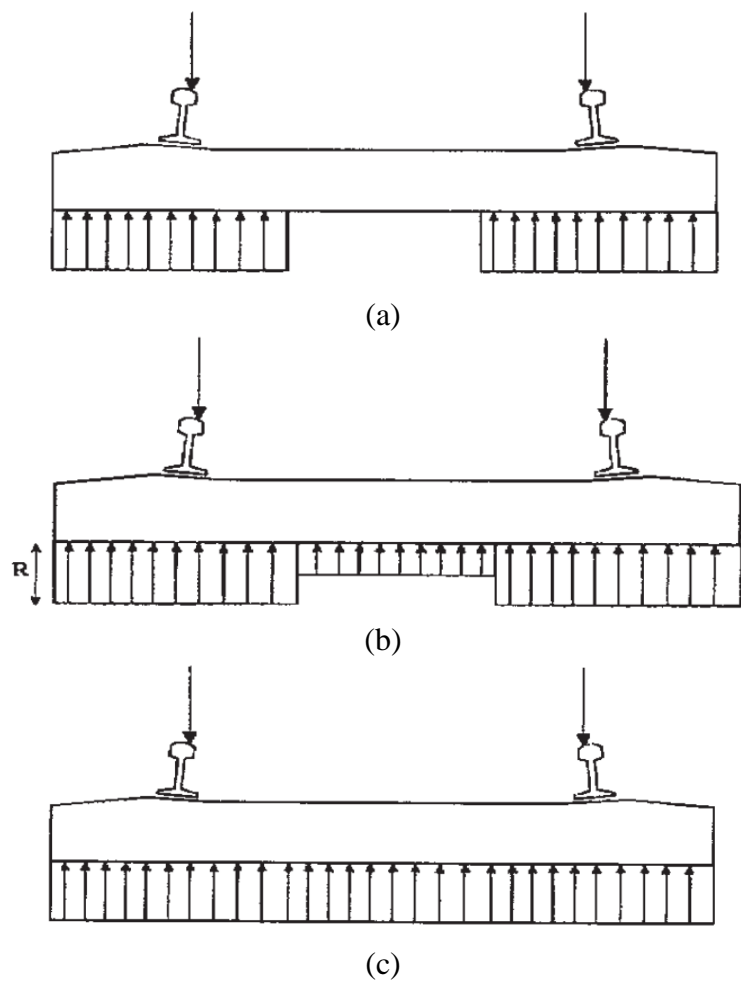


Figure 3.7: Analytical models proposed by UIC for (a) rail seat analysis, (b) center section analysis on prismatic crossties and (c) center section for waisted crossties (UIC, 2004)

Rail seat positive bending moments can then be calculated using Equation 3-6.

$$RS_+ = \frac{R\lambda}{2} \quad 3-6$$

The factor λ is referred to as the effective lever arm and is calculated in accordance with Equation 3-7

$$\lambda = \frac{L_p - e}{2} \quad 3-7$$

Where L_p is the distance from the rail seat axis to the end of the crosstie, and e is the width of the load distribution; in the case of UIC this is considered at the level of the neutral axis and also factors in the depth of the crosstie (Figure 3.8).

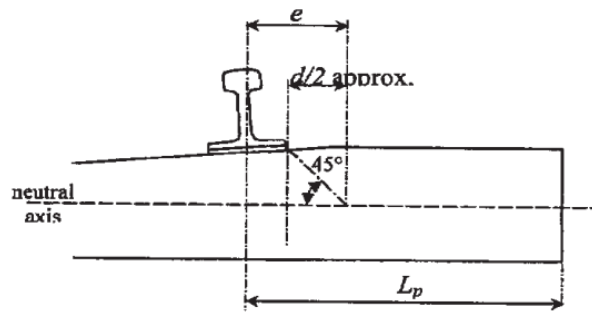


Figure 3.8: Assumed load distribution and lever arm derivation for rail seat bending (UIC, 2004)

In the case of center negative bending moments, the calculation is performed using Equation 3-8. Where L is the length of the crosstie, f is the length of the center zone of reduced reaction (normally $2g-L$), and c is the rail seat gauge distance (commonly referred as g in other models)

$$-R \left(\frac{c}{2} - \frac{2L^2 - f^2}{4(2L - f)} \right) \quad 3-8$$

3.3.3 Australian Standard AS 1085.14 Railway Track Material, Part 14: Prestressed concrete sleepers

The Australian Standard presents two different models, both of which are identical to the ones proposed by the UIC. The first model (Figure 3.9a) is generalized to both standard and narrow-gauge scenarios showing an effective bearing length dependent on the cross-tie length. For standard gauge, this value becomes $(l-g)$ and therefore is identical to both the UIC and Schramm models. The model for center negative bending moment calculation (Figure 3.9b) is the same as UIC proposed model.

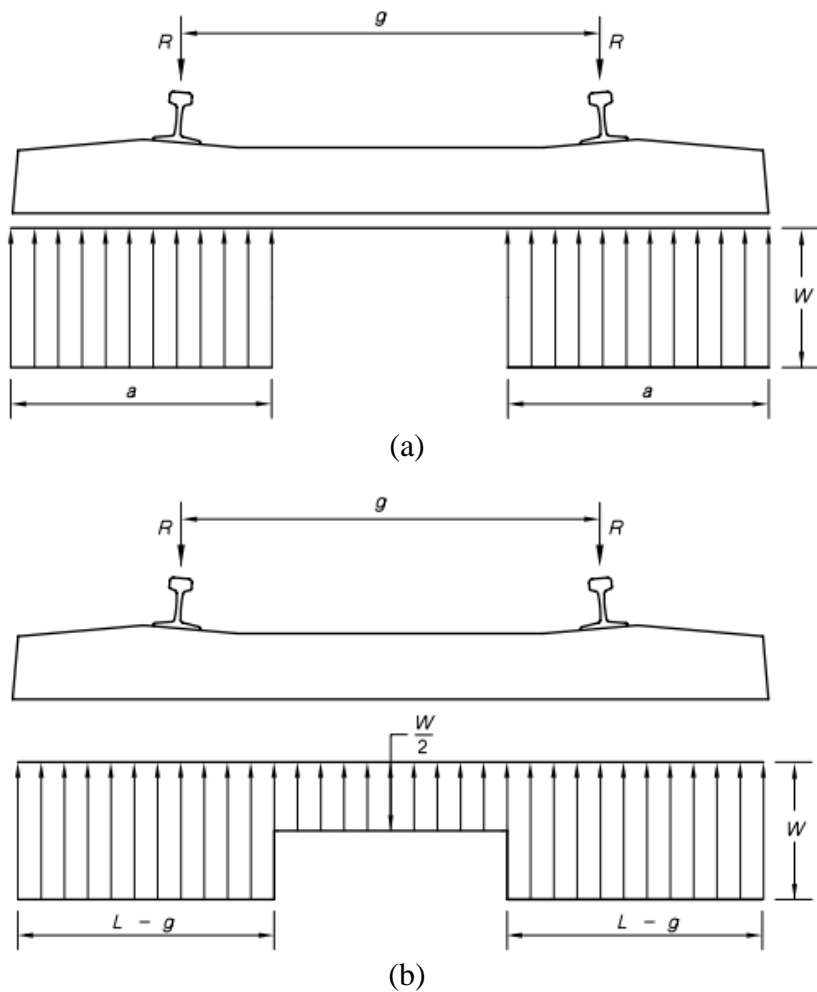


Figure 3.9: Analytical models proposed by Australian Standards for (a) rail seat analysis and (b) center section analysis (Council of Standards Australia, 2003)

Equations 3-9 and 3-10 are used for derivation for rail seat positive and center negative bending moments, respectively.

$$RS_+ = 0.05 R (L - g) \quad 3-9$$

$$C_- = \frac{R(2g - L)}{4} \quad 3-10$$

3.4 Generalized structural modeling

Any attempt to explain the interaction mechanism between crosstie and ballast requires a structural analysis model that can allow both flexibility in how the support distribution is defined, and facilitate efficient computation of crosstie internal forces. It is also desirable for the model to be robust enough to calculate element deflections. Finally, the model should be able to handle asymmetrical loading conditions, which are commonly found in the field.

For this purpose, a two-dimensional analytical model was developed (Figure 3.10). It is composed of a prismatic beam of length L and stiffness EI . The beam is supported by two rocker bearings allowing one rotational degree of freedom. Wheel loads (V_i) are represented by two distributed rail seat loads of fixed length I (RS_i). The separation between rail seats and support is set by a rail seat gauge distance of 60 in. (1,529 mm).

Ballast reaction is modeled under each rail seat as uniform with variable length B_i . The location of the ballast support force is defined by its “skew” (S_i), which is defined as the offset from the support centerline to the ballast support centroid where the resultant reaction force (R_i) is applied. Skew is defined as positive if the support is located toward the center (center bound condition) and negative if support is toward the end of the crosstie (end bound condition). The parameter S_i is a quantitative value that defines how center bounded or end bounded a crosstie is.

These parameters are defined for each rail seat allowing the model to handle asymmetrical loading conditions.

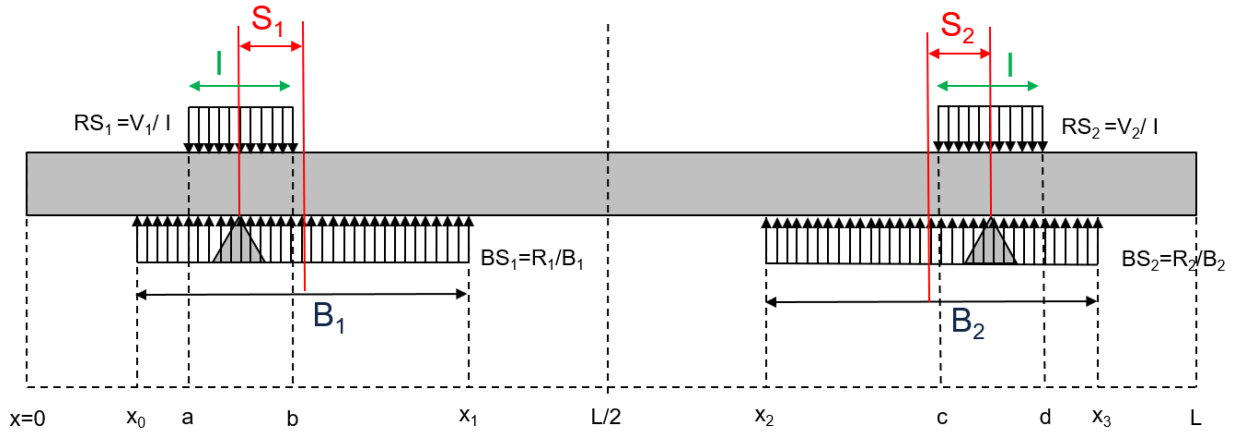


Figure 3.10: Proposed structural model used for the analysis of crossties

The magnitude of support forces, BS_i , is given by the equilibrium of loads and moments around the center of the crosstie. The function of the supports is to provide a boundary condition to the displacements of the crosstie and therefore do not provide an external reaction to the model. The equilibrium conditions are presented in Equations 3-11 and 3-12 in terms of resultant forces V_i and R_i and are valid for crossties for standard gauge track.

$$0 = V_1 + V_2 - R_1 - R_2 \quad 3-11$$

$$0 = 30 * (V_1 - R_2) + R_2(30 - s_2) - R_1(30 - s_1) \quad 3-12$$

By solving the system of equations previously defined, it is possible to compute the expressions for the ballast reaction forces that guarantee equilibrium given any magnitude of wheel loads (Equation 3-13 and 3-14).

$$R_1 = \frac{(s_2 - 60)V_1 + s_2V_2}{s_1 + s_2 - 60} \quad 3-13$$

$$R_2 = \frac{V_2(s_1 - 60) + s_1V_1}{s_1 + s_2 - 60} \quad 3-14$$

The values x_i define the start and end of the ballast distributed reaction forces. The rail seat gauge distance is set to 1,524 mm (60 in) and the total crosstie length to 2,590 mm (102 in). The position of the rocker bearings is defined at 533.4 mm (21 in) and 2,057.4 mm (81 in) from the coordinate system origin. With the aforementioned parameters, it is possible to define a set of equations for all x_i (Equations 3-15 through 3-18).

$$x_0 = 21 + S_1 - \frac{B_1}{2} \quad 3-15$$

$$x_1 = 21 + S_1 + \frac{B_1}{2} \quad 3-16$$

$$x_2 = 81 - S_2 - \frac{B_2}{2} \quad 3-17$$

$$x_3 = 81 - S_2 + \frac{B_2}{2} \quad 3-18$$

These values should be positive and less than the total crosstie length. At the same time, it is necessary to avoid potential overlap between the ballast reactions. Therefore, the relationship shown in Equation 3-19 shall hold true for every set of values of x_i .

$$0 > x_0 > x_1 > \frac{L}{2} > x_2 > x_3 > L \quad 3-19$$

Considering a standard concrete crosstie length of 102 in. (2,590 mm), it's possible to develop the set of restrictions for S_1 , S_2 , B_1 , and B_2 (Equations 3-20 through 3-23).

$$42 + 2 \times S_1 > B_1 \quad 3-20$$

$$42 + 2 \times S_2 > B_2 \quad 3-21$$

$$2 \times S_1 + B_1 < 60 \quad 3-22$$










$$2 \times S_2 + B_2 < 60 \quad 3-23$$

Presently, the model is capable of handling any of the support distribution idealizations used for the analysis or design of concrete crossties, in particular, those models that characterize

the ballast support distribution as a single uniform load under the rail seat. Any other model not based on this definition can be transformed into an equivalent model by calculating an equivalent uniform effective bearing length (b_{eq}) and equivalent skew (s_{eq}). For the equivalent effective bearing length, the equivalent model will have the same average bearing pressure. For the equivalent skew value, the ballast bearing distribution will have the same centroid with respect of the center axis of the crosstie as that of the original model. This method guarantees that the calculated bending moment flexural response in the center of the crosstie remains unchanged; however, the calculation of bending moments at other points of the crosstie might show small deviations compared to the original, non-equivalent model.

This generalized model also allows the user to directly compare the characteristics of the previous models (Table 3.4). Given that the skew value is a direct numeric value for quantifying how center bound a crosstie is, models with higher positive skew values will generate higher center negative bending moments. Models with a skew value of zero will produce no center negative moments, while negative skew values will generate center positive bending moments.

Table 3.4: Equivalent ballast support parameter for different idealized design support conditions for a cross-tie 8'-6" in length

| Name | Model | Equivalent B Value (in) | Equivalent S Value (in) |
|-----------------|---|-------------------------|-------------------------|
| Uniform |  | 51 | 4.5 |
| Scharamm/UIC/AS |  | 42 | 0 |
| Magee |  | 39 | -1.5 |
| Clarke |  | 34 | -4.0 |
| Cope |  | 44.25 | 1.30 |
| Profillidis |  | 32.04 | 2.74 |
| Sadeghi |  | 49.4 | 3.81 |
| AREMA |  | 49.56 | 3.88 |
| UIC/AS Center |  | 46.5 | 2.47 |

3.5 Structural analysis

The development of a closed form solution for the beam flexural bending analysis will facilitate expedient and straightforward calculations. The definition of multiple non-continuous distributed loads made the traditional (direct integration) method impractical as it required solving for up to 18 different integration constants. In an alternative method, the use of singularity functions (Macaulay, 1919) has proven useful in similar scenarios and is computationally efficient to implement (Beer et al., 2015). This technique is applicable to Euler-Bernoulli beams and it is particularly suited to elastic, homogeneous, and isotropic prismatic beams with uniformly distributed loads (Wittrick, 1965). The analysis is limited, however, to prismatic beams as the method becomes impractical for elements with a variable cross-section (Popov, 1998).

The method makes use of discontinuity equations represented using the “Macaulay bracket” ($\langle \rangle$) as defined by Equation 3-24.

$$\langle f(x - a) \rangle = \begin{cases} 0 & \text{if } x < a \\ f(x - a) & \text{if } x \geq a \end{cases} \quad 3-24$$

Based on the prior definition it is possible to develop a generalization for power functions (Equation 3-25):

$$\langle x - a \rangle^n = \begin{cases} 0 & \text{if } x < a \\ (x - a)^n & \text{if } x \geq a \end{cases} \quad 3-25$$

The exponent n defines the shape of the singularity function and is related to specific loading conditions. In the case of the model being considered, only distributed loads are used, and they are defined with a value of $n=0$ (Popov, 1998). This has the advantage of providing a simple, yet powerful way to describe discontinuous loading (Macaulay, 1919). The functions

described are open-ended to the right, and therefore a “finite distributed load must be replaced by an equivalent combination of open-ended loadings” (Beer et al., 2015).

Considering the aforementioned methodology, the loading condition of the crosstie is defined by Equation 3-26.

$$w(x) = BS_1 \langle x - x_0 \rangle^0 - BS_1 \langle x - x_1 \rangle^0 - RS_1 \langle x - a \rangle^0 + RS_1 \langle x - b \rangle^0 + BS_2 \langle x - x_2 \rangle^0 - BS_2 \langle x - x_3 \rangle^0 - RS_2 \langle x - c \rangle^0 - RS_2 \langle x - d \rangle^0 \quad 3-26$$

Successive direct integrations of the loading function are performed in order to obtain shear, moment, rotation, and deflection expressions (Equation 3-27 through 3-30).

$$V(x) = BS_1 \langle x - x_0 \rangle^1 - BS_1 \langle x - x_1 \rangle^1 - RS_1 \langle x - a \rangle^1 + RS_1 \langle x - b \rangle^1 + BS_2 \langle x - x_2 \rangle^1 - BS_2 \langle x - x_3 \rangle^1 - RS_2 \langle x - c \rangle^1 + RS_2 \langle x - d \rangle^1 + C_1 \quad 3-27$$

$$M(x) = \frac{BS_1}{2} \langle x - x_0 \rangle^2 - \frac{BS_1}{2} \langle x - x_1 \rangle^2 - \frac{RS_1}{2} \langle x - a \rangle^2 + \frac{RS_1}{2} \langle x - b \rangle^2 + \frac{BS_2}{2} \langle x - x_2 \rangle^2 - \frac{BS_2}{2} \langle x - x_3 \rangle^2 - \frac{RS_2}{2} \langle x - c \rangle^2 + \frac{RS_2}{2} \langle x - d \rangle^2 + C_1 \times x + C_2 \quad 3-28$$

$$EI \theta(x) = \frac{BS_1}{6} \langle x - x_0 \rangle^3 - \frac{BS_1}{6} \langle x - x_1 \rangle^3 - \frac{RS_1}{6} \langle x - a \rangle^3 + \frac{RS_1}{6} \langle x - b \rangle^3 + \frac{BS_2}{6} \langle x - x_2 \rangle^3 - \frac{BS_2}{6} \langle x - x_3 \rangle^3 - \frac{RS_2}{6} \langle x - c \rangle^3 + \frac{RS_2}{6} \langle x - d \rangle^3 + \frac{C_1 \times x^2}{2} + C_2 \times x + C_3 \quad 3-29$$

$$EI \delta(x) = \frac{BS_1}{24} \langle x - x_0 \rangle^4 - \frac{BS_1}{24} \langle x - x_1 \rangle^4 - \frac{RS_1}{24} \langle x - a \rangle^4 + \frac{RS_1}{24} \langle x - b \rangle^4 + \frac{BS_2}{24} \langle x - x_2 \rangle^4 - \frac{BS_2}{24} \langle x - x_3 \rangle^4 - \frac{RS_2}{24} \langle x - c \rangle^4 + \frac{RS_2}{24} \langle x - d \rangle^4 + \frac{C_1 \times x^3}{6} + \frac{C_2 \times x^2}{2} + C_3 \times x + C_4 \quad 3-30$$

Boundary conditions allow the calculation of the first two integration constants (Equation 3-31 and 3-32).

$$V(0) = 0 \therefore C_1 = 0 \quad 3-31$$

$$M(0) = 0 \therefore C_2 = 0 \quad 3-32$$

Constants C_3 and C_4 require extensive calculations as certain loading cases can create multiple scenarios that have an impact on the calculation of each variable. In general terms, the

calculation of those constants is dependent on the relationship between parameters a, b, c, d, and the value of x_i . Solutions valid for the typical rail seat bearing length of 6 in (150mm) are provided in Table 3.5.

Table 3.5: Definition of integration constants for certain loading scenarios

| Primary scenario | Secondary scenario | C_3 | C_4 |
|-----------------------|--------------------|--------------------------------|--|
| $x_0 < 21$ < x_1 | $x_2 < 81 < x_3$ | $C_3 = \frac{A+C-D-E}{60}$ | $C_4 = \frac{-27(A+C)+7(D+E)}{20}$ |
| | $x_3 < 81$ | $C_3 = \frac{A+C-D-E-F}{60}$ | $C_4 = \frac{-27(A+C)+7(D+E+F)}{20}$ |
| | $x_2 > 81$ | $C_3 = \frac{A+C-D}{60}$ | $C_4 = \frac{-27(A+C)+7(D)}{20}$ |
| $x_1 < 21$ | $x_2 < 81 < x_3$ | $C_3 = \frac{A+B+C-D-E}{60}$ | $C_4 = \frac{-27(A+B+C)+7(D+E)}{20}$ |
| | $x_3 < 81$ | $C_3 = \frac{A+B+C-D-E-F}{60}$ | $C_4 = \frac{-27(A+B+C)+7(D+E+F)}{20}$ |
| | $x_2 > 81$ | $C_3 = \frac{A+B+C-D}{60}$ | $C_4 = \frac{-27(A+B+C)+7(D)}{20}$ |
| $x_0 > 21$ | $x_2 < 81 < x_3$ | $C_3 = \frac{C-D-E}{60}$ | $C_4 = \frac{-27(C)+7(D+E)}{20}$ |
| | $x_3 < 81$ | $C_3 = \frac{C-D-E-F}{60}$ | $C_4 = \frac{-27(C)+7(D+E+F)}{20}$ |
| | $x_2 > 81$ | $C_3 = \frac{C-D}{60}$ | $C_4 = \frac{-27(C)+7(D)}{20}$ |

The constants A through F are defined by equations 3-33 through 3-36.

$$A = \frac{BS_1}{24}(21 - x_0)^4 \quad 3-33$$

$$B = -\frac{BS_1}{24}(21 - x_1)^4 \quad 3-34$$

$$C = -\frac{RS_1 \times 27}{8} \quad 3-35$$


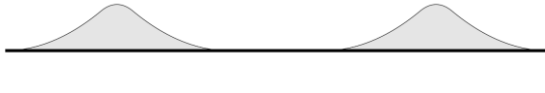




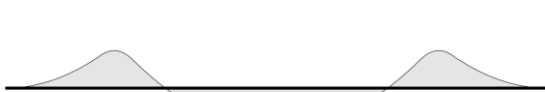


$$D = \frac{BS_1}{24}(81 - x_0)^4 - \frac{BS_1}{24}(81 - x_1)^4 - \frac{RS_1}{24}(63)^4 + \frac{RS_1}{24}(57)^4 - \frac{RS_2}{8}27 \quad 3-36$$

$$E = \frac{BS_2}{24}(81 - x_2)^4 \quad 3-37$$

$$F = -\frac{BS_2}{24}(81 - x_3)^4 \quad 3-38$$

Table 3.6 shows the flexural bending moment diagrams for each of the support conditions previously described for 10 kips (44.48 kN) rail seat load. Small differences in theoretical bending moment calculations are present and are to be expected due to differences in the characterization of the rail seat load.

Table 3.6: Structural analysis results for different models for a crosstie 8'-6" in length

| Name | Flexural Bending Moment Diagram | Rail seat BM (kip-in) | Center BM (kip-in) |
|-----------------|--|-----------------------------|--------------------------|
| Uniform |  | 72 | -90 |
| Scharamm/UIC/AS |  | 90 | 0 |
| Magee |  | 98 | 30 |
| Clarke |  | 115 | 80 |
| Cope |  | 83 | -26 |
| Profillidis |  | 40.0 | -54.8 |
| Sadeghi |  | 73.4 | -76.2 |
| AREMA |  | 73.1 | -77.6 |
| UIC/AS Center |  | 77.9 | -49.4 |

CHAPTER 4: EFFECT OF WHEEL LOAD ON SUPPORT CONDITION DEFINITION

4.1 Introduction

The analytical models included within the common international design standards presented in Chapter 3 exhibit slight differences. Nevertheless, they are consistent in their description of a linear relationship between flexural bending moments and rail seat loads. This linearity can be seen by comparing the bending moment equations of all three standards (Table 4.1) and noticing that in all cases, the equation has the form $M = R \times c$, where R is the rail seat load and c is a set of numeric constants.

Table 4.1: Summary of design standards design equations

| Standard | Rail Seat Positive | Center Negative |
|----------------------------|--|---|
| AREMA MRE 2017 | $\frac{1}{8} \left[\left(\frac{2R}{2(L-g) + \alpha(2g-L)} \right) (L-g)^2 - R_s \right]$ | $-\frac{1}{2} R \left[\frac{-L^2 - (1-\alpha)(2g-L)^2}{2(L-(1-\alpha)(2g-L))} - g \right]$ |
| UIC 713 | $\frac{R\lambda}{2}$ | $-R \left(\frac{c}{2} - \frac{2L^2 - f^2}{4(2L-f)} \right)$ |
| Australian Standard | $0.05R(L-g)$ | $-R(2g-L)/4$ |

The reason for this implicit linear relationship is due to the static modeling of the ballast support condition. In these models, ballast bearing is independent of any wheel loads and crosstie-ballast interaction. However, the same set of field data recorded on Amtrak’s NEC that was presented in Chapter 2 suggest that the relationship is highly non-linear for center flexural bending moments (Figure 4.1). These data represent a subset of the complete dataset and were selected in a manner that isolates the effects of loading in the crosstie flexural response. Wheels with high impact factors were excluded, and the data were filtered to show only points captured

when the cross-ties exhibit a temperature gradient (top to bottom) between -2 and -1 degrees Fahrenheit. The nonlinear relationship implies the existence of an unknown mechanism that modifies the support condition of the cross-tie as the wheel load increases.

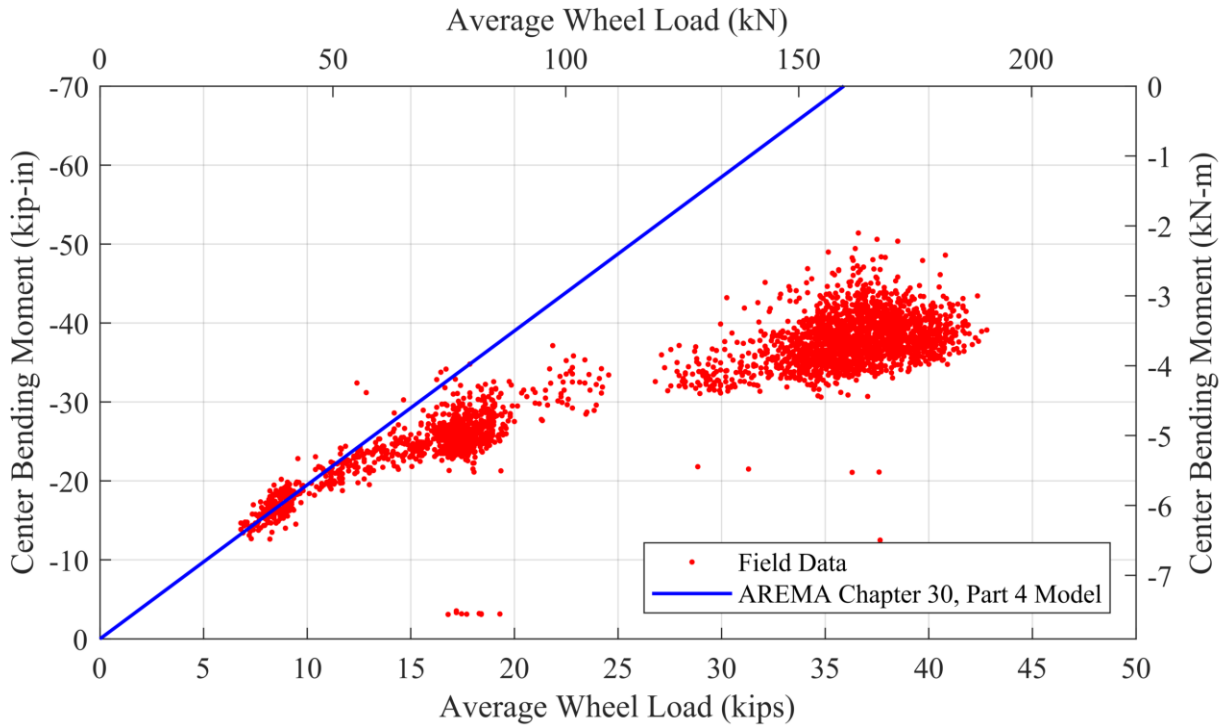


Figure 4.1: Comparison of wheel load-center bending moment relationship for field-collected data and AREMA Chapter 30 (Ties), Part 4 structural analysis model

In the case of the rail seat area, under most loading scenarios the support remains concentrated below that zone of the cross-tie. Previous authors have noted that the rail seat area is much less sensitive to changes in the support condition (Bastos, 2016). The changes of the support bearing magnitude under the center of the cross-tie have little to no effect on the rail seat as bearing is still provided below the rail seat area (Gao et al., 2017b). Field data suggest that while there might be an interaction similar to the one observed at the cross-tie center, the data

follow a more linear wheel load-bending moment relationship (Figure 4.2). It is also evident that the data conforms more closely to the relationship defined by the AREMA MRE (2017a).

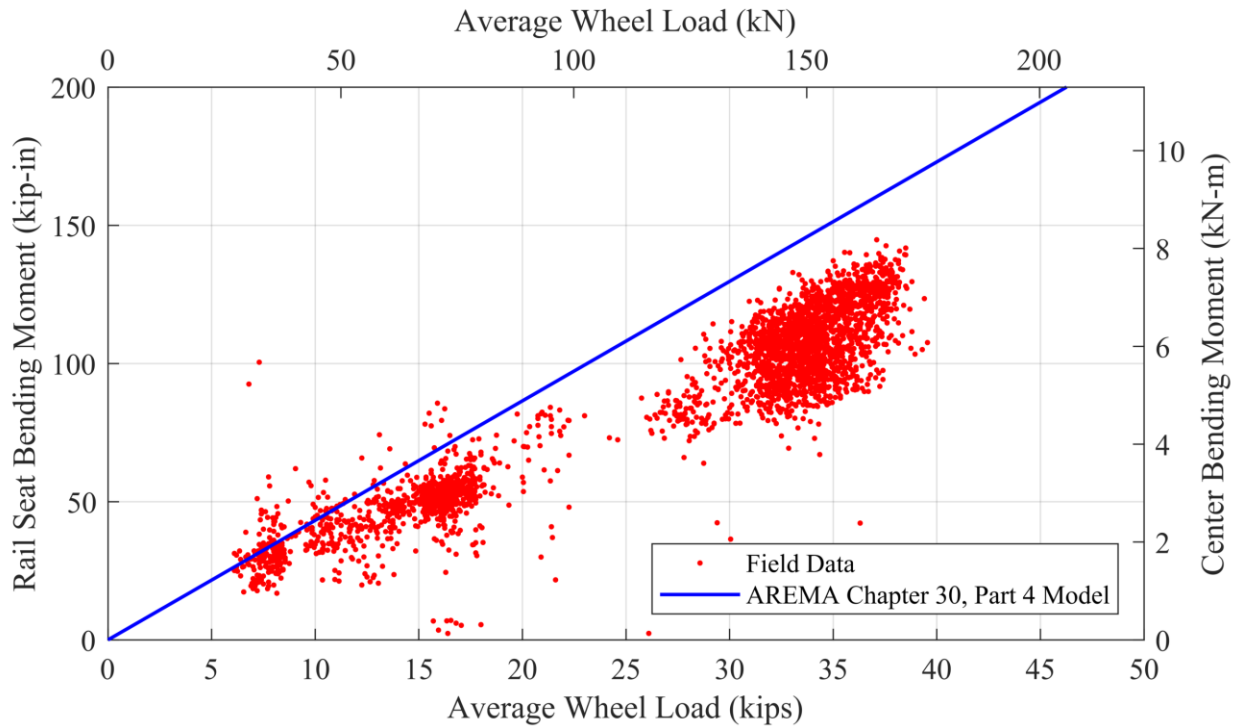


Figure 4.2: Comparison of wheel load-rail seat bending moment relationship for field-collected data and AREMA Chapter 30 (Ties), Part 4 structural analysis model

4.2 Support Redistribution Hypothesis

4.2.1 Hypothesis background

The results of early railroad track instrumentation showed that increases in rail seat load were accompanied by apparent changes in the crosstie support condition. In particular, Prause et al. (1977) noted that in some cases with very light wheel loads, the crosstie behaved as center-bound while for heavier cars the crosstie exhibited end-bounded or well-supported behavior (Figure 4.3). Specifically, Prause et al. (1977) expressed that “The load-dependent center binding effect was evident from the data, and it has a significant effect on the tie/ballast

pressure distribution.” Note that the pressure distribution varies significantly ranging from a center bound to a more common rail seat support condition.

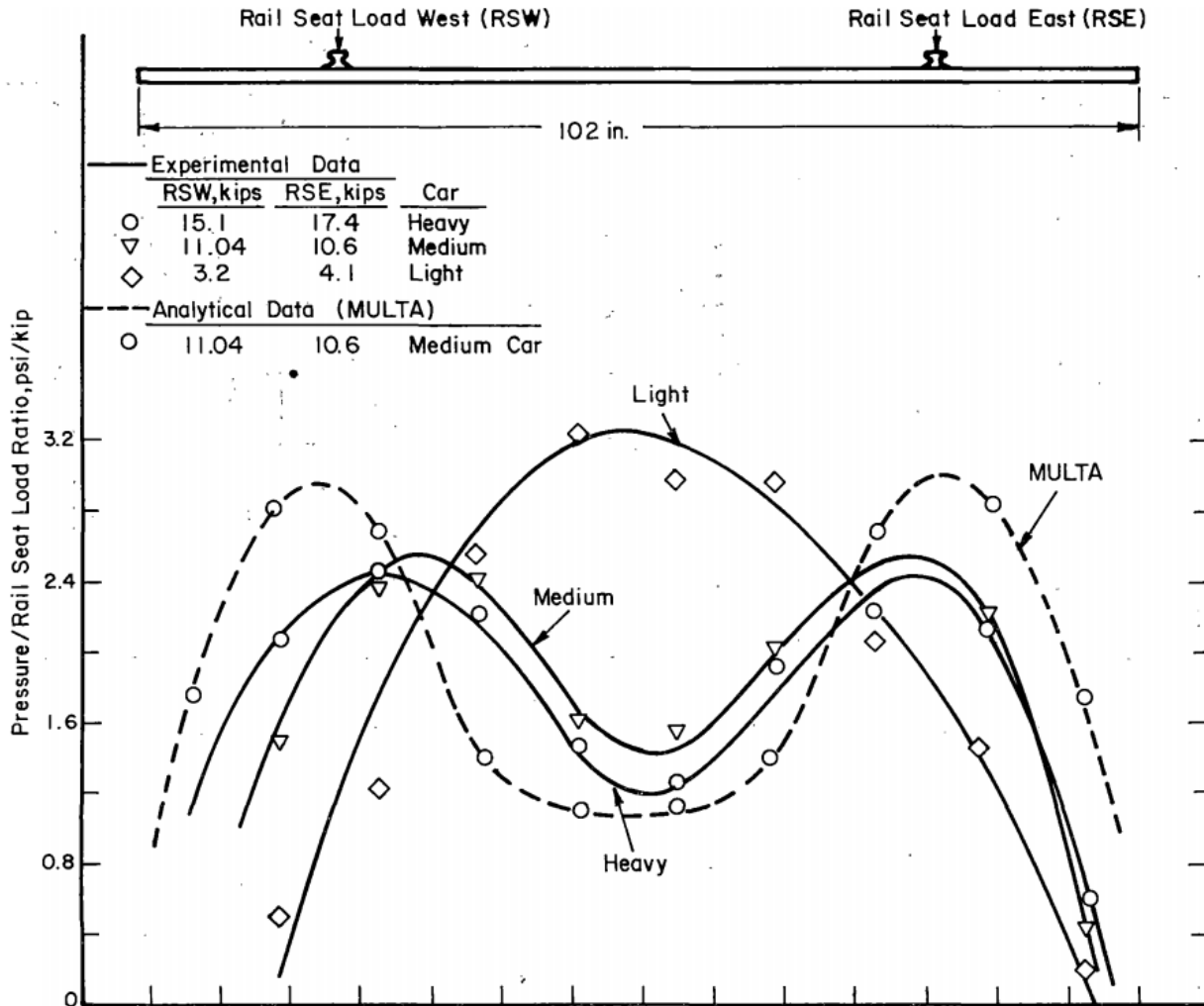


Figure 4.3: Ballast-Crosstie interface pressures normalized to rail seat load for three different load levels (Prause et al., 1977)

In particular, Prause et al. (1977) stated that the data collected “indicates a nonlinear support condition whereby the distribution of reaction loads along the length is changing with the load to maintain a relatively constant bending moment.” Regarding the mechanism behind this phenomenon, Prause et al. (1977) noted that “the tie deflection into the ballast plus some tie

bending under heavy loads would be sufficient to shift the reaction loads towards the tie ends and maintain a nearly constant bending moment.”

Previous research related to quantification of ballast pressure under timber cross-ties also provides useful information related to this phenomenon. Song et al. (2017) measured the pressure distribution at five discrete locations under steel and timber cross-ties using of pressure cells under laboratory conditions varying external load levels (Figure 4.4). Their results indicate that as load increases, the change in ballast pressures at five discrete locations is considerably different. On timber cross-ties, in particular, it was found that “as the external load increased, the pressure under the timber cross-tie increased from outside to inside, indicating that the four outside locations experienced a higher increase that did the center location” (Song et al., 2017). In summary, under low loads, the cross-tie showed a distinct center binding behavior, while as load increased, the support distribution shifted to provide more and more support to the rail seat.

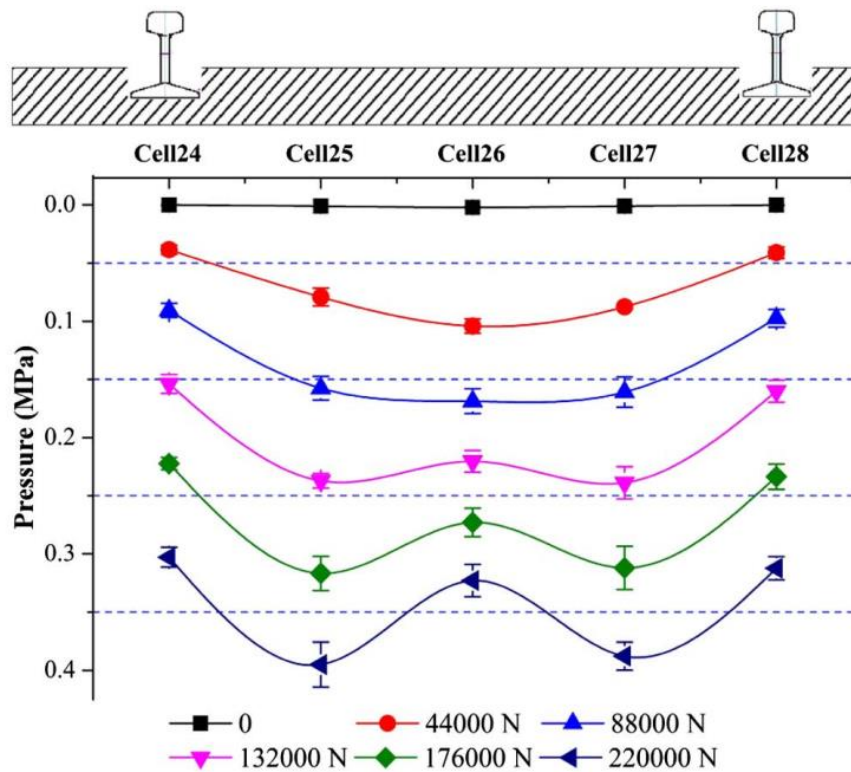


Figure 4.4: Pressure distributions under cross-tie at different load levels (Song et al., 2017).

Support redistribution is referenced indirectly by Talbot (1919) citing that “a more usual condition for what is commonly included as an end bound condition develops positive moments at the middle of the crosstie for the smaller loads and negative moments for the larger loads”, which implies a change in the support condition due to increase in loading. Talbot (1919) also commented on the effects of crosstie bending and ballast interaction, specifically on the development of center-bound conditions noting that “It is possible that at the point of greatest depression, as immediately under the rail, a permanent depression will be formed, and the tie will not touch the bed until it has bent considerably at this point.” On flexibility, Talbot (1919) noted that increased flexibility of the crosstie resulted in the greater variability of support intensity under the rail seats.

While noted in prior research, support redistribution effects on the development of bending moments have not been specifically explored and documented in the literature. On track segments with uniform wheel loads the effect, while present, is not of critical importance due to the fact that flexural behavior develops as expected. Underestimation of the specific flexural demand of light rail cars could arise on corridors with mixed shared traffic. In this case, the bending moment induced by light vehicles can be significantly higher than the expected moments for that specific wheel-load level. Furthermore, the stiffness of the crosstie can accentuate this phenomenon even more.

4.2.2 Analytical model

I developed a hypothetical redistribution approach that mathematically describes the change in support condition as loading increases. I assumed that the mechanism behind this phenomenon is the interaction of the deflected shape of the crosstie with the ballast particles. As

the crosstie deflects, certain portions of the crosstie enter in direct contact with the ballast particles and cause a change in the location of the effective support location. Modeling the phenomenon requires an iterative algorithm with successive increases in load values. As it was described in Chapter 3, the crosstie structural model defines the ballast support characteristics of each rail seat (i) in terms of the support width (B_i) and skew (S_i), defined as the distance between the rail seat center line and the ballast reaction center line. The sign of the skew describes an end bound (negative skew) or center bound (positive skew) condition (Figure 4.5). The support redistribution algorithm assumes that on every iteration, the skew of the ballast support will change, while the support width will remain constant. Tests of this assumption will be described in the following sections.

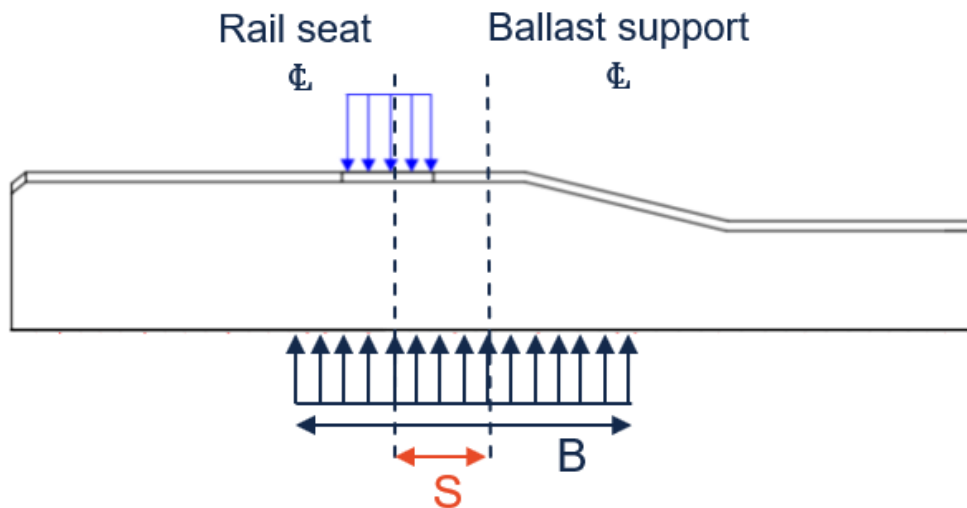


Figure 4.5: Definition of ballast support width (B) and skew (S)

The first stage of the algorithm requires the definition of initial values of rail seat load, support width (b_i), and support skew (s_i). The structural analysis developed in Chapter 3 uses the input values to calculate the crosstie's deformed shape (Figure 4.6). I assumed that the ballast

behaves as an elastic (Winkler) foundation with a stiffness value k_s . Therefore, positive deflections (downward) are related to an additional reaction force (BL'). The ratio of the additional reaction (BL') to the static ballast reaction (BL) is used to modify the value of skew (s) for the next iteration (Equation 4-1).

$$S_{i+1} = S_i \times \left(1 - \frac{BL'}{BL}\right) \quad 4-1$$

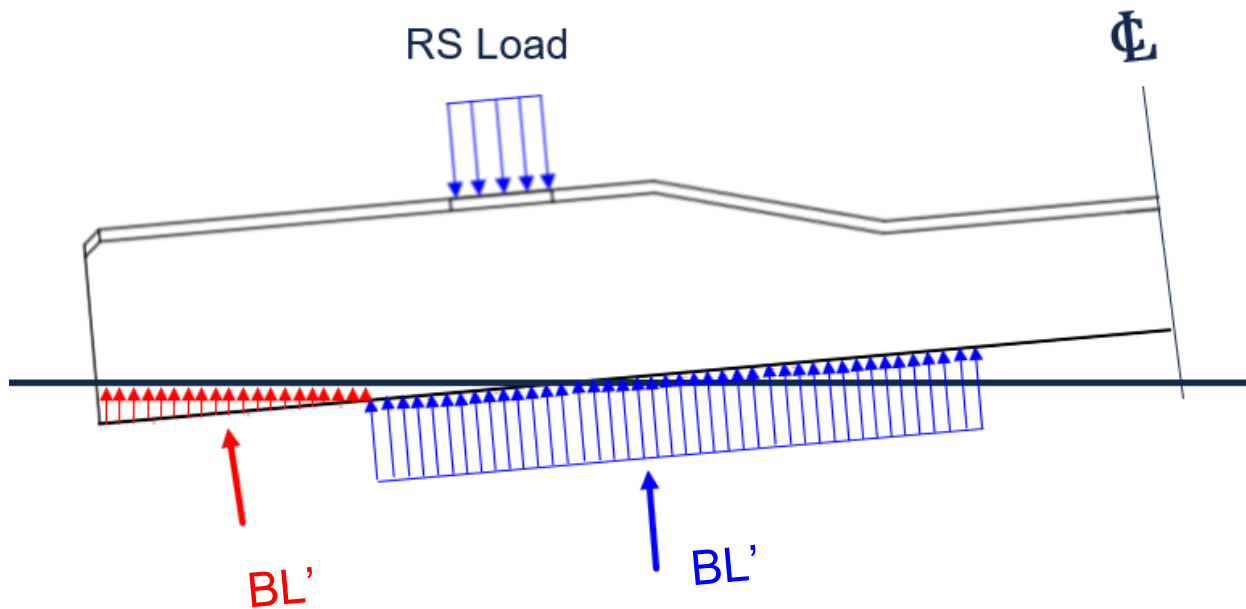


Figure 4.6: Definition of additional ballast forces on cross-tie deflected shape.

This method models the cross-tie as a beam on a Winkler foundation with an across-track ballast modulus k_s as described by Cai et al. (1994). This parameter can be calculated based on the method developed by Gailin and described by Selvadurai (1979) (Equation 4-2) for a narrow finite beam resting on an isotropic elastic half-space.

$$k_s = \frac{\pi E_s}{2b(1 - \nu^2) \log(l/b)} \quad 4-2$$

Parameters E_s and ν are the effective elastic modulus and Poisson's ratio for the combined ballast and subgrade layers, b is the crosstie width, and l is the crosstie length.

4.3 Model validation

The proposed model behavior can be compared with the wheel-load flexural-bending moment relationship proposed by AREMA (Figure 4.6). Also, the field collected data is incorporated into the figure and serves to verify the performance of the model. In general terms, for the initial conditions established ($S_0=6.5$ in, $B_0=32$ in, $EI=2,600,000$ k-in²), the model follows more closely the field data and therefore, provides a better estimate of the actual dynamic demand experienced by the crossties in revenue service.

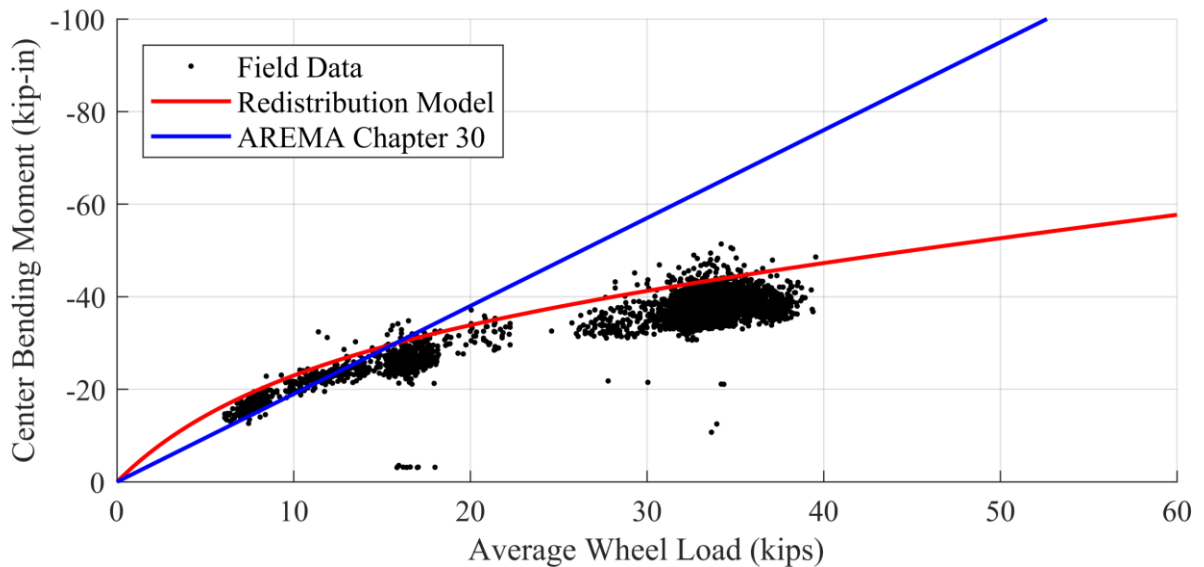


Figure 4.7: Comparison of redistribution model and AREMA recommend wheel load-flexural bending moment relationship

While this model makes several assumptions that limit its applicability, it aims to be a first approximation of the mechanical behavior observed on the field data. A more refined

approach making use of contact mechanics and two-parameter foundation models could be further developed based on this initial model.

An initial model validation requires evidence that supports the two primary hypotheses and assumptions behind the proposed model: 1) skew reduces in a non-linear manner as load increases and 2) effective ballast bearing length remains constant as wheel load increases.

Back-calculation of the support condition from strain gauge data has proven to be a useful technique to characterize the support parameters of concrete crossties (Gao et al., 2017a). I used the algorithm they developed (Gao et al., 2017a, 2017c) as a basis to develop a revised back-calculator using the structural analysis model described in Chapter 3. The optimization algorithm of the back-calculator has four outputs: effective ballast support length for each rail seat (B_1 , and B_2), and the ballast support skew for each rail seat (S_1 and S_2).

The field data shown in Figure 4.7 were grouped into 1-kip bins based on their wheel loads. Within each bin, all wheel passes were analyzed with the support condition back-calculator. Outputs from this analysis were an average rail-seat-effective width and average rail-seat-support skew. Each of the bins were characterized by the average value and standard deviation of the parameters, back-calculated for each wheel pass.

Data presented in Figure 4.8 show the average field data, back-calculated support-skew values. 95% confidence intervals were computed and presented in the graph. Also shown are the lines representing the proposed skew value relationship for different crosstie structural analysis models and the wheel-load skew relationship estimated by the redistribution algorithm. Initial skew values were defined at 6.5 in. as estimated from visual analysis of the field data. The constant effective support length of 33 in. was selected based on the one-third effective support length proposed by Clarke (1957) and recommended by the AREMA MRE Chapter 16

(2017b). The non-linearity of the wheel load and skew relationship is evident, and the results of the redistribution model proposed are satisfactory.

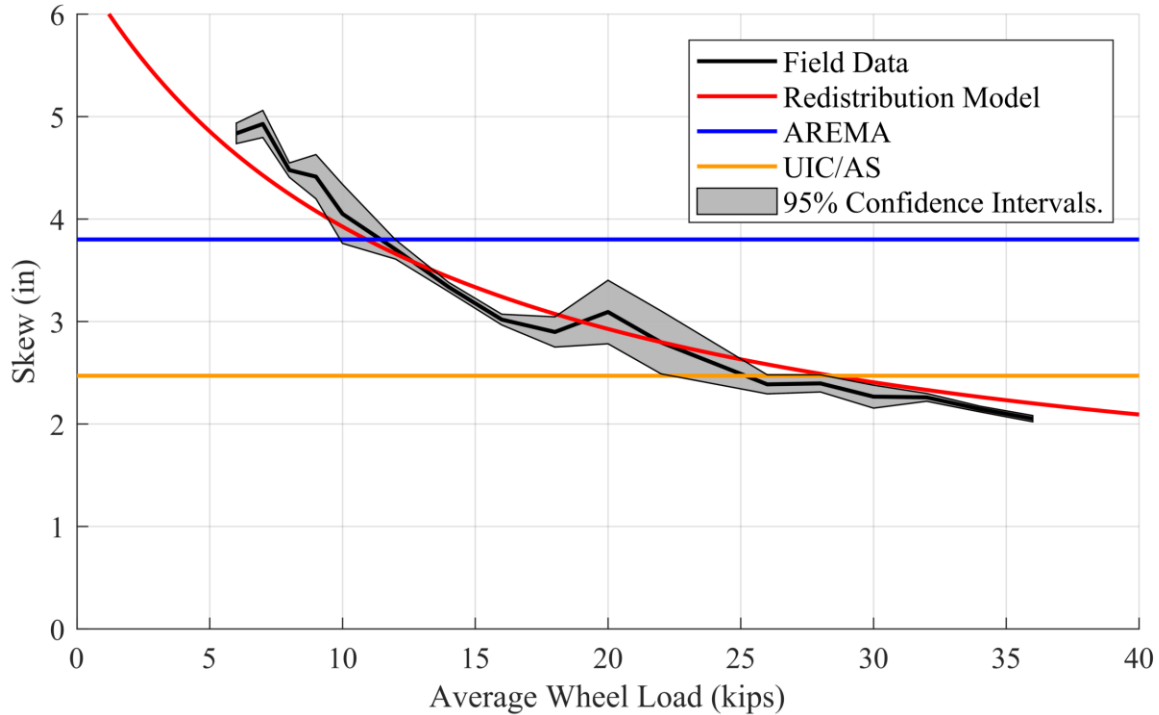


Figure 4.8: Comparison of wheel load-skew relationship values for multiple ballast support models

From an analytical point of view, the skew value is proportional to the magnitude of the center bending moment. Therefore, there are two areas of key importance in Figure 4.8. The first is all the field data points falling below the line representing the AREMA MRE Chapter 30 implicit skew value. In this region, AREMA recommendations will generate a higher flexural bending moment than field data suggests. In this sense, the model is conservative. The second area includes the field data located above the aforementioned line, an area in which the model underestimates bending demand (i.e. field data indicate greater bending moments).

The AREMA MRE is a set of recommended practices for design, while the support redistribution model presented in this work is an analysis tool. As such, the objectives of both are different. The latter aims to quantify the expected average behavior of the components, while the former is conservative by nature, trying to model a *reasonable* worst-case scenario. On this basis, I expected that the AREMA methodology would prove conservative; however, it also shows that strict use of the current design method could be marginally appropriate for light wheel load applications. Nevertheless, the current use of impact load factors could offset this deficiency and provide reasonably-conservative values.

The relationship between wheel load and effective rail seat bearing length was also back-calculated (Figure 4.8). No clear trend is visible in the relationship between wheel load and effective support width. While in general, the effective bearing length is lower than any other model, the value tends to stabilize around 33 in. which is approximately one-third of the crosstie length. The absence of any visible trend indicates that the assumption of constant bearing support length is valid.

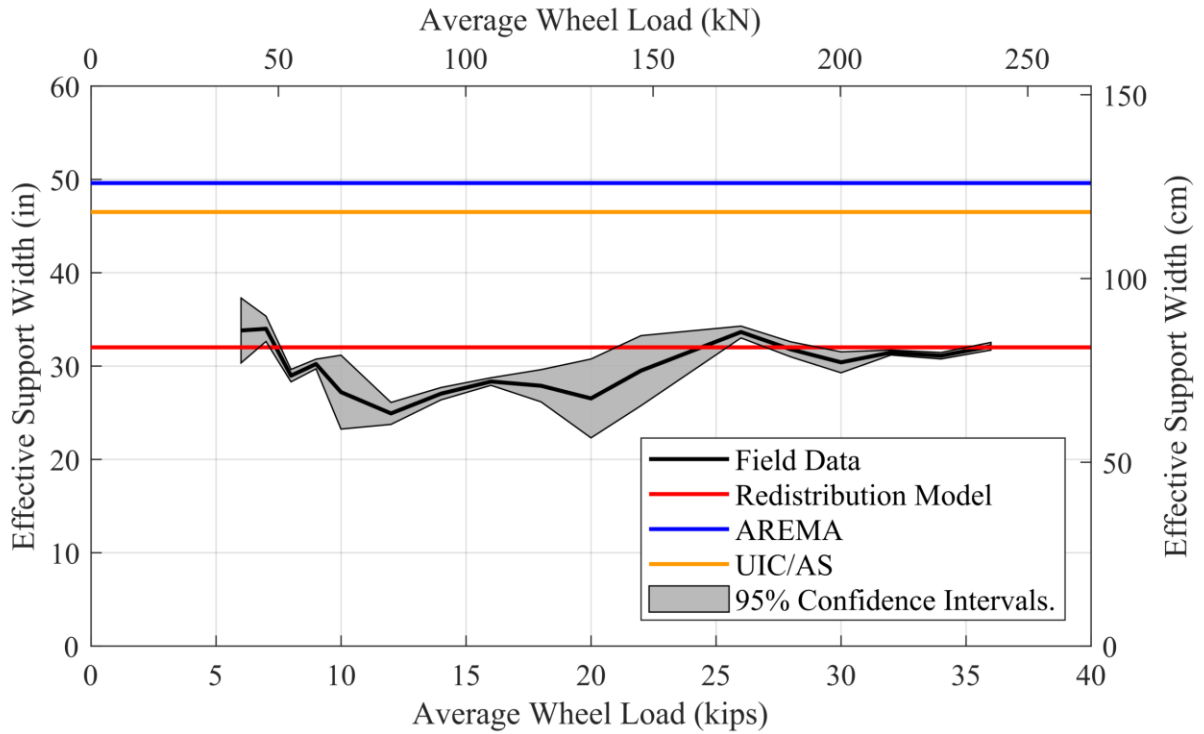


Figure 4.9: Comparison of wheel load-effective ballast support length relationship for multiple ballast support models

Once these assumptions are validated, the model could be used to improve upon the support condition extrapolation analysis performed in Chapter 2. The results presented in Figure 2.14 and Figure 2.15 did not consider any dynamic change of the support condition as a result of the interaction between the deflected cross-tie shape and ballast layer. Considering the observed phenomenon of support redistribution, the data presented in the aforementioned figures could be overestimating the possible flexural demand. The use of the proposed support redistribution algorithm on the analysis of the center region of the cross-tie allows a more realistic estimation of the probable flexural demand levels for different initial support conditions (Figure 4.10).

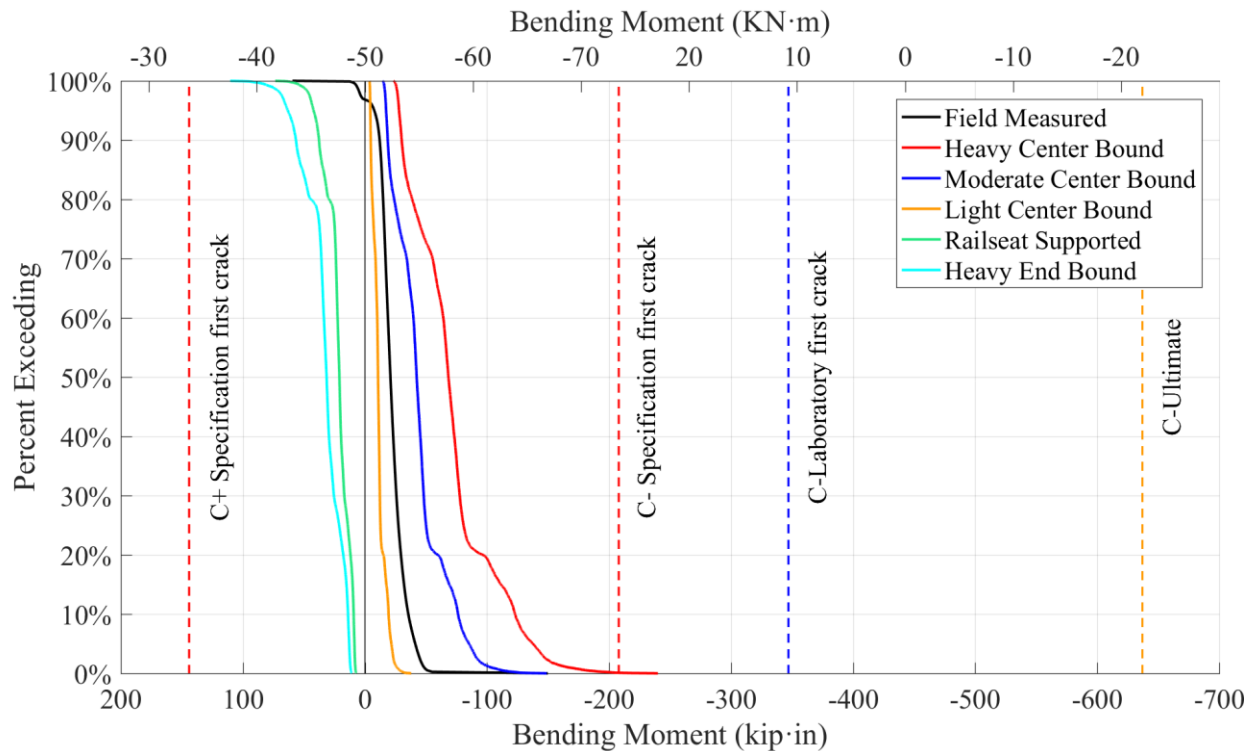


Figure 4.10: Extrapolated bending flexural bending moments of prestressed concrete cross-ties on center region incorporating support redistribution algorithm.

Considering the observed wheel loads and the empirically observed performance of the cross-ties, it is evident that the updated estimations show a more realistic distribution. In this case, it is possible for the bending moments to surpass the specification thresholds and therefore, cracking should be expected at places with highly degraded support conditions. However, ultimate failure is not expected, which aligns with the observed field performance of cross-ties. In the case of Amtrak’s NEC, these data offer an upper bound for the feasible bending moments based on the current wheel loading distribution.

In terms of the rail seat behavior, the results show little to no change with the inclusion of the support redistribution algorithm (Figure 4.11). The data are in close alignment with the extrapolation presented in Figure 2.15, and once again it is not expected for the bending moments to surpass the specified capacity.

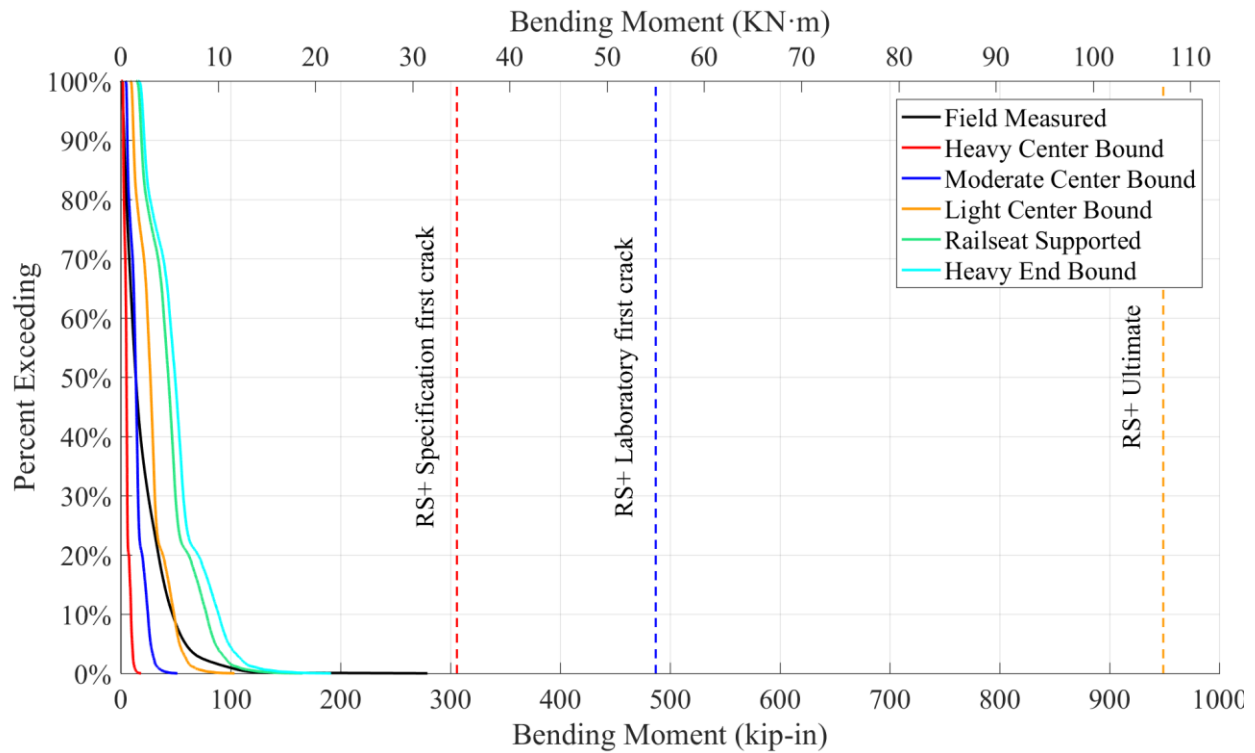


Figure 4.11: Extrapolated bending flexural bending moments of prestressed concrete cross-ties on rail seat region incorporating support redistribution algorithm.

4.4 Conclusions and recommendations

The observed discrepancy between wheel load and measured bending moments under shared corridor field loading conditions could be explained by a dynamic support condition phenomenon that has not previously been quantified. The model I developed closely matches the revenue service field data obtained on Amtrak’s NEC and provides an accurate estimate of the field demand that quasi-static loads produce on the cross-ties. Outside of the scope of this model is the effect of high frequency, low deflection impact loads that can cause sudden spikes in the internal stresses of concrete cross-ties leading to the development of cracks under revenue service conditions. However, this model provides an initial theoretical background for the structural analysis of cross-ties and the effects of the interaction on the cross-tie-ballast interface.

In general terms, it can be concluded that:

- There is evidence of a dynamic support condition under concrete crossties that is dependent on rail seat loads and component mechanical properties.
- There is evidence that support redistribution is related to the mechanics of ballast-crosstie interaction.
- Current design methodologies may be overestimating center-negative bending moments under heavy axle load (HAL) freight railroad loading environments.
- Current design methodologies may be underestimating center-negative bending moments in light wheel load environments.

CHAPTER 5: SENSITIVITY OF REDISTRIBUTION MODEL AND EFFECTS OF TEMPERATURE ON SUPPORT CONDITION DEFINITION

5.1 Introduction

The support redistribution model introduced in the previous chapter provides an analytical explanation of the non-linearity between wheel loads and bending moments in crossties. The model incorporates multiple geometrical and material parameters and requires the user to define the initial ballast support conditions. In this chapter I present a sensitivity analysis of the model with the objectives of:

- Increasing the understanding of the relationships between model input and outputs, and their physical meanings.
- Validating the expected behavior of the model under common input values and expected deviations from these values.
- Finding essential connections between input characteristics and output results that could explain empirical track behavior observations.

5.2 Model sensitivity analysis

5.2.1 Model variables

The support redistribution model requires four parameters: 1) initial support width (B_0), 2) initial support skew (S_0), 3) crosstie stiffness (EI), and 4) ballast support reaction (k). The first two values define the initial support conditions and describe the ballast distribution under the crosstie before any load application. Crosstie stiffness is directly related to the material constituent properties such as Young's Modulus and component geometry (Moment of Inertia). Finally, the ballast support reaction (k_b) characterizes the ballast layer as a Winkler foundation,

where a layer of closely spaced springs support the crosstie, in a similar arrangement as proposed by Cai et al. (1994).

5.2.2 Methodology

Based on observations from field data used for the validation of the model that were presented in Chapter 4, a realistic base scenario was selected. Variations of this initial base scenario were prepared by modifying the magnitude of a specific parameter while keeping the others constant, in order to isolate the effect of each input on the model output values. I used an axle load of 80 kips, which based on the WILD data represents a reasonable upper bound for most wheel loads in the field. For the concrete crosstie I assumed a stiffness value of 2,600,000 kip·in² (experimentally measured in the laboratory), and a ballast support stiffness of 7 ksi/in based the results of Cai et al. (1994).

5.2.3 Effects of initial support with (B_0) on model response

The maximum theoretical value of support width per rail seat is half the crosstie length (i.e., 51 in. for most crosstie designs). This length corresponds to a uniformly supported crosstie and could serve as an upper bound for the purposes of this sensitivity analysis. However, due to the geometry constraints described by Equation 3-19, it would imply a fixed skew value of 4.5 in. Any proposed increase for sensitivity purposes would violate the mathematical model relationships. Therefore, a practical upper limit for support width was defined as 45 in. Reductions of this value in increments of 5 in. down to a minimum value of 10 in. were included.

In both the center (Figure 5.1) and rail seat (Figure 5.2) sections of the crosstie, it can be seen that the narrow support widths are related to lower bending moments. In other words, a

reduced support width maximizes the effect of the support redistribution phenomenon. At the rail seat section, this reduced support width even facilitates the development of rail seat negative bending moments, albeit at a low magnitude. As part of the validation analysis of the model presented in the previous chapter, I found that the back-calculated value of B_0 had very low variability and varied primarily between 25 and 35 in. Therefore, the extreme cases observed in this sensitivity analysis are not expected under actual field conditions.

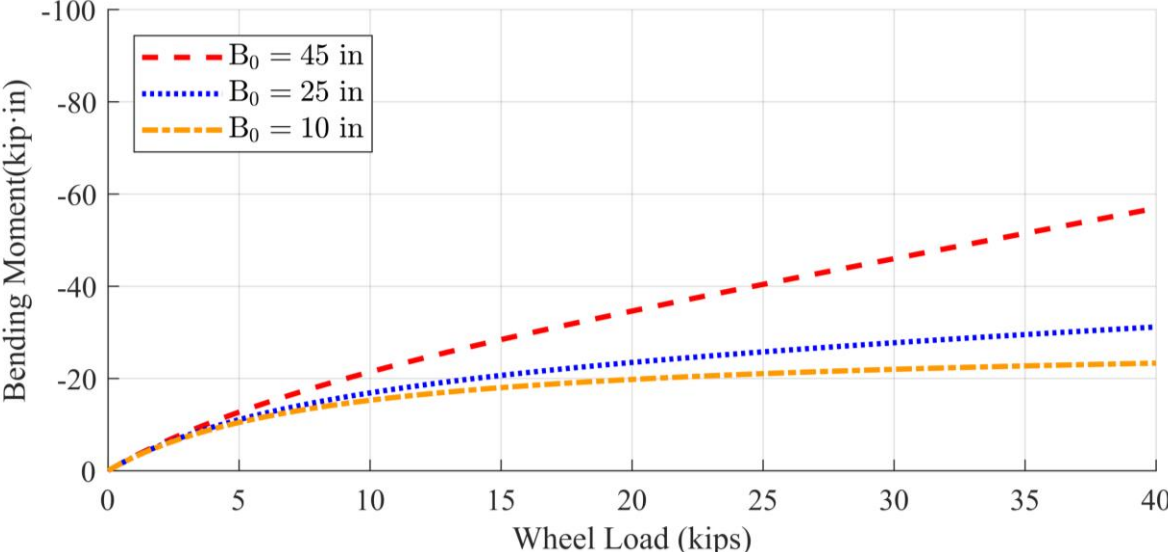


Figure 5.1: Flexural response of crosstie center region to changes in the initial support width in the proposed support redistribution model

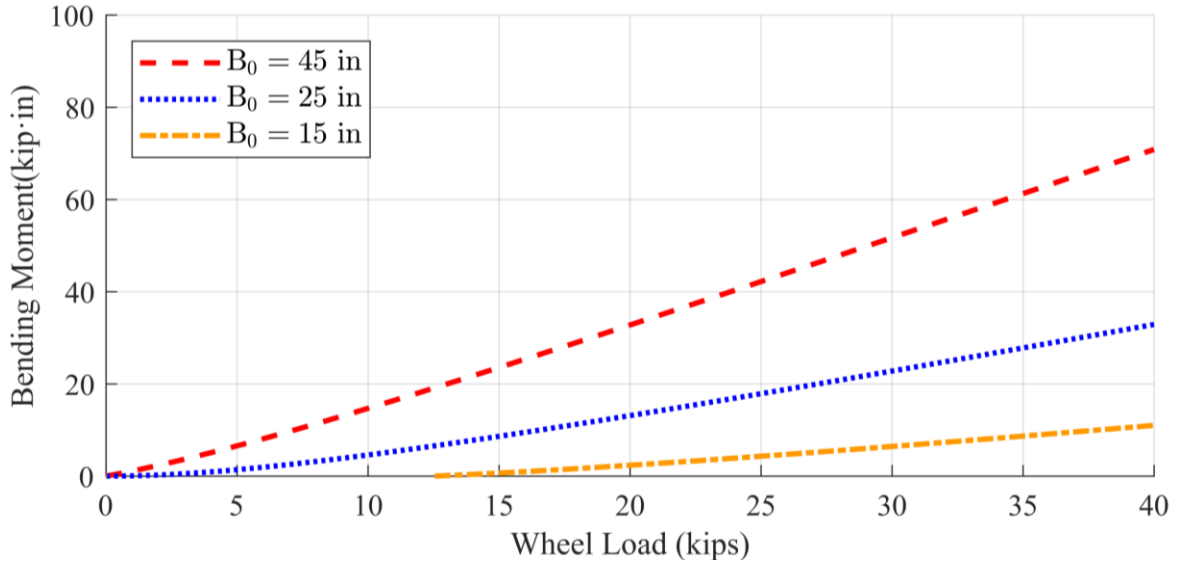


Figure 5.2: Flexural response of a crosstie rail seat region to changes in the initial support width in the proposed support redistribution model

5.2.4 Effects of initial support skew (S_0) on model response

The magnitude of support skew is a direct measurement of how center bound a crosstie is in the field. I hypothesize that the initial support skew of the crosstie is related to interval since last tamping, tonnage since last tamping, thermally-induced crosstie curling and possibly other factors. Long-term experimentation would allow the inclusion of these parameters into the structural analysis of concrete crossties. Based on the model validation discussion presented in Chapter 4, I selected a practical maximum support skew value of 12 in. I decreased this value in 2 in. decrements to a minimum value of 2 in. A skew value of zero corresponds to the condition of perfectly symmetrical support relative to the center of the rail seat, and therefore it is expected to generate no flexural effect on the center of the crosstie.

In both the center (Figure 5.3) and rail seat (Figure 5.4) sections of the crosstie, it can be seen that the flexural response was highly non-linear for high skew values (i.e., $S_0=12$ in) and gradually transitioned to a linear response. This implies that support redistribution is a factor

that plays a significant role in cross-ties with a high center-bound condition. Well maintained track, where support skew is expected to be low, should exhibit a response that is in alignment with current design practices.

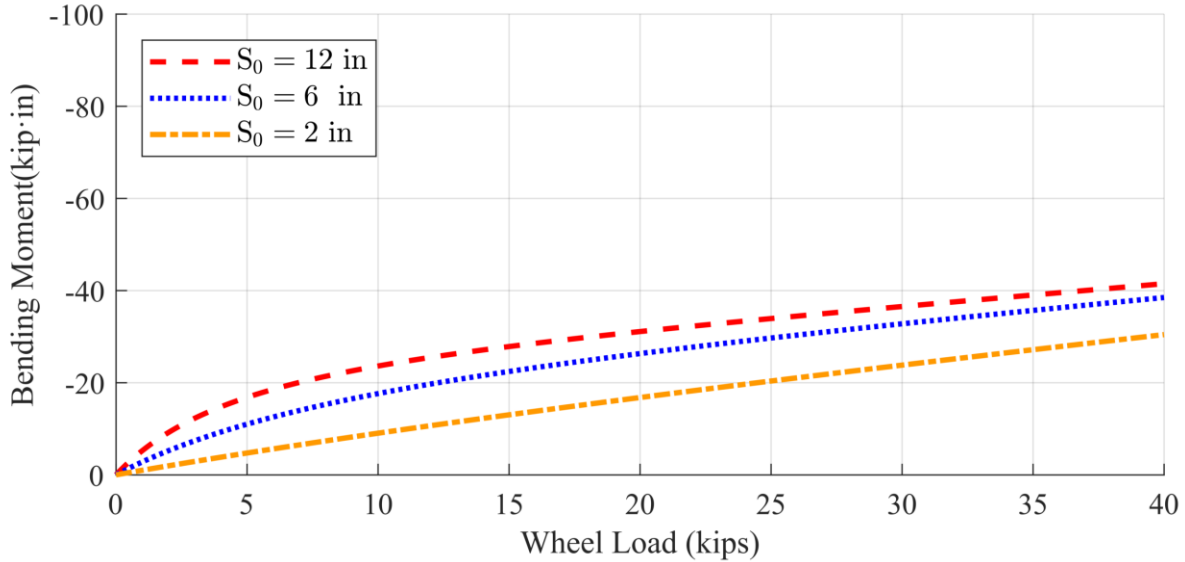


Figure 5.3: Flexural response of a cross-tie center region to changes in the initial skew width in the proposed support redistribution model

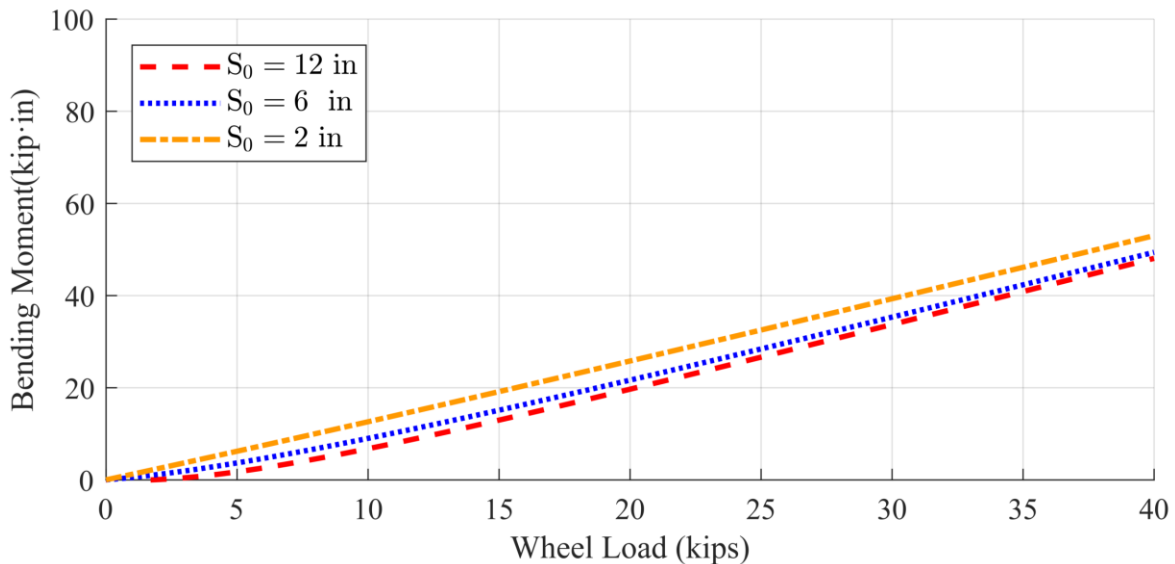


Figure 5.4: Flexural response of a cross-tie rail seat region to changes in the initial skew width in the proposed support redistribution model

5.2.5 *Effects of crosstie stiffness (EI) on model response*

Crosstie stiffness is related to the mechanical properties of the material and geometry. The inclusion of this parameter in the model allows for the calculation of crosstie deflections and normalizes the model outputs for different crosstie materials. Therefore, from a theoretical point of view, the proposed redistribution model could be used for the calculation of the flexural response of timber, composite, steel, and concrete crossties. However, as the model validation was only performed on data obtained from a section of track using concrete crossties, further analysis is required to validate the use of the model in different conditions.

Laboratory measured stiffness of concrete crossties has been performed by Bastos et al. (2018) as part of a proposed testing protocol for AREMA. The base scenario of $EI=2,600,000$ $\text{ksi}\cdot\text{in}^2$ represents the laboratory-measured stiffness of the crossties located at the field site where the data used for model validation were obtained. An upper bound of $3,500,000$ $\text{ksi}\cdot\text{in}^2$ was selected considering the potential use of higher strength concrete and a deeper crosstie section. Based on AREMA Chapter 30 (Ties) (2017a) material property reference data, a lower bound was selected considering a smaller rail transit concrete crosstie cross-section. This value was set as $500,000$ $\text{ksi}\cdot\text{in}^2$, representative of the most flexible (lowest flexural rigidity) concrete crossties in use in North America.

I used the model to analyze the effect of crosstie stiffness at three values for the center region of the crosstie (Figure 5.5). A more flexible crosstie will deflect more and therefore have a more pronounced interaction with the underlying ballast. As such, the effects of support redistribution are more evident and minimize the flexural response of the crosstie over time. This could explain the generally satisfactory performance of timber crossties on high density, well-maintained track, even in today's HAL freight railroad operating environment. On the

other hand, a rigid crossie will induce higher bending moments to the component for the same base scenario. In the case of the rail seat (Figure 5.6) the model sensitivity is significantly lower, and the observed trend is linear, indicating that crossie stiffness plays a limited role on the flexural response of the rail seat with or without support redistribution.

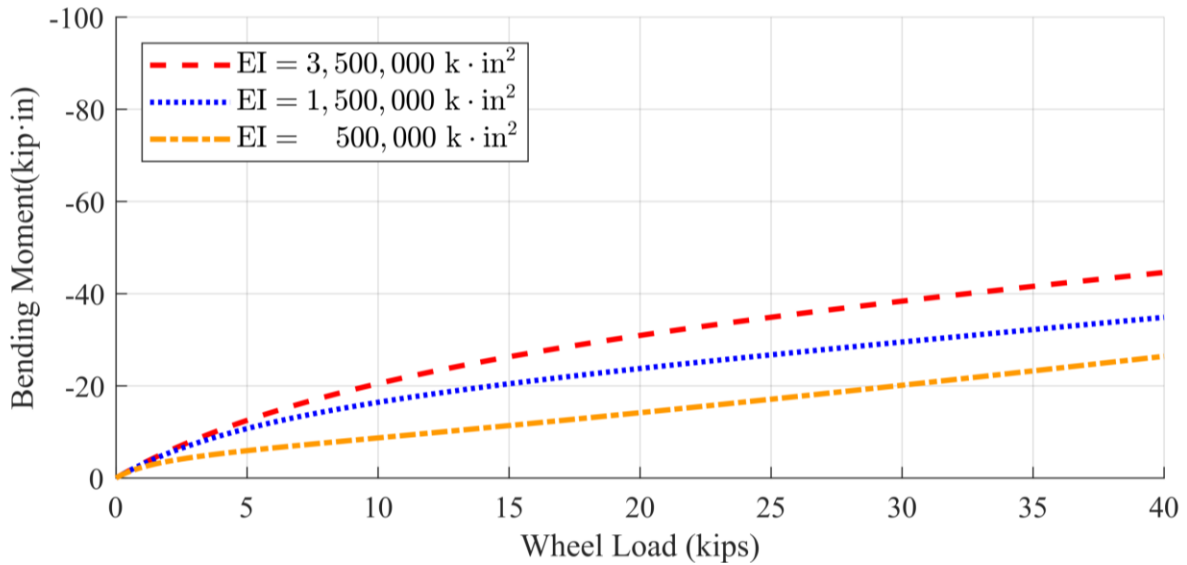


Figure 5.5: Flexural response of a crossie center region due to changes in the crossie stiffness in the proposed support redistribution model

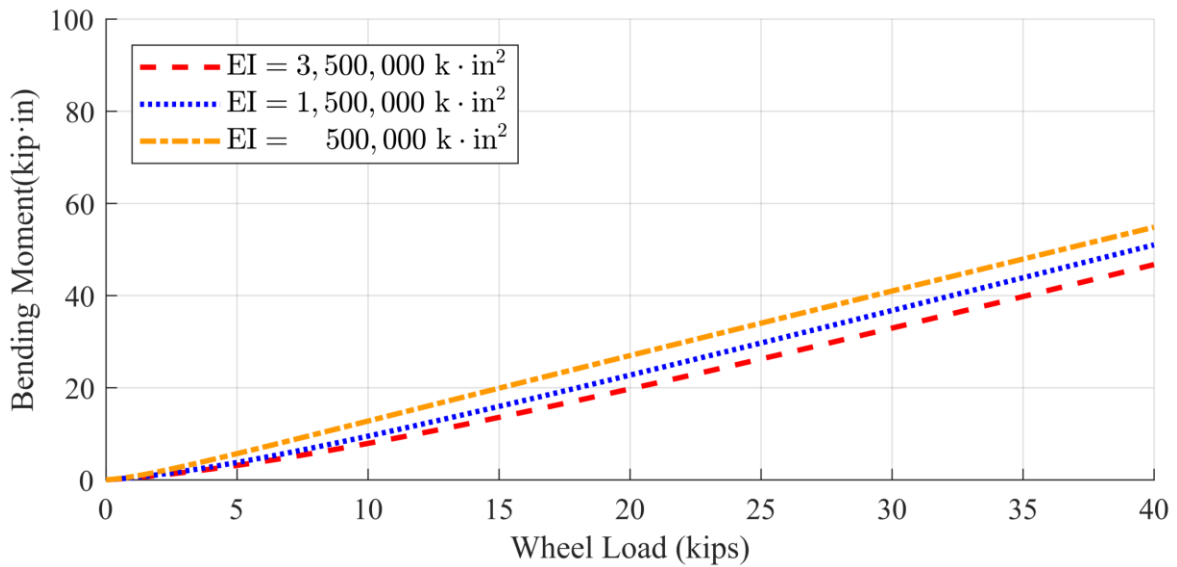


Figure 5.6: Flexural response of a crossie rail seat region due to changes in the crossie stiffness in the proposed support redistribution model

5.2.6 *Effects of ballast stiffness (k_s) on model response*

The crosstie is modeled as a body on an elastic Winkler foundation. This foundation is characterized by closely spaced linear springs with an elastic constant k_s connecting the bottom of the crosstie with an infinitely stiff subgrade. As described in previous chapters, k_s is related to ballast mechanical properties such as the material elastic modulus and Poisson's ratio and geometric parameters related to the crosstie length and width. Based on Equation 4-2 and common ballast mechanical properties according to Cai et al. (1994), it is possible to calculate a common range of values for k_s . I selected a maximum value of 7 ksi/in as an upper bound, corresponding to a rigid compacted ballast layer. The lower bound, 1 ksi/in characterizes a soft ballast/subgrade, with poor compaction and possibly saturated with water.

This parameter (k_s) proved to be the most significant component of the redistribution model, which was expected, given the influence of track stiffness on other track component loading demands (Kerr, 2003). Figure 5.7 and Figure 5.8 show the results of the sensitivity analysis for the center and rail seat flexural response, respectively. Flexible support reduces the effects of support redistribution and therefore, approaches the linear behavior described by the current design guides. Increasing the support stiffness magnifies the effect of support redistribution as the crosstie's deflected shape must overcome a higher reaction imparted by the ballast.

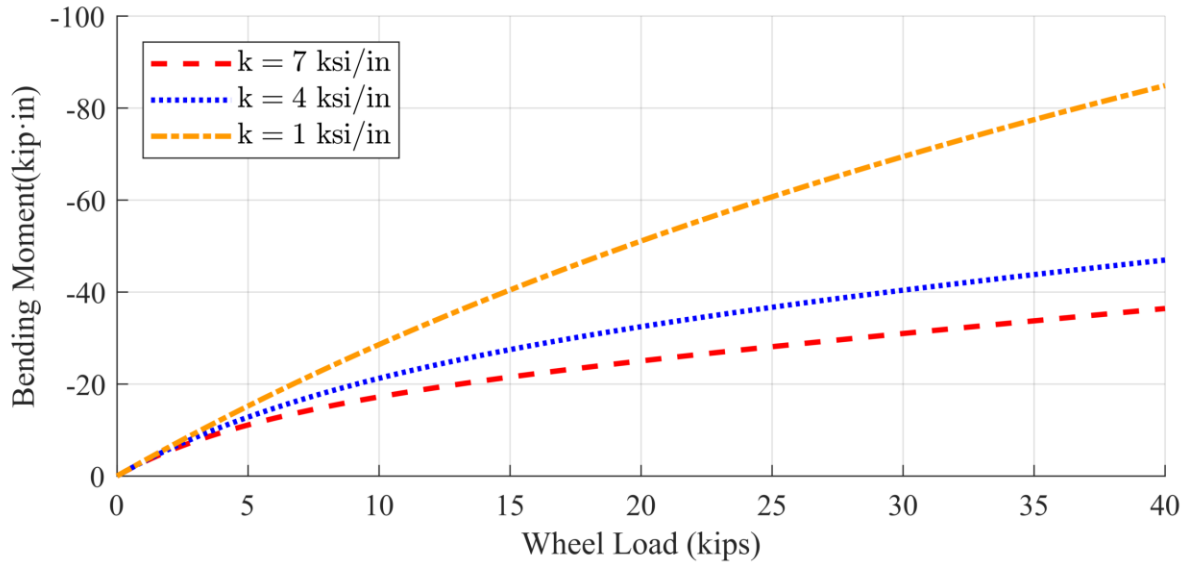


Figure 5.7: Flexural response of a crosstie center region due to changes in ballast stiffness in the proposed support redistribution model

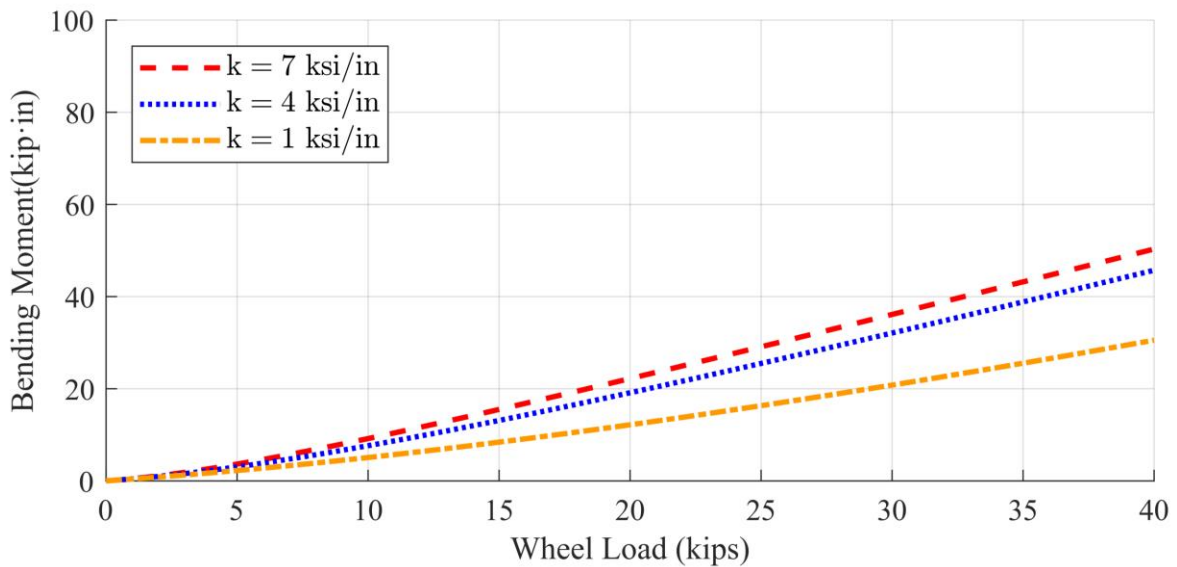


Figure 5.8: Flexural response of a crosstie rail seat region due to changes in ballast stiffness in the proposed support redistribution model

5.2.7 Effect of parameter variability on model sensitivity

Based on the previous analysis, it is possible to identify an adequate combination of support and component characteristics that would originate an optimal or suboptimal scenario for

the development of the flexural demand. In the case of the center region of the crosstie, Figure 5.9 shows these scenarios in comparison with the field captured values. These are also compared to a projection obtained using the AREMA recommended analysis model. The suboptimal scenario for the crosstie flexural response involves a rigid crosstie on a soft ballast layer. Under these conditions, the bending moments could be substantially higher than the specified capacity of a crosstie designed in accordance with AREMA. AREMA only aims to quantify a *reasonable* worst-case scenario for flexural demand under typical operating conditions. While not common under an effective ballast maintenance schedule, the combination of rigid crossties in poor ballast might be the explanation for cracks and failure of concrete crossties even when field data at other locations indicate that the demand is lower than the crosstie’s capacity. Soft spots, or “mud spots,” are not generally found at track instrumentation sites but may magnify the flexural response of the crossties as well as wheel loads and impacts, increasing the total demand of the crosstie.

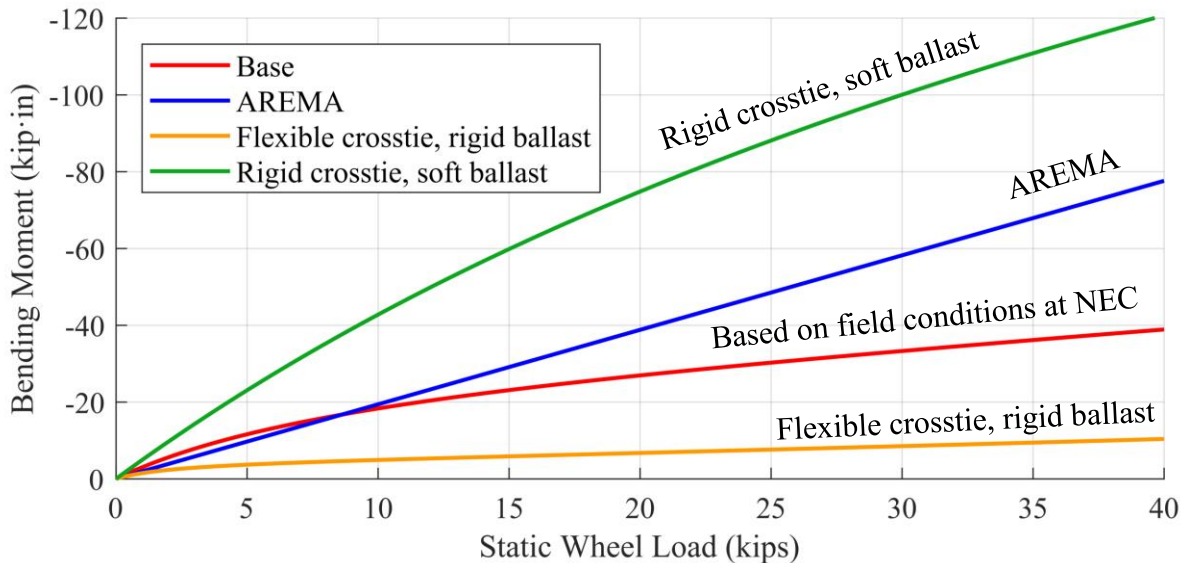


Figure 5.9: Potential variability of crosstie center flexural response as a function of support redistribution model parameters

In the case of the rail seat, the effects of the support redistribution are not as significant (Figure 5.10). As previously noted, the sensitivity of the rail seats to changes in the support condition is limited. Therefore, most of the curves reflect a quasi-linear relationship. The AREMA recommended model follows closely the suboptimal scenario characterized in this case by flexible crosstie on rigid support. Based on these scenarios it is possible to explain the adequate rail seat performance of concrete crossties under heavy axle loads. The high stiffness of both the component and the ballast on those sections minimizes the development of flexural demand and therefore improves performance. Concrete crossties are not expected to experience flexural cracks in the rail seat provided that the rolling stock condition results in reasonably low impact factors.

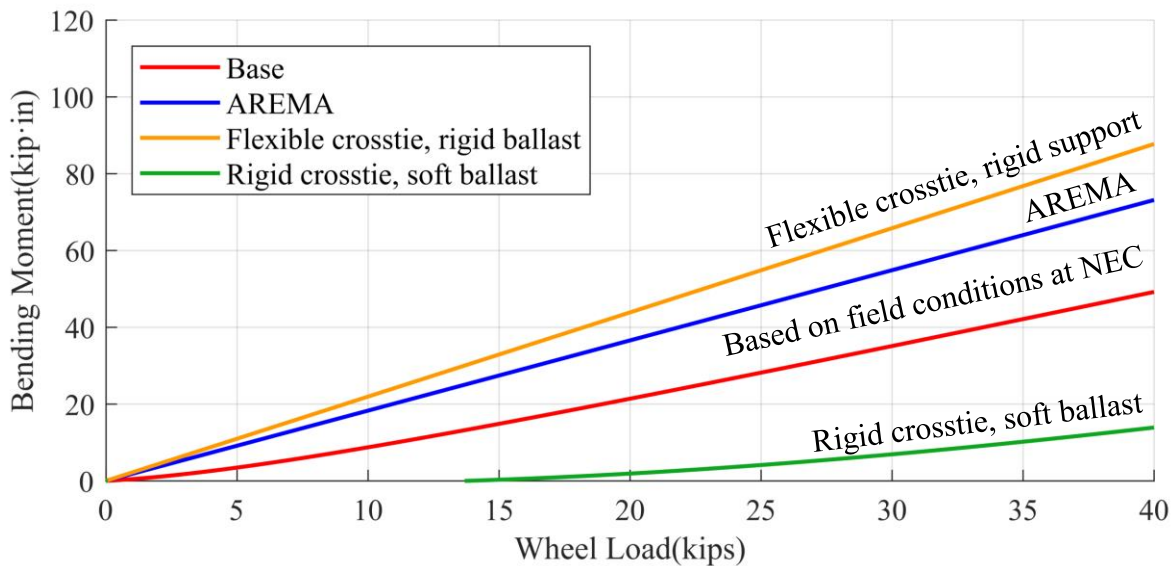


Figure 5.10: Potential variability of rail seat center flexural response as a function of support redistribution model parameters

5.3 Temperature effects on initial support conditions

In addition to support and loading conditions, crossties are subjected to various environmental conditions. Temperature-induced thermal gradients due to solar radiation and

thermal properties of concrete have the potential to generate important internal strains. This has been studied extensively on prestressed concrete girders (Barr et al., 2005), pavement concrete slabs (Armaghani et al., 1987; Richardson and Armaghani, 1987; Thompson et al., 1987; Mohamed and Hansen, 1996; Yu et al., 1998), and concrete crossties (Wolf et al., 2016; Canga Ruiz, 2018). In the particular case of concrete crossties, laboratory and field experimentation on HAL freight railroad sites (Wolf et al., 2016) and rail transit locations (Canga Ruiz, 2018) show that high negative temperature differentials increase the flexural bending moments at the center of the crosstie, while high positive temperature differentials tend to minimize the development of center bending moments.

Changes in the support condition of the crosstie due to the induced thermal curling have been identified as the leading reason for the variation of flexural bending moments due to temperature gradients (Wolf et al., 2016). As the crosstie is not rigidly constrained by the ballast, the crosstie will exhibit unrestrained changes in its geometry (Figure 5.11). This will change the contact points in the crosstie-ballast interface and therefore alter the support condition of the crosstie.

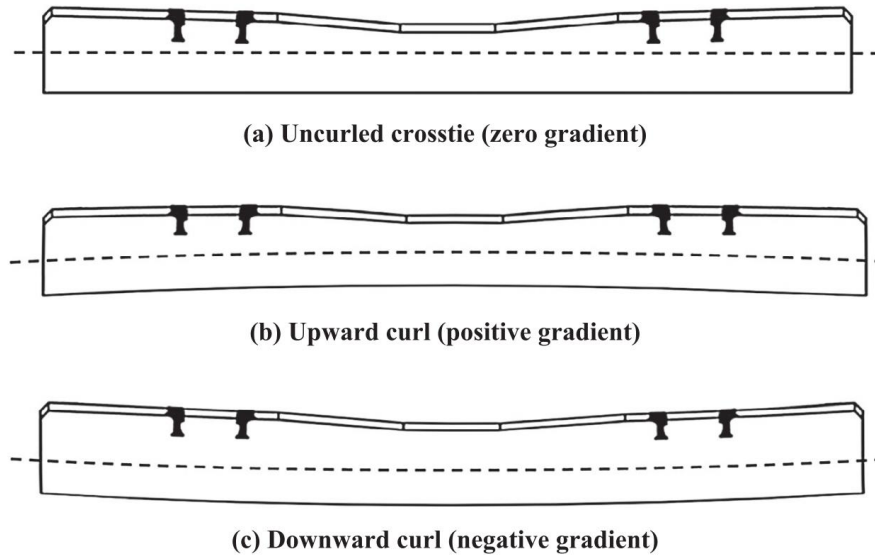


Figure 5.11: Schematic drawings of concrete crosstie curling geometry (Wolf et al., 2016)

Since the proposed crosstie analytical model provides a parametric method for characterizing the support condition, it can be used to analyze the effects of temperature-induced curling of crossties. The back-calculator previously developed provides a tool to measure the changes in the support condition as the crosstie experiences varying temperature differentials, following a similar methodology as the one used for the redistribution model validation. Furthermore, the effects of curling could be incorporated into the redistribution model in terms of an initial skew value. In this way, the initial skew value can serve as an indicator of center binding due to ballast degradation and also due to the temperature induced curling.

5.3.1 *Effect of temperature differentials on crosstie behavior*

The previously-used dataset for model validation also contains crosstie temperature data of the top and bottom chamfers. Therefore, I was able to calculate the temperature differential of the crosstie and then correlate it with the measured bending moment. Filtering the dataset to include only peak wheel loads within a narrow range (in this case between 22.5 and 23.5 kips)

allowed me to isolate the effect of temperature gradient on the flexural response of the crosstie. (Figure 5.12). The previously-observed trend of high-temperature differentials mapping to a reduction of bending moments is evident on the filtered data set.

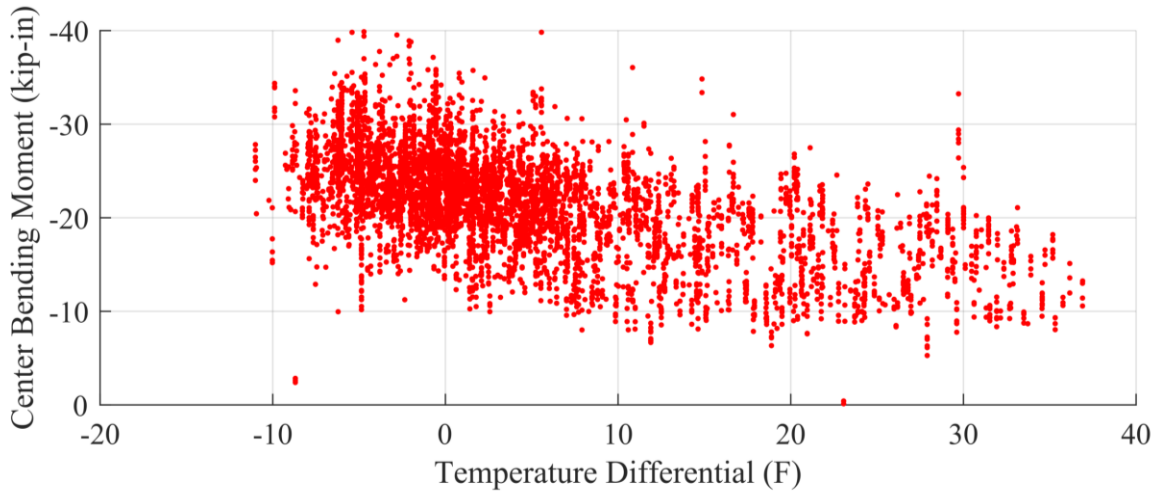


Figure 5.12: Relationship between field-measured temperature differential and the flexural bending moment at the center of the crosstie for peak wheel loads between 22.5 and 23.5 kips.

5.3.2 *Effect of temperature differentials on crosstie support condition*

The field temperature differential data shown in Figure 5.12 were grouped into one-degree Fahrenheit bins. Within each bin, all wheel passes were analyzed with the support condition back-calculator. Outputs obtained from this analysis include an average rail seat effective support width (B_i) and average rail seat support skew (S_i). The standard deviation of each average value was calculated to characterize its variability.

Figure 5.13 shows the results of the average back-calculated skew as a function of the temperature differential between the top and bottom of the crosstie. The observed linear trend aligns well with the observed behavior of the relationship between temperature differential and flexural bending moment (Wolf et al., 2016; Canga Ruiz, 2018). The crosstie curling modifies

the support condition, reducing how center bound the crosstie is as the temperature differential increases. This is consistent with the expected behavior as positive temperature facilitates upward curl that minimizes contact at the center of the crosstie and therefore, reduces the center bound condition.

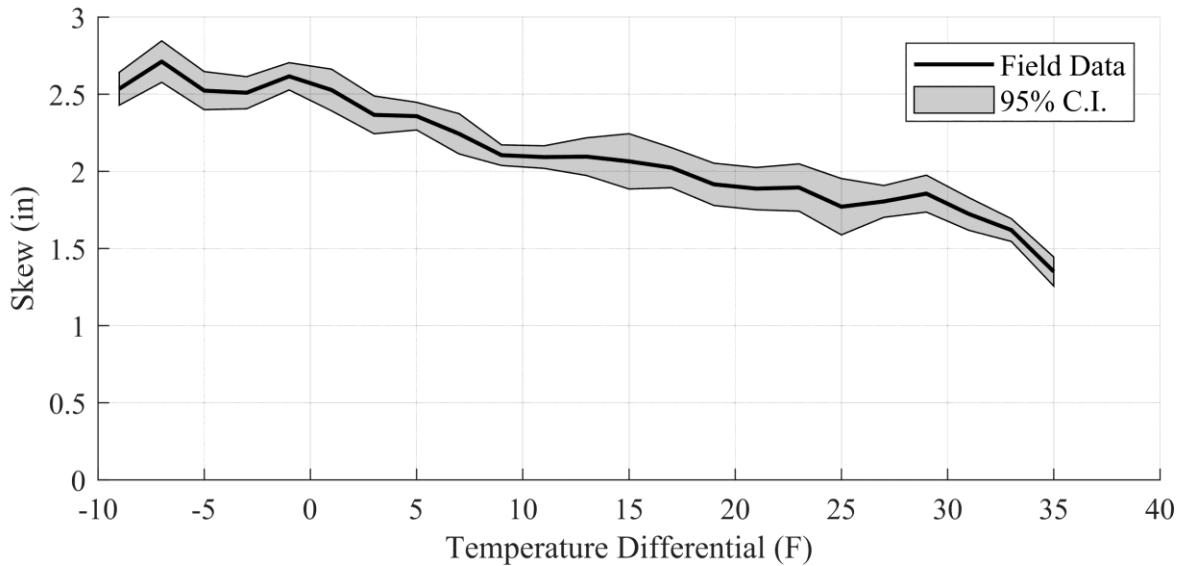


Figure 5.13: Back-calculated support skew values as a function of temperature differential

While the support skew declines as the crosstie curls upwards, the support width remains more or less constant (Figure 5.14). The data suggest little to no correlation between increasing temperature differentials and the magnitude of the parameter over all temperatures.

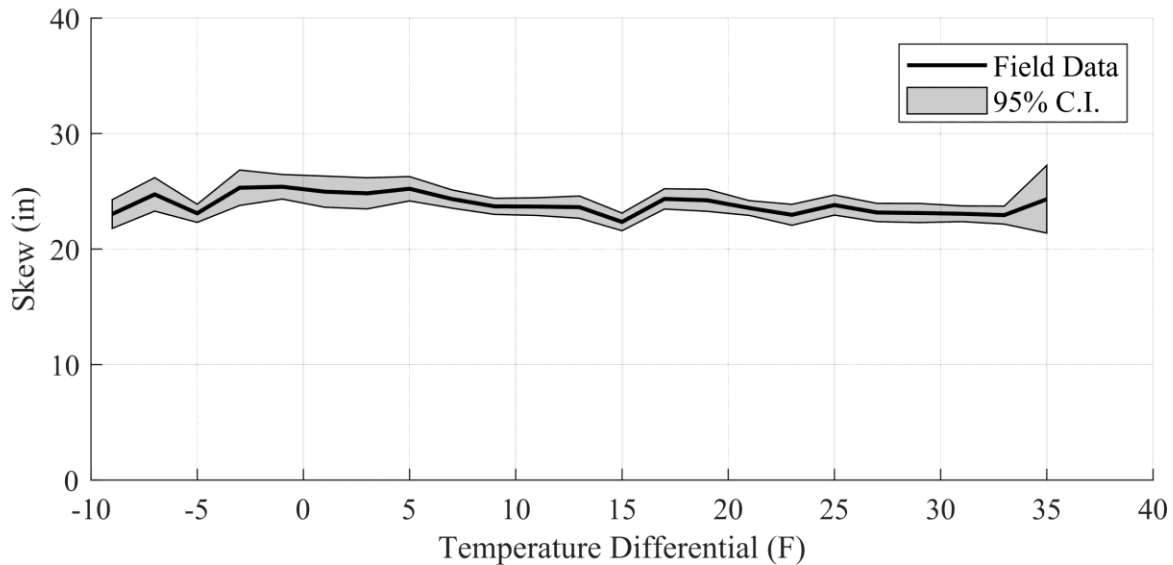


Figure 5.14: Back-calculated support width values as a function of temperature differential

5.4 Conclusions

While the support redistribution model explains the non-linearity in the effect of wheel loads and bending moments in concrete crossties, the effects of each model parameter in the flexural response of the crosstie was not fully understood. The sensitivity analysis I performed enabled identification the key metrics and relationships that describe the development of the phenomenon. The study highlights the critical importance of performing ballast maintenance throughout the life of the crosstie. The results of the model suggest the reduction of center negative bending moments, but it does not explain the observed presence of cracks in crossties in specific regions. The sensitivity analysis showed that poor ballast layer stiffness could induce bending moments that exceed design recommendations and/or crosstie capacity. This is consistent with observed field behavior and observations.

Crosstie stiffness also has an essential role in the model mechanics. Timber crossties have long been the principal type used in North America and continue to have the largest market share compared to concrete or composite materials (Railway Tie Association, 2017). Based on

the results of the model, the timber crosstie's record of field performance can be partially explained by its flexibility, as it allows greater conformity with the ballast and therefore induces support redistribution much more effectively than the more rigid concrete crossties. Recent developments in high-strength, low-modulus concrete could improve this aspect of concrete crossties, and narrow this performance gap (Rizos, 2016; Zeitouni et al., 2018).

The final parameters in terms of importance are the initial crosstie conditions before loading. These values could be characterized for a particular crosstie in relation to the following parameters: 1) crosstie temperature distribution, 2) time since ballast maintenance cycle and 3) tonnage since last ballast maintenance cycle. This chapter provides preliminary data and conclusions related to the effects of temperature differentials and shows how the crosstie curling affects the support parameters (skew and width). Those changes in support condition explain the observed temperature dependence of the flexural response of crossties. Future research is needed to characterize the unloaded support characteristics of concrete crossties. Specifically, long-term instrumentation of crossties is necessary to analyze the effects of ballast maintenance cycles and tonnage in the support characteristics.

CHAPTER 6: RECOMMENDATIONS AND FUTURE WORK

In this thesis I present research aimed at better understanding and characterizing the mechanical behavior of crossties with a specific focus on the crosstie-ballast interface.

Additionally, the thesis provided an analysis of field measured wheel load and crosstie flexural bending data that allowed the validation of the proposed crosstie analytical models.

In Chapter 1, I present an overview of the different interfaces of the track structure and the development and execution of a research plan that succeeded in filling voids in the body of knowledge related to the mechanics of the ballast-crosstie interface. Chapter 2 describes the methodology and results of the field data collected and analyzed from Amtrak's Northeast Corridor (NEC) that served as the basis for the analytical models developed. An overview of historical and current crosstie analysis models is presented in Chapter 3 along with the primary limitations of each. This chapter also establishes a new, generalized analysis model for crossties. Using this model, I develop and describe a model in Chapter 4 a model to explain the observed mechanics of the ballast-crosstie interface from an analytical point of view, which was validated using field data. Lastly, in Chapter 5 I describe an analysis that provides insight into the sensitivity of the support redistribution algorithm and evaluates the effect of temperature in the support parameters of concrete crossties.

6.1 Summary of findings

6.1.1 *The use of instrumentation for the quantification of the loading environment on mixed-use corridors (Chapter 2)*

The data captured from existing commercial field sensors such as WILD sites and experimental monitoring equipment such as instrumented crossties proved to be a valuable

resource for characterizing the loading environment of discrete points along Amtrak's NEC. While extremely valuable, it was insufficient on its own to provide meaningful information for characterizing the loading demands along an entire railroad or rail corridor. Therefore, data analysis techniques allowed for the extrapolation of the information and quantification of variability in such a way that allows for more holistic characterization of the corridor behavior and its potential variability, thereby allowing decisions to be made based on information collected at a set of discrete points. Additionally, they provide a basis for the future implementation of a reliability-based design approach, in alignment with the vision for the mechanistic design of track systems.

6.1.2 The non-linearity of wheel load-bending moment relationship and the development of a support redistribution algorithm (Chapter 4)

The observed discrepancy between wheel load and measured bending moments could have significant effects on the existing crosstie design guidelines. The modeling of static support condition independent of wheel load could be insufficient in specific load ranges and overly conservative in others. While generally not critical from a safety perspective, the analysis of this phenomenon is necessary to understand the underlying track mechanics that from which this non-linearity originate. The refinement of crosstie analytical models relates, however, to potential optimization of the component and related cost reductions. The model developed provides an efficient analytical solution based on the mechanics of the ballast-crosstie interface, incorporating elements of the ballast and crosstie stiffness and concepts from structural mechanics. The model was validated against the field data and provides an estimate of the field demand that quasi-static loads produce on the crossties.

6.1.3 The influence of parameters in the development of the support redistribution phenomenon and effects of thermal curling on crosstie support definitions (Chapter 5)

Based on the support redistribution model it was possible to analyze the effects of the system parameters on the crosstie flexural response. Increased ballast stiffness and reduced crosstie flexibility are the key ways to reduce the flexural response of the crosstie, and therefore they play a significant role in the performance of the components on field applications. Flexural failure in revenue service of concrete crossties could be related to excessive ballast degradation, low ballast quality, or low compaction, causing low ballast stiffness and therefore developing insufficient support conditions under the crossties, thereby magnifying the effects of wheel loads and exceeding component capacity. The model also provides a case for crossties with a reduced modulus of elasticity that could conform better to the ballast profile and minimize development of flexural bending moments.

Finally, the chapter introduces the effects of temperature curling on the support characteristics of concrete crossties. This curling alters the location of the support and therefore has an essential role in both the flexural response and the support redistribution phenomenon. Further analysis is necessary to understand the role of both temperature and ballast degradation on the crosstie support distribution to develop a global model for use on mechanistic track design procedures.

6.2 Recommendations and future work

6.2.1 A vision for the mechanistic-empirical design of track components and structure

Historically, railroad track design has been based on the concept of allowable stresses (Doyle, 1980; Kerr, 2003) that addresses uncertainty in load and materials using global safety

factors. However, this and other design methodologies such as Load Resistance Factor Design (LRFD) are oriented towards minimizing the probability of failure of a structure over its design life (Bulleit, 2008). Implicitly, the designer expects that the structure will not experience structural failure, at least during its specified design life. However, much like highway pavements, railroad track is a structure where failure is ultimately. After millions of cycles and vulnerability to environmental conditions, components will degrade, fatigue, and fail. The similarities in materials and function of railroad track and highway pavement make a compelling case for adopting the concepts developed for pavements in the design of track components.

The design of pavements has shifted towards predicting the life of structures, rather than directly designing components capable of handling a specified design load. This design approach provides adequate performance for a specific amount of time, rather than providing adequate performance for a specific loading scenario. From an economic perspective, knowing the life cycle performance evolution of railroad assets such as track components is compelling. It could refine railroad economic models and provide input for data-driven track maintenance practices.

The need for developing a framework for the mechanistic-empirical design of concrete crossties was identified based on some of the current research topics presented in this thesis. This high-level framework could delineate the future research needs in the area. The theoretical procedure delineated in the following sections, revolves around the design of concrete crossties, although it could be easily expanded to incorporate different components, materials, and even the complete track structure.

6.2.1.1 The general philosophy of a mechanistic-empirical design procedure

The mechanistic-empirical design method makes use of both structural mechanics for the analysis of structures and empirical relationships for damage quantification. The mechanistic portion of the procedure takes inputs such as wheel load and material properties to generate a measurable physical output such as strains, stresses, and deflections. This portion of the method is based on pure physical relationships and existing classical or modern mechanical analysis tools (i.e., beam on elastic foundation, finite element modeling (FEM), etc.). The empirical portion of this method takes the outputs of those models and relates the mechanical responses to damage with the use of transfer functions. The transfer functions calculate the relative damage a particular load application causes on the capacity of the component. Damage accumulation theories and reliability concepts are introduced to quantify the accumulated damage throughout the desired service life of the component.

This design procedure differs fundamentally from other design procedures: it does not directly provide a design (dimensions, number of prestressing strands, material strength) as an output; instead, it analyzes a candidate design and calculates the expected service life of the component/structure. Therefore, the design of a component becomes an iterative process, where candidate components with different material properties and dimensions are evaluated until one satisfies the design objectives. The process can be then repeated to obtain multiple adequate configurations that can be finally assessed from an economic standpoint to achieve the final design. The mechanistic-empirical procedure for flexible pavements is shown in Figure 6.1 and serves as a basis for the current framework.

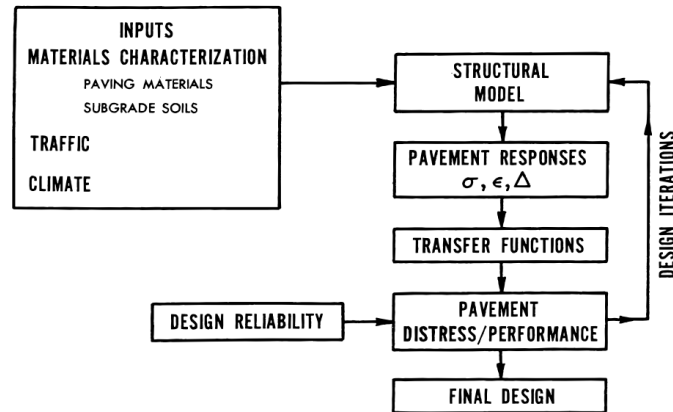


Figure 6.1: Components of mechanistic-empirical design procedure for pavements (Thompson, 1996)

When working in life cycles that are measured by decades, it must be understood that the inputs incorporated in a model will demonstrate time dependency. All materials and components will exhibit evolution of their properties due only to passage of time and exposure to environmental factors. For instance, in both railroad track structures and pavement, it is well understood that the substructure bearing capacity and modulus will change dramatically during wet or winter conditions (Huang, 2004). Previous authors (Wolf et al., 2016; Canga Ruiz, 2018) showed how the cross-tie thermal curling varies during the day due to changes in thermal gradients. Besides environmental factors, repeated loading due to traffic will degrade ballast and modify support conditions as well. Eventually, surfacing maintenance will restore partially the mechanical behavior of the ballast layer. Therefore, the mechanistic section of the procedure will change its inputs during the analysis period.

Considering all the previous factors, Figure 6.2 shows a proposed mechanistic-empirical design procedure for concrete cross-ties. An additional component of the flowchart in relation to Figure 6.1 was incorporated to recognize the previously described dynamic nature of railroad track. Further sections of the present document will briefly analyze each component of the

proposed mechanistic-empirical method and briefly identify the research needs for the development of a mechanistic-empirical design procedure.

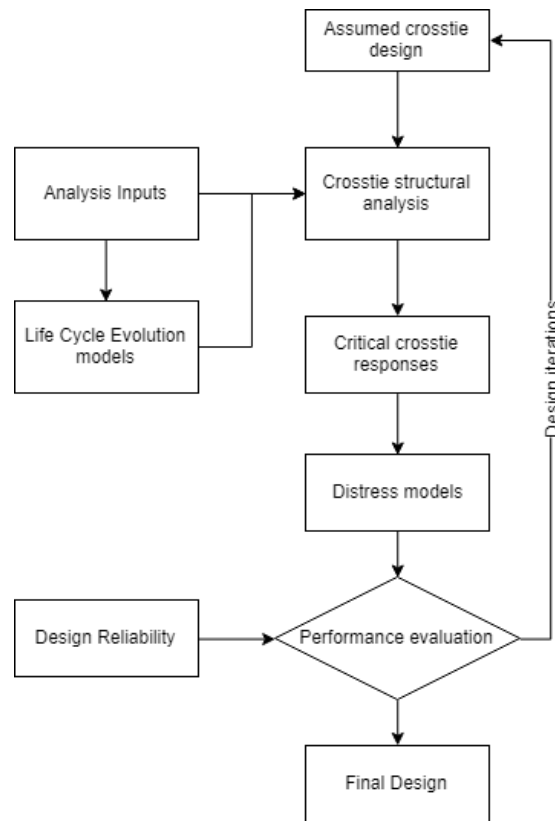


Figure 6.2: Proposed components of a mechanistic-empirical design procedure for concrete cross-ties

6.2.1.2 Analysis inputs

Of primary importance to understand the problem of designing a long-term component or system subject to cyclical loads is incorporating the time dependency of the inputs. All inputs in the model are subject to change throughout the expected life cycle of the component. Traffic is one of the traditional inputs that exhibits time dependency. Although year to year growth of traffic is relatively easy to model, assuming it can be predicted, more detailed and granular information such as seasonal or hourly distribution may be necessary for accurate service life

predictions. If the material properties are subject to seasonal or daily variation, it is also desirable to know these distributions of traffic. In addition to the total number of repetitions, traffic also incorporates the distribution of maximum gross weight of cars, empty versus loaded railcars, wheel condition, and impact loads.

When considering crossties, the properties of the subgrade and ballast layers are fundamental to their expected performance. In addition to traditional static values such as material type, gradation or resilient modulus, their variation in time is critical. Granular materials show temperature and moisture dependency that must be adequately addressed to characterize the existing support condition of a crosstie at a given time. For this, climatic models may need to be incorporated as an input. Among other parameters, moisture level of subgrade, daily precipitation, resilient modulus of granular materials, snow cover, subgrade freezing depth, air temperature, and crosstie temperature differential must be aspects the climatic model should be able to provide.

In terms of specific crosstie materials, information regarding the evolution of concrete strength and loss of prestressing are essential factors that must be considered. All the previous parameters are based around the critical last design input: a desired life cycle length. This value should be one that balances the economic aspects of producing an engineered component such as crossties. From a railroad perspective, this value might be driven by other factors such as making the life cycle of crossties similar to that of other track components, in such a way that maintenance cycles could effectively be planned to exhaust the complete service life of multiple track elements simultaneously. Thus, maximizing the use of assets and minimizing the impact of track maintenance.

6.2.1.3 Life Cycle Evolution models

While the support characteristics and evolution in time of the subgrade and even ballast layers could be adopted from sources outside the railroad engineering domain, the topic of track condition evolution is an area that requires extensive research in order to be incorporated in a mechanistic-empirical design procedure. Anecdotally, it has been observed that in the case of crossties, track degradation induces a center-bound condition, which in response increases the flexural demand on the component. The exact mechanisms of this degradation and its relationship with crosstie flexural response are not as clear. At the same time, track surfacing maintenance techniques such as tamping allow the track substructure to recover a portion of its initial support characteristics and therefore decreases the flexural demand on crossties.

From the perspective of the proposed design procedure, two different track evolution models must be developed: 1) ballast degradation model as a function of tonnage, and 2) quantification of the effects of surfacing on the ballast support characteristics. Long-term experimentation of high frequency and high tonnage railroad corridors could provide the necessary data to develop both of these models. As an indirect result of this experimentation, railroads could calibrate their maintenance cycles based on the expected degradation curves obtained through the models, providing additional and tangible value for the industry even before the complete development of a mechanistic-empirical design guide.

6.2.1.4 Structural analysis of concrete crossties

The selection of a structural model for use on a design guide must be made in accordance with the required outputs for the transfer functions (capable of providing the adequate analysis outputs) and capable of taking the inputs provided by the necessary track and material evolution

models. Proper structural modeling represents the “heart of a mechanistic-based design procedure” (Applied Research Associates, 2004). The structural analysis model I developed in Chapter 4, could be used as a starting point, although the movement towards a model based on Finite Element Analysis (FEA) could be necessary depending on the computational needs of the final product. Alternatively, linear regression or neural network models have been used for mechanistic-empirical procedures as they require significantly less computational power and provide reasonable accuracy (Ceylan et al., 1999; Applied Research Associates, 2004; Quirós-Orozco et al., 2017).

6.2.1.5 Distress models and critical crosstie responses

The evaluation and quantification of damage comprise the empirical portion of the proposed design methodology. The model of this phenomenon is complex and highly variable, so it has been generally accepted that regression-based analysis can provide satisfactory predictions that account for the underlying damage mechanisms sufficient for design purposes (Huang, 2004). Two different kinds of distresses are identified: 1) structural, where the component loses the capacity to safely handle loads and 2) functional, where the component loses its ability to provide even support condition. The first of these distresses relates to the classical crosstie capacity problem, while the second is related to the indirect effects of poor crosstie performance. These effects also include track geometry deviations, development of soft spots, or accelerated damage to other track components. The selected distresses must be correlated with a mechanical response of interest, in order to develop transfer functions that quantify the unit damage a unit load causes.

Among the crosstie distresses that could be considered as part of a mechanistic-empirical design guide are 1) flexural crack of rail seat, 2) flexural crack of center, 3) rail seat deterioration, 4) bursting cracks, and 5) gauge widening. These distresses could be related to extreme fiber tensile stresses, strains, crosstie deflection and/or bond stresses. Models capable of relating the mechanical responses to these or another potential distresses must be developed or adapted from other engineering disciplines.

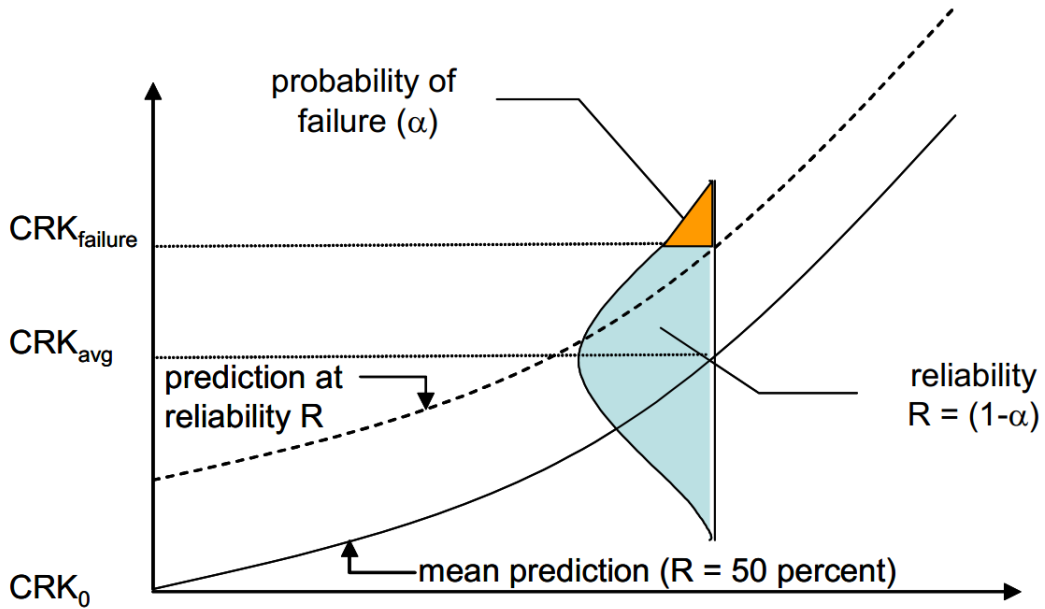
6.2.1.6 Design reliability

Practical application of a mechanistic-empirical design guide for track components must recognize the uncertainty and variable nature of all life cycle and loading stages. Materials, traffic, construction methods, and models introduce inherent uncertainty that must be managed so that a new design can be developed for a desired level of reliability. A common way to address reliability (R) is to quantify the probability (P) that the distress prediction (d) will be less than the failure criteria (D) (Equation 6-1).

$$R = 1 - P[d > D] \quad 6-1$$

During all stages of the design process, the variability of the inputs and the models can be quantified, so a probability distribution of the transfer function outputs could be developed. The variability of the inputs would be a function of the methods used for the characterization of materials or the inherent uncertainty on traffic growth. For instance, in terms of flexural cracking, the final transfer function output would be the mean value prediction of cracking development. This mean value has a particular variability, due to the variability of the inputs and it is characterized in terms of standard deviation or coefficient of variability. The complete

distribution could be then compared with the performance thresholds defined by design, and a probability of failure could be computed (Figure 6.3).



**Figure 6.3: Design reliability concept for a given distress
(Applied Research Associates, 2004)**

REFERENCES

- American Railway Engineering and Maintenance-of-Way Association (AREMA). 2017a. *Manual for Railway Engineering*, Chapter 30: Ties. The American Railway Engineering and Maintenance of Way Association, Landover, MD, USA.
- American Railway Engineering and Maintenance-of-Way Association (AREMA). 2017b. *Manual for Railway Engineering*, Chapter 16: Economics of Railway Engineering and Operations. The American Railway Engineering and Maintenance of Way Association, Landover, MD, USA.
- Amtrak. 2003. *Concrete Crosstie And Fastening Assembly Specification (CT-10)*. National Railroad Passenger Corporation. Wilmington, DE, USA.
- Amtrak. 2012. *The Amtrak Vision For The Northeast Corridor 2012 Update Report*. National Railroad Passenger Corporation. Washington, DC, USA.
- Applied Research Associates. 2004. *Guide For Mechanistic-Empirical Design Of New And Rehabilitated Pavement Structures*. National Cooperative Highway Research Program Report 1-37A. Champaign, Illinois, USA.
- Armaghani, J.M., T.J. Larsen and L.L. Smith. 1987. Temperature response of concrete pavements. *Transportation Research Record: Journal of the Transportation Research Board*, 1121: 23–33.
- Barke, D. and W.K. Chiu. 2005. Structural health monitoring in the railway industry: a review. *Structural Health Monitoring*, 4(1): 81–93.
- Barr P. J., Stanton J. F. and Eberhard M. O. 2005. Effects of temperature variations on precast, prestressed concrete bridge girders. *Journal of Bridge Engineering*, 10(2): 186–194.
- Bastos, J.C. 2016. *Analysis Of The Performance And Failure Of Railroad Concrete Crossties With Various Track Support Conditions*. Master's Thesis, University of Illinois at Urbana-Champaign, Department of Civil and Environmental Engineering. Urbana, IL, USA.
- Bastos, J.C., M.S. Dersch, J.R. Edwards and B. Andrawes. 2017. Flexural behavior of concrete crossties under different support conditions. *Journal of Transportation Engineering, Part A: Systems*, 143(12). DOI: 10.1061/JTEPBS.0000097.
- Bastos, J.C., A. Álvarez-Reyes, M.S. Dersch, J.R. Edwards and C.P.L. Barkan. 2018. Laboratory characterization of structural capacity of North American heavy haul concrete crossties. *Transportation Research Record: Journal of the Transportation Research Board*. DOI: 10.1177/0361198118782250.
- Beer, F.P., E.R. Johnston, J.T. DeWolf and D.F. Mazurek. 2015. *Mechanics Of Materials*, 7th ed. McGraw-Hill Education, New York, NY, USA.

- Boedecker, C. 1887. *Die Wirkungen Zwischen Rad Und Schiene Und Ihre Einflüsse Auf Den Lauf Und Den Bewegungswiderstand Der Fahrzeuge In Den Eisenbahnzügen*. Hahn'sche Buchhandlung, Hannover, Germany.
- Boussinesq, J. 1885. *Application Des Potentiels À L'étude De L'équilibre Et Du Mouvement Des Solides Élastiques*. Gauthier-Villars, Paris, France.
- Bulleit, W.M. 2008. Uncertainty in structural engineering. *Practice Periodical on Structural Design and Construction*, 13(1): 24–30.
- Cai, Z., G.P. Raymond and R.J. Bathurst. 1994. Estimate of static track modulus using elastic foundation models. *Transportation Research Record: Journal of the Transportation Research Board*, 1470: 65–72.
- Canadian National. 2011. Wheel Impact Load Detectors: The Early History On CN. In: *Proceedings Of The 31st Annual North American Rail Mechanical Operations Seminar*, St. Louis, MO, USA.
- Canga Ruiz, Á.E. 2018. *Analysis Of The Design Of Railroad Track Superstructure Components For Rail Transit Applications*. Master's Thesis, University of Illinois at Urbana-Champaign, Department of Civil and Environmental Engineering, Urbana, IL, USA.
- Carter, F.W. 1916. The electric locomotive. *Proceedings of the Institute of Civil Engineers*, 201: 221–252.
- Ceylan, H., E. Tutumluer and E. Barenberg. 1999. Artificial neural networks for analyzing concrete airfield pavements serving the Boeing B-777 aircraft. *Transportation Research Record: Journal of the Transportation Research Board*, 1684: 110–117.
- Clarke, C.W. 1957. Track loading fundamentals: part III. *The Railway Gazette* 104: February, pp. 157-163.
- Cope, G.H. 1993. *British Railway Track. Design, Construction And Maintenance*, 6th ed. The Permanent Way Institution, Loughborough, Leicestershire, England.
- Council of Standards Australia. 2003. *Railway Track Material Part 14: Prestressed Concrete Sleepers (AS 1085.14)*. Sydney, Australia.
- Doyle, N.F. 1980. *Railway Track Design: A Review Of Current Practice*. BHP Melbourne Research Laboratory. Canberra, Australia.
- Edwards, J.R., M.S. Dersch and R.G. Kernes. 2017a. *Improved Concrete Crosstie And Fastening Systems For US High Speed Passenger Rail And Joint Corridors - Project Summary Report (Volume 1)*. Federal Railroad Administration (FRA). Washington, DC, USA.
- Edwards, J.R., Z. Gao, H.E. Wolf, M.S. Dersch and Y. Qian. 2017b. Quantification of concrete railway sleeper bending moments using surface strain gauges. *Measurement*, 111: 197–207.

- Edwards, J.R., A. Cook, M. Dersch and Y. Qian. 2018a. Quantifying rail transit concrete monoblock sleeper field bending moments. *Journal of Transportation Engineering –Part A (Systems)*. DOI: 10.1061/JTEPBS.0000125.
- Edwards, J.R., A. Cook, M. Dersch and Y. Qian. 2018b. Quantification of rail transit wheel loads and development of improved dynamic and impact loading factors for design. *Journal of Rail and Rapid Transit*. DOI: 10.1177/0954409718770924.
- Fisher, R.B. 1990. Introduction of static frequency converters on SEPTA's 25 Hz commuter rail system. In: *Technical Papers Presented At The 1990 ASME/IEEE Joint Conference*. Institute of Electrical and Electronics Engineers (IEEE). Chicago, IL, USA, pp. 149–155.
- Gao, Z., M.S. Dersch, Y. Qian, M.V. Csenge and J.R. Edwards. 2017a. Use of ballast support condition back-calculator for quantification of ballast pressure distribution under concrete sleepers, In: Loizos, A., I. Al-Qadi & T. Scarpas, (Eds.). *Bearing Capacity of Roads, Railways and Airfields: Proceedings of the 10th International Conference on the Bearing Capacity of Roads, Railways and Airfields*, Athens, Greece.
- Gao, Z., H.E. Wolf, M.S. Dersch, Y. Qian and J.R. Edwards. 2017b. Non-destructive estimation of concrete crosstie support conditions using field bending moments. In: *Proceedings Of The 96th Annual Meeting Of The Transportation Research Board Of The National Academies*, Washington, DC, USA.
- Gao, Z., Y. Qian, M.S. Dersch and J.R. Edwards. 2017c. Compressive stress distribution in prestressed concrete and its effect on railroad crosstie design. *Construction and Building Materials*, 151: 147–157.
- Giannakos, K. 2010. Loads on track, ballast fouling, and life cycle under dynamic loading in railways. *Journal of Transportation Engineering*, 136(12): 1075–1084.
- Gräbe, P.J., B.F. Mtshotana, M.M. Sebati and E.Q. Thünemann. 2016. The effects of under-sleeper pads on sleeper-ballast interaction. *Journal of the South African Institution of Civil Engineering*, 58(2): 35–41.
- Greve, M. 2015. *Quantification Of Rail Seat Load Distributions On Concrete Crossties*. Master's Thesis, University of Illinois at Urbana-Champaign, Department of Civil and Environmental Engineering, Urbana, IL, USA.
- Hanson, C.E. and H.L. Singleton. 2006. Performance of ballast mats on passenger railroads: measurement vs. projections. *Journal of Sound and Vibration*, 293(3): 873–877.
- Harrison, H.D., L.R. Cheng and W. GeMeiner. 2006. Tracking the performance of heavy axle load vehicles in revenue service. In: *Proceedings Of ASME 2006 International Mechanical Engineering Congress And Exposition*. American Society of Mechanical Engineers (ASME). Chicago, IL, USA, pp. 137–143.

- Harrison, H.D. and J.M. Tuten. 1984. Wheel load measurement. WO1986003582A1.
- Hay, W.W. 1982. *Railroad Engineering*, 2nd ed. John Wiley & Sons, Incorporated, New York, NY, USA.
- Heath, D., J. Waters, M. Shenton and R. Sparrow. 1972. Design of conventional rail track foundations. *Proceedings of the Institution of Civil Engineers*, 51(2): 251–267.
- Hertz, H. 1881. Ueber die berührung fester elastischer körper. *Journal für die reine und angewandte Mathematik (Crelle's Journal)*, 1882(92): 156–171.
- Hou, W., B. Feng, W. Li and E. Tutumluer. 2018. Ballast support condition affecting crosstie performance investigated through discrete element method. In: *Proceedings Of The 2018 Joint Rail Conference*. American Society of Mechanical Engineers (ASME). Pittsburgh, PA, USA.
- Huang, Y.H. 2004. *Pavement Analysis And Design*, 2nd ed. Pearson, Upper Saddle River, NJ, USA.
- Indraratna, B., W. Salim and C. Rujikiatkamjorn. 2011. *Advanced Rail Geotechnology - Ballasted Track*. CRC Press, London, United Kingdom.
- International Union of Railways (UIC). 2004. *Design Of Monoblock Sleepers (UIC 713)*, 1st ed. L'Union Internationale des Chemins de Fer, Paris, France.
- Johansson, A., J.C.O. Nielsen, R. Bolmsvik, A. Karlström and R. Lundén. 2008. Under sleeper pads—Influence on dynamic train–track interaction. *Wear*, 265(9–10): 1479–1487.
- Kerr, A.D. 2003. *Fundamentals Of Railway Track Engineering*, 1st ed. Simmons-Boardman Books, Inc., Omaha, NE, USA.
- Klingel, W. 1883. Über den lauf der eisenbahnwagen auf gerader bahn. *Organ für Die Fortschritte des Eisenbahnwesens*, 20(4): 113–123.
- Knothe, K. 2008. History of wheel/rail contact mechanics: from Redtenbacher to Kalker. *Vehicle System Dynamics*, 46(1–2): 9–26.
- LB Foster Salient Systems. 2015. Wheel Impact Load Detector Product Sheet. URL http://www.lbfoster-salientsystems.com/pdf/LBF_Wild_Product_sheet_LOWRES.pdf. Accessed 2017-07-10.
- Lewis, R. and U. Olofsson. 2009. *Wheel-Rail Interface Handbook*, 1st ed. Woodhead Publishing, Cambridge, United Kingdom.
- Li, D. and E.T. Selig. 1998. Method for railroad track foundation design. I: Development. *Journal of Geotechnical and Geoenvironmental Engineering*, 124(4): 316–322.

- Lima, A de O. 2017. *Under Ballast Mats For Railway Infrastructure – A North American Approach To Component Characterization*. Master's Thesis, University of Illinois at Urbana-Champaign, Department of Civil and Environmental Engineering, Urbana, IL, USA.
- Macaulay, W.H. 1919. Note on the deflection of beams. *Messenger of Mathematics*, 48: 129–130.
- Mayville, R.A., L. Jian and M. Sherman. 2014. *Performance Evaluation Of Concrete Railroad Ties On The Northeast Corridor*. US Department of Transportation, Federal Railroad Administration Report DOT/FRA/RPD-14/03. Washington, DC, USA.
- McHenry, M.T., M. Brown, J. LoPresti, J. Rose and R. Souleyrette. 2015. Use of matrix-based tactile surface sensors to assess fine-scale ballast–tie interface pressure distribution in railroad track. *Transportation Research Record: Journal of the Transportation Research Board*, 2476: 23–31.
- Mohamed, A.R. and W. Hansen. 1996. Prediction of stresses in concrete pavements subjected to non-linear gradients. *Cement and Concrete Composites*, 18(6): 381–387.
- National Instruments. 2012. Making Accurate Strain Measurements - National Instruments. URL <http://www.ni.com/white-paper/6186/en/>. Accessed 2017-07-11.
- Popov, E.P. 1998. *Engineering Mechanics Of Solids*, 2nd ed. Pearson, Upper Saddle River, N.J, USA.
- Prause, R.H., H.C. Meacham, H.D. Harrison, T.A. Johns and W.A. Glaeser. 1974. *Assessment Of Design Tools And Criteria For Urban Rail Track Structures (Volume I: At-Grade Tie-Ballast Track)*. US Department of Transportation, Urban Mass Transportation Administration Report UMTA-MA-06-0025-74-4. Washington, DC, USA.
- Prause, R.H., H.D. Harrison, J.C. Kennedy and R.C. Arnlund. 1977. *An Analytical And Experimental Evaluation Of Concrete Crosstie And Fastener Loads*. US Department of Transportation, Federal Railroad Administration Report FRA/ORD-77/71. Washington, DC, USA.
- Profillidis, V.A. 2014. *Railway Management And Engineering*, 4th ed. Ashgate Publishing Company, Burlington, VT, USA.
- Quirós-Orozco, R.J., L.G. Loría-Salazar and P. Leiva-Padilla. 2017. Models to predict mechanical responses in rigid pavements. *Journal of Transportation Engineering, Part A: Systems*. DOI: 10.1061/JTEPBS.0000027.
- Quirós-Orozco, R.J., J.R. Edwards, Y. Qian and M.S. Dersch. 2018. Quantification of loading environment and flexural demand of prestressed concrete crossties under shared corridor operating conditions. *Transportation Research Record: Journal of the Transportation Research Board*. DOI: 10.1177/0361198118793500.

- Railway Tie Association. 2017. Frequently Asked Questions. URL <https://www.rta.org/faqs-main>. Accessed 2018-10-14.
- Rapp, C.T., J.R. Edwards, M.S. Dersch, C.P.L. Barkan, J. Mediavilla and B.M. Wilson. 2012. Measuring concrete crosstie rail seat pressure distribution with matrix based tactile surface sensors. In: *Proceedings Of The 2012 ASME Joint Rail Conference*. American Society of Mechanical Engineers (ASME). Philadelphia, PA, USA, pp. 85–92.
- Raymond, G.P. 1978. Design for railroad ballast and subgrade support. *Journal of the Geotechnical Engineering Division*, 104(1): 45–60.
- Richardson, J.M. and J.M. Armaghani. 1987. Stress caused by temperature gradient in Portland cement concrete pavements. *Transportation Research Record: Journal of the Transportation Research Board*, (1121): 7–13.
- Rizos, D.C. 2016. High-strength reduced-modulus high performance concrete (HSRM-HPC) for prestressed concrete tie applications. In: *Proceedings Of The 2016 Joint Rail Conference*. American Society of Mechanical Engineers (ASME). Columbia, SC, USA.
- Rose, J.G. and J.C. Stith. 2004. Pressure measurements in railroad trackbeds at the rail/tie interface using Tekscan sensors. In: *Proceedings Of The AREMA 2004 Annual Conference*. American Railway Engineering and Maintenance-of-Way Association (AREMA). Nashville, TN, USA.
- Sadeghi, J.M. 2008. Experimental evaluation of accuracy of current practices in analysis and design of railway track sleepers. *Canadian Journal of Civil Engineering*, 35(9): 881–893.
- Sadeghi, J.M. and P. Barati. 2010. Evaluation of conventional methods in analysis and design of railway track system. *International Journal of Civil Engineering*, 8(1): 44–56.
- Sadeghi, J.M. and P. Barati. 2012. Comparisons of the mechanical properties of timber, steel and concrete sleepers. *Structure and Infrastructure Engineering*, 8(12): 1151–1159.
- Sadeghi, J.M. and M. Youldashkhan. 2005. Investigation on the accuracy of the current practices in analysis of railway track concrete sleepers. *International Journal of Civil Engineering*, 3(1): 15.
- Schneider, P., R. Bolmsvik and J.C.O. Nielsen. 2011. In situ performance of a ballasted railway track with under sleeper pads. *Journal of Rail and Rapid Transit*, 225(3): 299–309.
- Schramm, G. 1961. *Permanent Way Technique And Permanent Way Economy*. 1st ed. Otto Elsner Verlagsgesellschaft, Darmstadt, Germany.
- Selig, E.T. and J.M. Waters. 1994. *Track Geotechnology And Substructure Management*, 1st ed. Thomas Telford Publishing, London, United Kingdom.
- Selvadurai, A.P.S. 1979. *Elastic Analysis Of Soil-Foundation Interaction*, 1st ed. Elsevier, New York, NY, USA.

- Shenton, M.J. 1978. Deformation of railway ballast under repeated loading conditions, In: Kerr, A. D., (Ed.) *Railroad Track Mechanics and Technology*. Pergamon Press, Princeton, NJ, USA. pp.405–425.
- Song, W., X. Shu, B. Huang, Y. Sun, H. Gong and D. Clarke. 2017. Pressure distribution under steel and timber crossties in railway tracks. *Journal of Transportation Engineering, Part A: Systems*, 143(9): 04017046.
- Stratman, B., Y. Liu and S. Mahadevan. 2007. Structural health monitoring of railroad wheels using wheel impact load detectors. *Journal of Failure Analysis and Prevention*, 7(3): 218–225.
- Talbot, A.N. 1918. First progress report of special committee to report on stresses in railroad track. In: *Proceedings Of The 19th American Railway Engineering Association Annual Convention*. American Railway Engineering Association (AREA). Chicago, IL, USA.
- Talbot, A.N. 1919. Second progress report of special committee to report on stresses in railroad Track. In: *Proceedings Of The 21st American Railway Engineering Association Annual Convention*. American Railway Engineering Association (AREA). Chicago, IL, USA.
- Thompson, D. 2008. *Railway Noise And Vibration: Mechanisms, Modelling And Means Of Control*, 1st ed. Elsevier, Amsterdam, The Netherlands.
- Thompson, M.R. 1996. Mechanistic-empirical flexible pavement design: an overview. *Transportation Research Record: Journal of the Transportation Research Board*, 1539: 1–5.
- Thompson, M.R., B.J. Dempsey, H. Hill and J. Vogel. 1987. Characterizing temperature effects for pavement analysis and design. *Transportation Research Record: Journal of the Transportation Research Board*, (1121): 14–22.
- Tutumluer, E., H. Huang, Y.M.A. Hashash and J. Ghaboussi. 2007. Discrete element modeling of railroad ballast settlement. In: *Proceedings Of The American Railway Engineering and Maintenance-of-way Association 2007 Annual Conference*. The American Railway Engineering and Maintenance-of-way Association (AREMA). Chicago, IL, USA.
- Tutumluer, E., H. Huang, Y.M.A. Hashash and J. Ghaboussi. 2009. AREMA gradations affecting ballast performance using discrete element modeling (DEM) approach. In: *Proceedings Of The American Railway Engineering and Maintenance-of-way Association 2009 Annual Conference*. The American Railway Engineering and Maintenance-of-way Association (AREMA). Chicago, IL, USA, pp. 20–23.
- Tutumluer, E., Y. Qian, Y.M.A. Hashash, J. Ghaboussi and D.D. Davis. 2011. Field validated discrete element model for railroad ballast. In: *Proceedings Of The American Railway Engineering and Maintenance-of-way Association 2011 Annual Conference*. The American Railway Engineering and Maintenance-of-way Association (AREMA), Minneapolis, MN, USA, pp. 18–21.

- Van Dyk, B. 2015. *Characterization Of The Loading Environment For Shared-Use Railway Superstructure In North America*. MS Thesis, University of Illinois at Urbana-Champaign, Department of Civil and Environmental Engineering, Urbana, IL, USA.
- Van Dyk, B.J., C.T. Rapp, M.S. Dersch, J.R. Edwards, C.J. Ruppert Jr and C.P.L. Barkan. 2013. Evaluation of existing loading environment in North America for improved concrete sleepers and fastening systems. In: *Proceedings Of The 2013 World Congress Of Railway Research*, Sydney, Australia.
- Van Dyk, B., M. Dersch, J. Edwards, C. Ruppert and C. Barkan. 2014. Load characterization techniques and overview of loading environment in North America. *Transportation Research Record: Journal of the Transportation Research Board*, (2448): 80–86.
- Van Dyk, B.J., J.R. Edwards, M.S. Dersch, C.J. Ruppert and C.P. Barkan. 2017. Evaluation of dynamic and impact wheel load factors and their application in design processes. *Proceedings of the Institution of Mechanical Engineers, Part F: Journal of Rail and Rapid Transit*, 231(1): 33–43.
- Winkler, E. 1867. *Die Lehre Von Der Elastizität Und Festigkeit*. Verlag von H. Dominicius, Prague, Czech Republic.
- Wittrick, W.H. 1965. A generalization of Macaulay’s method with applications in structural mechanics. *American Institute of Aeronautics and Astronautics Journal*, 3(2): 326–330.
- Wolf, H.E. 2015. *Flexural Behavior Of Prestressed Concrete Monoblock Crossties*. Master’s Thesis, University of Illinois at Urbana-Champaign, Department of Civil and Environmental Engineering, Urbana, IL, USA.
- Wolf, H.E., J.R. Edwards, M.S. Dersch and C.P. Barkan. 2015. Flexural analysis of prestressed concrete monoblock sleepers for heavy-haul applications: methodologies and sensitivity to support conditions. In: *Proceedings Of The International Heavy Haul Association 2015 Conference*. International Heavy Haul Association (IIHA), Perth, Australia.
- Wolf, H.E., Y. Qian, J.R. Edwards, M.S. Dersch and D.A. Lange. 2016. Temperature-induced curl behavior of prestressed concrete and its effect on railroad crossties. *Construction and Building Materials*, 115: 319–326.
- Yu, H., L. Khazanovich, M. Darter and A. Ardani. 1998. Analysis of concrete pavement responses to temperature and wheel loads measured from instrumented slabs. *Transportation Research Record: Journal of the Transportation Research Board*, 1639: 94–101.
- Yu, H., B.P. Marquis and D.Y. Jeong. 2017. Failure analysis of railroad concrete crossties in the center negative flexural mode using finite element method. *Proceedings of the Institution of Mechanical Engineers, Part F: Journal of Rail and Rapid Transit*, 231(5): 610–619.

- Zeitouni, A.I., D. Rizos and Y. Qian. 2018. Benefits of prestressed HSRM concrete ties for center binding conditions. In: *Proceedings Of The 2018 Joint Rail Conference*. American Society of Mechanical Engineers (ASME). Pittsburgh, PA, USA.
- Zeman, J.C. 2010. *Hydraulic Mechanisms Of Concrete-Tie Rail Seat Deterioration*. Master's Thesis, University of Illinois at Urbana-Champaign, Department of Civil and Environmental Engineering, Urbana, IL, USA.
- Zimmermann, H. 1941. *Die Berechnung Des Eisenbahnoberbaues*, 3rd ed. Verlag W. Ernst & Sohn, Berlin, Germany.